

PREDICTION OF AIRCRAFT FUSELAGE VIBRATION

by

Rohan J. Thomas  
Bachelor of Technology, National Institute of Technology Warangal, 2012

A Thesis

Submitted to the Graduate Faculty

of the

University of North Dakota

in partial fulfillment of the requirements

for the degree of

Master of Science

Grand Forks, North Dakota

May  
2015

UMI Number: 1594387

All rights reserved

INFORMATION TO ALL USERS

The quality of this reproduction is dependent upon the quality of the copy submitted.

In the unlikely event that the author did not send a complete manuscript and there are missing pages, these will be noted. Also, if material had to be removed, a note will indicate the deletion.



UMI 1594387

Published by ProQuest LLC (2015). Copyright in the Dissertation held by the Author.

Microform Edition © ProQuest LLC.

All rights reserved. This work is protected against unauthorized copying under Title 17, United States Code



ProQuest LLC.  
789 East Eisenhower Parkway  
P.O. Box 1346  
Ann Arbor, MI 48106 - 1346

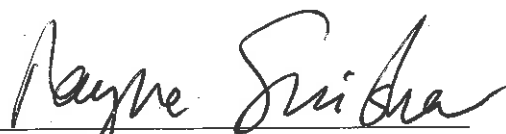
This thesis, submitted by Rohan J. Thomas in partial fulfillment of the requirements for the Degree of Master of Science from the University of North Dakota, has been read by the Faculty Advisory Committee under whom the work has been done and is hereby approved.

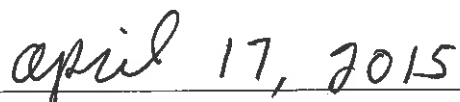
  
\_\_\_\_\_  
Dr. Marcellin Zahui

  
\_\_\_\_\_  
Dr. Bishu Bandyopadhyay

  
\_\_\_\_\_  
Dr. George Bibel

This thesis is being submitted by the appointed advisory committee as having met all of the requirements of the School of Graduate Studies at the University of North Dakota and is hereby approved.

  
\_\_\_\_\_  
Wayne Swisher  
Dean of the School of Graduate Studies

  
\_\_\_\_\_  
Date

## PERMISSION

Title            Prediction of Aircraft Fuselage Vibration  
Department    Mechanical Engineering  
Degree         Master of Science

In presenting this thesis in partial fulfillment of the requirements for a graduate degree from the University of North Dakota, I agree that the library of this University shall make it freely available for inspection. I further agree that permission for extensive copying for scholarly purposes may be granted by the professor who supervised my thesis work or, in his absence, by the Chairperson of the department or the dean of the School of Graduate Studies. It is understood that any copying or publication or other use of this thesis or part thereof for financial gain shall not be allowed without my written permission. It is also understood that due recognition shall be given to me and to the University of North Dakota in any scholarly use which may be made of any material in my thesis.

Rohan Thomas

30<sup>th</sup> April 2015

## TABLE OF CONTENTS

LIST OF FIGURES .....	vi
LIST OF TABLES .....	x
ACKNOWLEDGEMENTS .....	xi
ABSTRACT .....	xii
CHAPTER	
I.INTRODUCTION .....	1
Research Objective .....	2
Background.....	2
Turbulence Effects.....	3
Human Control.....	6
Conventional Turbulence Sensors.....	7
Piezoelectric Materials as Sensors.....	8
II. DEVELOPMENT OF A LUMPED MASS MODEL.....	10
Modal Analysis of the Lumped Mass System.....	10
Finite Element Modeling and Simulation of the Lumped Mass System.....	14
Forced Vibration Analysis using Modal Superposition Equations .....	17
Finite Element Forced Vibration Simulation of the Lumped Mass System .....	23
Theoretical State Space Model.....	25
System Identification State Space Model.....	29

Frequency Response Function .....	33
III. DEVELOPMENT OF A THREE DIMENSIONAL MODEL .....	37
Free Vibration Simulation of the Three Dimensional Aircraft .....	37
Forced Vibration Simulation .....	41
Deriving State Space Models using System Identification .....	43
Validation of Derived State Space Models .....	49
Frequency Response Function .....	56
IV. VIBRATION SENSOR DESIGN .....	62
Development of a Theoretical Sensor .....	62
MATLAB® Simulation of the Theoretical Sensor .....	65
ANSYS® Simulation .....	68
Displacement Sensors on an Airplane Wing .....	71
Slope Correction .....	73
V. VIBRATION SENSORS ON AN AIRPLANE .....	75
Fixed Fuselage Simulation .....	75
Elastically Supported Fuselage Simulation .....	77
VI. CONCLUSIONS AND RECOMMENDATIONS .....	88
APPENDICES .....	91
APPENDIX A .....	92
APPENDIX B .....	98
REFERENCES .....	101

## LIST OF FIGURES

Figure	Page #
1. Constraints imposed on UAVs and their side effects.....	5
2. Effects of asymmetric gust loading on an aircraft.....	5
3. Approaches towards aircraft stability.....	7
4. Aircraft model.....	10
5. Lumped mass system.....	11
6. Representation of the lumped mass system as a spring mass system.....	11
7. First mode shape of the lumped mass system.....	15
8. Second mode shape of the lumped mass system.....	15
9. Third mode shape of the lumped mass system.....	16
10. Comparison between calculated and simulation results for a step force input.....	24
11. Comparison between calculated and simulation results for a sine force input.....	25
12. Comparison between derived state space model and MATLAB® model for a step input.....	31
13. Comparison between derived state space model and MATLAB® model for a sine input.....	31
14. Comparison between the two state space models.....	32
15. Amplitude comparison between simulation results and state space models.....	35
16. Phase comparison between simulation results and state space models.....	36

17. Three dimensional model of the aircraft used for analysis.....	37
18. BTE Super Hauler.....	38
19. Constraints placed on the three dimensional plane.....	39
20. Locations of the elastic supports on the aircraft.....	41
21. Loads applied on the faces of the wings.....	42
22. Comparison between simulation results and state space output for fuselage motion in the X direction.....	50
23. Comparison between simulation results and state space output for fuselage motion in the Y direction.....	50
24. Comparison between simulation results and state space output for fuselage motion in the Z direction.....	51
25. Comparison between simulation results and state space output for fuselage rotation about the X direction.....	51
26. Comparison between simulation results and state space output for fuselage rotation about the Y direction.....	52
27. Comparison between simulation results and state space output for fuselage rotation about the Z direction.....	52
28. Comparison between simulation results and state space output for fuselage motion in the X direction.....	53
29. Comparison between simulation results and state space output for fuselage motion in the Y direction.....	53
30. Comparison between simulation results and state space output for fuselage motion in the Z direction.....	54
31. Comparison between simulation results and state space output for fuselage rotation about the X direction.....	54
32. Comparison between simulation results and state space output for fuselage rotation about the Y direction.....	55
33. Comparison between simulation results and state space output for fuselage rotation about the Z direction.....	55



34. Amplitude comparison between simulation results and state space model.....	57
35. Phase comparison between simulation results and state space model.....	57
36. Comparison between FRF state space model and transient analysis.....	60
37. Cantilever beam covered with piezoelectric patches.....	62
38. Comparison between results for a cantilever beam displacement for an arbitrary force excitation frequency of 298 Hz.....	67
39. Comparison between results for the Frequency Response Function of the displacement of a cantilever beam.....	67
40. Prismatic beam with piezoelectric patches.....	68
41. Voltages on a single sensor patch.....	70
42. Comparison between measured displacement and patch output for a clamped-clamped beam.....	70
43. Piezoelectric displacement sensors on an airplane wing.....	71
44. Force applied to the airplane wing.....	71
45. Comparison between measured displacement and patch output for a fixed airplane wing.....	72
46. Cantilever beam.....	73
47. Comparison between measured displacement and patch output for a fixed airplane wing with an applied correction factor.....	74
48. Aircraft with distributed displacement sensors on its wings.....	76
49. Comparison between the measured displacement and calculated displacement of wing 1.....	76
50. Comparison between the measured displacement and calculated displacement of wing 2.....	77
51. Calculated displacement of wing 1.....	78
52. Calculated displacement of wing 2.....	78

53. Comparison between state space outputs and simulation results for fuselage motion about the X-axis.....	85
54. Comparison between state space outputs and simulation results for fuselage motion about the Y-axis.....	85
55. Comparison between state space outputs and simulation results for fuselage motion about the Z-axis.....	86
56. Comparison between state space outputs and simulation results for fuselage rotation about the X-axis.....	86
57. Comparison between state space outputs and simulation results for fuselage rotation about the Y-axis.....	87
58. Comparison between state space outputs and simulation results for fuselage rotation about the Z-axis.....	87
59. Data input options in the system identification toolbox.....	95
60. Data being imported into the toolbox.....	95
61. State space model window.....	96
62. Model order selection window.....	96
63. Model output.....	97

## LIST OF TABLES

Table	Page #
1. Parameter values used for simulation.....	12
2. Summary of ANSYS® modal analysis results.....	15
3. Comparison between calculated results and simulation results.....	16
4. Summary of calculated damping values.....	19
5. Specifications used to develop the 3D model.....	38
6. Material specifications used for three dimensional simulation.....	39
7. Summary of the 3D modal analysis results.....	40
8. Summary of beam and sensor parameters used during simulation.....	66
9. Parameter values used to simulate a clamped-clamped beam.....	69
10. Parameters used for the PVDF displacement sensor.....	69

## ACKNOWLEDGEMENTS

I would like to express my sincere appreciation to the Mechanical Engineering Department at the University of North Dakota, especially Dr. Marcellin Zahui for all his guidance and wisdom. I would also like to thank my committee members, Dr. Bishu Bandyopadhyay and Dr. George Bibel for their advice and expertise.

I would also like to thank my father, Junu Thomas and mother, Susan Thomas for their extensive support and for believing in me.

## ABSTRACT

Modern unmanned aerial vehicles (UAV) are made of lightweight structures, owing to the demand for longer ranges and heavier payloads. These lightweight aircraft are more susceptible to vibrations caused by atmospheric turbulence transmitted to the fuselage from the wings. These vibrations, which can cause damage to the payload or on board avionics present a serious problem, since air turbulence is expected to increase over the next few decades, due to climate change.

The objective of this thesis is to predict the vibration of an aircraft fuselage by establishing a relationship between wing and fuselage vibration. A combination of ANSYS® and MATLAB® modeling are used to simulate aircraft vibrations. First, the displacement of a lumped mass aircraft model to step and sinusoidal forces acting on the wings are compared to displacements calculated using modal superposition equations. Next, a state space representation of this system is found using system identification techniques, which uses wing displacement as input, and provides fuselage displacement as output. This state space model is compared to a derived state space model for validation. Finally, a three dimensional aircraft with distributed displacement sensors on its wings is modeled. A state space representation is established using the wing displacement output from the sensors as its input and the motion and rotation of the fuselage along the X, Y and Z axes as the output.

It is seen that the displacement results of the lumped mass system match with those calculated using modal superposition equations. The state space model can also

accurately predict the fuselage vibration of the lumped mass system, when provided with wing displacement as input. More importantly, results have shown that the distributed vibration sensors on the three dimensional plane model are able to measure the wing displacements. Using the output from these distributed sensors, the motion and rotation of the fuselage about all three axes can be effectively predicted.

## **CHAPTER I**

### **INTRODUCTION**

The Unmanned Aerial Vehicle (UAV) industry is a highly competitive market, ever since its popularity in both military and civil applications have drastically increased. Longer ranges and heavier payloads are currently areas of continuous improvement in this industry. A common approach to this demand is the use of lightweight materials for aircraft structures. Light airplane structures allow for longer ranges and heavier payloads, but are more difficult to control under turbulent conditions [1]. Turbulent loads can cause damage to the payload and aircraft structure as these loads are transmitted to the fuselage through the wings.

Modern unmanned aircraft carry avionics in their fuselage which are sensitive to vibration and high values of acceleration. A 50% reduction in vibrations experienced by these avionics can improve their lifetime by a factor of 100 to as much as 1000 [2].

Clear-air turbulence is frequently encountered by such aircraft at cruising altitudes, and are not often detected by conventional radar. The strength of clear-air turbulence is expected to rise by 10 – 40%, and its frequency is expected to rise by 40 – 170% by the middle of this century due to climate change [3].

This predicted increase in aircraft turbulence frequency and intensity could lead to shorter lifetimes for aircraft avionics and greater structural damage on aircraft. Ultimately, replacing unreliable avionics and damaged aircraft structures prompt steeper maintenance costs.

## **Research Objective**

The objective of this thesis is to predict the rigid body vibration of the aircraft fuselage by measuring the vibration of its wings. Modern commercial aircraft carry on board highly sophisticated avionics, which are able to significantly damp turbulence effects. Introducing sophisticated electronics to the UAV could prove to be counterproductive, and hence the need for a system that is lightweight, cost effective and reliable is noteworthy.

Piezoelectric materials are widely used for their electromechanical properties, as a sensor as well as an actuator [4]. They add very little weight to the receiving structure and are easy to cut and shape. These properties make piezoelectric materials very suitable in sensing the displacement caused by turbulent loads on the wings of the aircraft.

By establishing a state space model which uses the vibration of the wings through the sensor as its input, the vibration of the fuselage along all axes can be predicted. An Active/Passive Vibration Control system can be developed by predicting fuselage vibrations, which provides suitable actuator signals for countermeasures. With the introduction of such a control system, a reduction in vibration can be ensured by means of active vibration mounts, thus protecting the payload, on board avionics and the structural integrity of the aircraft.

## **Background**

Gust detection systems such as LiDAR (Light Detection and Ranging) are currently employed in aircraft to detect any turbulence that it may encounter in the near future. Another turbulence probe used in aircraft known as the Best Aircraft Turbulence (BAT) probe, which consists of an air data probe, an inertial measurement system, a global



positioning system and software to link the hardware together [5]. While such systems are indeed effective on larger aircraft, it would be counterproductive to incorporate them into small unmanned vehicles. In general, the avionics of small unmanned aircraft are focused on aircraft navigation and control [6]. Tracking changes in turbulence that lie ahead of the plane can be computationally expensive, which may ultimately interfere with the range and payload characteristics of the aircraft.

Therefore, there is a need for a system that can measure turbulence without undermining the basic functionalities of the aircraft. From a structural point of view, turbulent loads cause wing deformations, fuselage roll as well as disturbances in the pitch of the aircraft [7]. If this wing deformation could be measured, it could be related to the consequential fuselage disturbance by means of a state space model, which would be less processor intensive than a system that can predict fuselage motion by constantly tracking changes in turbulence that the aircraft would encounter in the near future. With the introduction of said state space model to predict the motion of the fuselage, effective countermeasures to maintain the stability of the avionics or payload can be made without largely impacting the range and payload carrying characteristics of the aircraft.

Research has been widely conducted on the effects of turbulent winds on small unmanned aircraft, the suitability of conventional sensors in detecting turbulence and potential solutions to this problem. These studies are briefly discussed, followed by the possibility of using piezoelectric materials as displacement sensors for an aircraft.

### **Turbulence Effects**

In this thesis, turbulence is defined as: Severe wind gusts that cause undesirable motion. Hoppe also describes turbulence as [8]: “Change in angle of attack or an added

vertical component of headwind”.

Unmanned aerial vehicles have a number of unique constraints imposed upon them such as size, range, payload capacity and others based on their requirements. These constraints can present a number of issues such as undesirable roll, difficulty in maneuvering and poor stability in turbulent wind conditions. Unmanned vehicles often operate at lower altitudes; an atmospheric region where turbulence intensity is much higher and much more frequent [1].

A study conducted in 2013 by Mohamed, Massey, Watkins and Clothier looks into the attitude stability of an aerial vehicle while encountering significant turbulence and evaluates the effects of constraints such as size on the performance of the aircraft.

While a smaller airplane size may be more desirable, it could also lower the stability of the aircraft. The study also found that the ability of an aircraft to damp rolls is directly proportional to the wing span of the aircraft [1]. The roll mode time constant ( $\tau_r$ ) can be approximated as the inverse of roll damping ( $L_p$ ) as [1]:

$$\tau_r = \frac{-1}{L_p}$$

This implies that [1]:

$$\tau_r \sim \sqrt{b}$$

where

$b$  = wingspan of the aircraft

Hence for small unmanned aerial vehicles, it can be assumed that its ability to maintain a given angle of attack and roll angle while encountering turbulent winds is rather poor.

Since UAVs have limited payload capacity, it is unable to carry highly sophisticated

avionics or stabilizing gimbals [1]. This further undermines the ability of these vehicles to navigate safely through gusty conditions. These problems are summarized in Fig. 1.

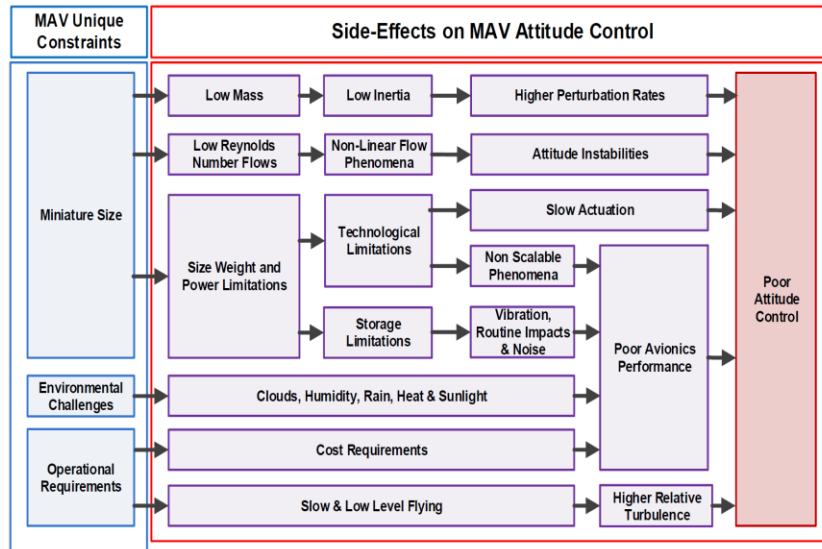


Figure 1. Constraints imposed on UAVs and their side effects [1].

One of the main consequences of turbulence is undesirable roll on UAVs. More often than not, turbulent loads acting on the wings of a UAV are unsymmetrical – such loads cause the UAV to roll, which can prove to be detrimental to its performance. Fig. 2 illustrates the effects of unsymmetrical loading.

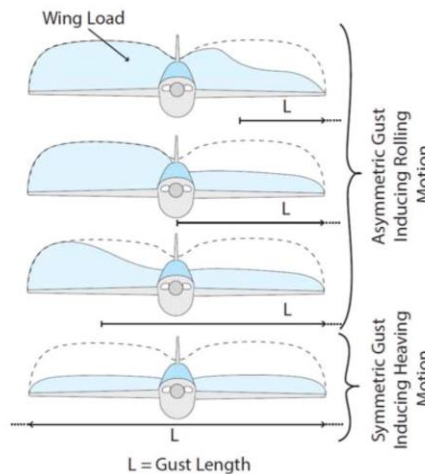


Figure 2. Effects of asymmetric gust loading on an aircraft [9].

## **Human control**

An experiment conducted in 2014 by Chen, Clothier, Mohamed and Badawy tries to determine if humans are able to control a small unmanned aircraft through turbulent conditions. In this experiment, a random sample of volunteers were asked to take part in a simulation which involved maneuvering an unmanned aircraft using a controller [10]. The simulation involved guiding the aircraft, which was allowed to rotate only about its roll axis, through turbulent winds [10]. Results showed that most of the volunteers were able to keep the wings level within  $\pm 20^\circ$  for 50% of the time [10]. The instability of an unmanned aerial vehicle through such conditions could have several implications such as damage to payload, reduced avionics lifetimes or total loss of the aircraft. UAVs are often involved in assignments that are stability intensive, and in such cases, the input from a human controlling the vehicle may not suffice. It is also a concern that turbulent winds are observed to act at frequencies as high as 25 Hz [11]. Making corrections to the attitude of the plane at such frequencies may prove to be highly strenuous to human beings, and their performance may decrease over time.

Potential solutions to this problem are discussed by the previous study, which suggests that this situation may be solved either by redesigning the physical characteristics of the aircraft, or by using control systems. Redesigning the aircraft involves reducing wing span, velocity and mass of the aircraft [9]. While this solution will stabilize the aircraft, it would diminish the maneuverability of the aircraft, which may be unacceptable in many operations. Control systems, which consists of a sensor, actuator and a processing unit provides a robust and attractive solution to this problem, since it would make the aircraft more maneuverable and completely autonomous [9]. The study emphasizes on minimizing

the latency between sensing the gust and providing suitable countermeasures to the actuator, so that the control system can be effective at dissipating the effects of turbulence. With the availability of advanced processors, this latency can be reduced to a minimum. These solutions are summarized in Fig. 3.

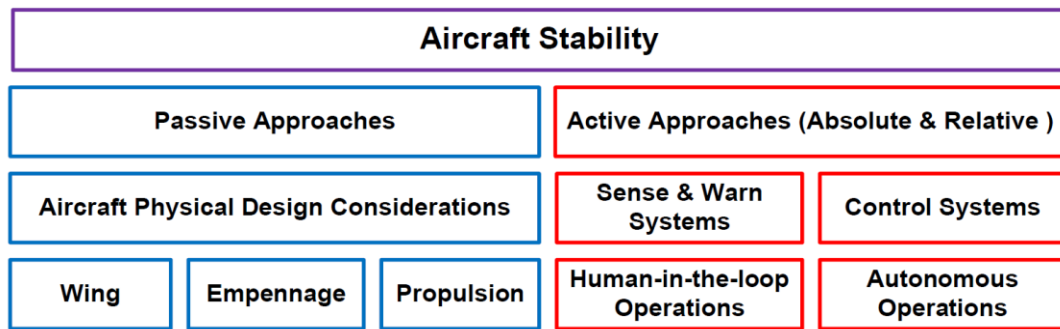


Figure 3. Approaches towards aircraft stability [9].

### Conventional turbulence sensors

A paper presented in 2014 by Mohamed, Clothier, Watkins, Sabatini and Abdulrahim explores the adequacy of conventional sensors in detecting turbulence. One of the most commonly used sensors are reactive sensors – these sensors estimate the inertial response of the unmanned vehicle due to a disturbance [12]. MEMS (Micro-ElectroMechanical Systems) are often used as accelerometers in unmanned vehicles. The downside to these accelerometers are that they are not only unable to differentiate between components of acceleration, but they are also susceptible to temperature changes and vibrations [12]. The technology to counter the effects of vibrations have still not been incorporated into the avionics of small unmanned vehicles owing to weight constraints [12]. MEMS gyroscopes, which are often used in larger commercial aircraft, have been miniaturized for use with UAVs. Miniaturization brings along with it a host of other problems, since MEMS devices are highly sensitive to manufacturing tolerances [12].

Other sensors used to aid navigate unmanned aerial vehicles are horizon sensors – these sensors may prove useful in certain situations, but in an urban scenario these sensors may not be effective at all due to presence of high rise buildings [12].

Studies show that conventional airplane sensors are not well suited for UAV applications. There is a need for a sensor that is accurate, reliable and robust since the effectiveness of the control system in dissipating the effects of gust are highly dependent on the accuracy of the sensors being employed.

### **Piezoelectric materials as sensors**

Piezoelectric materials have been widely studied for their properties as sensors as well as actuators [4]. Piezoelectric materials can used as lightweight, cost effective sensors which are able to monitor structural loadings in real time. Research has shown that by placing patches of piezoelectric materials along the length of a structure, each patch provides an output voltage based on the state of strain it experiences. The voltages from each of these patches are proportional to the slope of the lateral displacement curve of the patch [13]. The slope from each patch can effectively be used to determine the displacement curve of a beam [13].

This application of distributed piezoelectric patches as displacement or vibration sensors can be used in UAVs to measure the displacement curve of a wing. Deflection measurements can be made in real time, which when sent to the controller of an active/passive vibration control system, can provide suitable signals to dissipate the effects of gust load.

Observations from research conducted on UAVs indicate that instability while encountering turbulence is a problem that needs to be addressed with a solution that is

effective and robust. Human control in such situations is ineffective as well as strenuous on the controller. A more effective solution would be to use an active/passive vibration control system which can control the vibrations transferred to the avionics or payload by means of a controller, actuator and a sensor.

Hence, by predicting the rigid body motion of the fuselage, the vibrations can be reduced using two methods. One approach to this problem would be to mount the avionics or payload on an active mount, which would provide countermeasures to prevent the transmission of vibrations to the avionics or payload. Another approach to this problem would be to program the on board avionics to damp out the predicted fuselage vibrations.

## CHAPTER II

### DEVELOPMENT OF A LUMPED MASS MODEL

A simplified form of an aircraft is first analyzed in the form of a two dimensional lumped mass model. A lumped mass system assumes that the mass of a body is concentrated at its center of gravity, while maintaining links between bodies by means of massless springs or beams. This lumped mass system is easy to model and simulate, and the results are just as easy to calculate theoretically using natural frequency and modal superposition equations.

#### Modal Analysis of the Lumped Mass System

Fig. 4 shows a model of an aircraft, based on which a lumped mass system is modeled in ANSYS® as shown in Fig 5. This lumped mass system can then be represented as a series of spring mass systems for a mathematical analysis, as shown in Fig. 6.

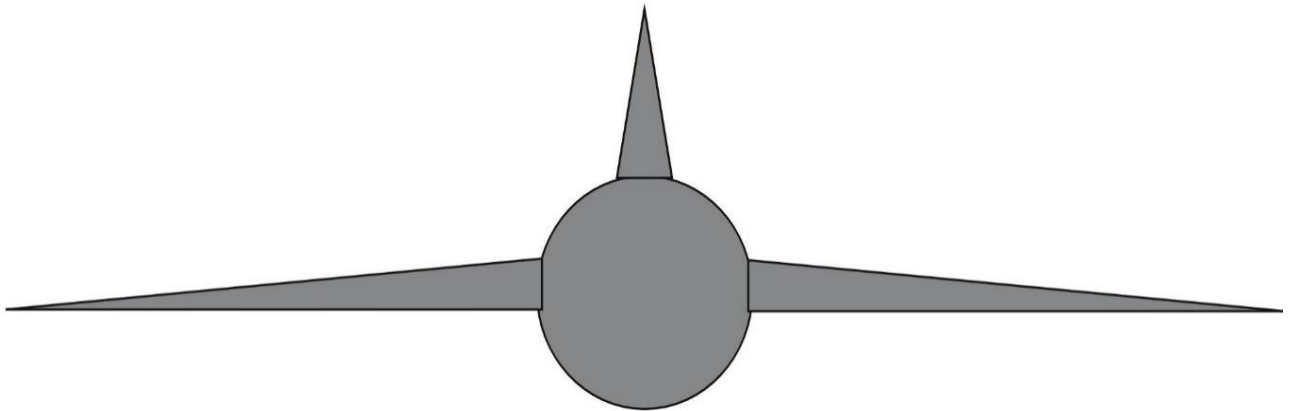


Figure 4. Aircraft model.



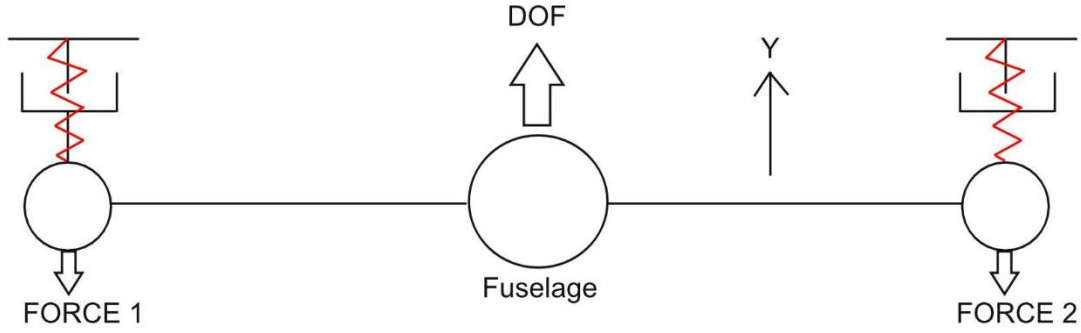


Figure 5. Lumped mass system.

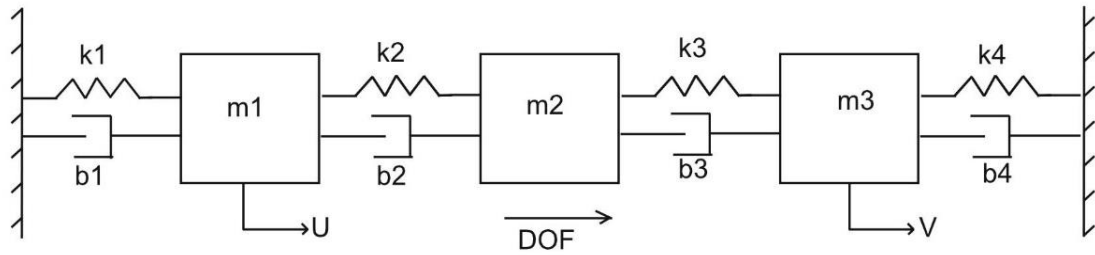


Figure 6. Representation of the lumped mass system as a spring mass system.

By determining the mass and stiffness matrices of the spring mass system, its natural frequencies can be calculated. This three degree of freedom system has springs  $k_2$  and  $k_3$  which represent the beams that connect the fuselage to the wings. Springs  $k_1$  and  $k_4$  represent the aerodynamic forces that hold the lumped mass model in the air. Dampers  $b_1, b_2, b_3, b_4$  represent the material damping exerted by the system. The equations of motion of the undamped spring mass system are:

$$\begin{cases} m_1 \ddot{x}_1 + (k_1 + k_2)x_1 - k_2 x_2 = 0 \\ m_2 \ddot{x}_2 + (k_2 + k_3)x_2 - k_2 x_1 - k_3 x_3 = 0 \\ m_3 \ddot{x}_3 + (k_3 + k_4)x_3 - k_3 x_2 = 0 \end{cases} \quad (2.1)$$

where

$m_1, m_3$  = masses of the wings (kg)

$m_2$  = mass of the fuselage (kg)

$x_1, x_3$  = displacements of the wings (m)

$x_2$  = displacement of the fuselage (m)

$k_1, k_4$  = spring stiffness (N/m)

$k_2, k_3$  = beam stiffness (N/m)

The parameter values assumed for the simulation procedure are shown in Table 1. It is arbitrarily assumed that the mass of the fuselage is five times the mass of the wings. The spring stiffness representing the aerodynamic forces is calculated such that the behavior of the lumped mass system is realistic.

Table 1. Parameter values used for simulation

Parameter	Stiffness (N/m)	Mass (Kg)
Wing ( $m_1, m_3$ )	Point Mass	2
Fuselage ( $m_2$ )	Point Mass	10
Beam ( $k_2, k_3$ )	10002	Massless
Spring ( $k_1, k_4$ )	17167.5	Massless

Equation 2.1 can also be represented in a matrix form as:

$$\begin{bmatrix} m_1 & 0 & 0 \\ 0 & m_2 & 0 \\ 0 & 0 & m_3 \end{bmatrix} \begin{pmatrix} \ddot{x}_1 \\ \ddot{x}_2 \\ \ddot{x}_3 \end{pmatrix} + \begin{bmatrix} k_1 + k_2 & -k_2 & 0 \\ -k_2 & k_2 + k_3 & -k_3 \\ 0 & -k_3 & k_3 + k_4 \end{bmatrix} \begin{pmatrix} x_1 \\ x_2 \\ x_3 \end{pmatrix} = \begin{pmatrix} 0 \\ 0 \\ 0 \end{pmatrix} \quad (2.2)$$

After substituting variables with values from Table 1, the mass matrix  $[m]$  and the stiffness matrix  $[k]$  are represented as:

$$[m] = \begin{bmatrix} 2 & 0 & 0 \\ 0 & 10 & 0 \\ 0 & 0 & 2 \end{bmatrix} \quad [k] = \begin{bmatrix} 27169.5 & -10002 & 0 \\ -10002 & 20004 & -10002 \\ 0 & -10002 & 27169.5 \end{bmatrix}$$

To solve for the natural frequency of the system, the characteristic Eigen value equation solved is [14]:

$$(-\omega^2[m]+[k])[x]=0 \quad (2.3)$$

where

$\omega$  = natural frequencies of the system (rad/s)

$[x]$  = displacements of the masses (m)

On solving Eq. 2.3, it becomes:

$$\begin{bmatrix} -2\omega^2 & 0 & 0 \\ 0 & -10\omega^2 & 0 \\ 0 & 0 & -2\omega^2 \end{bmatrix} + \begin{bmatrix} 27169.5 & -10002 & 0 \\ -10002 & 20004 & -10002 \\ 0 & -10002 & 27169.5 \end{bmatrix} = 0 \quad (2.4)$$

Equation 2.4 can be expressed as:

$$-40\omega^3 + 1166796\omega^2 - 9155651998.5\omega + 9330513554565 = 0 \quad (2.5)$$

On solving this polynomial equation, three natural frequencies are obtained. The calculated natural frequencies of the system are 5.49 Hz, 18.55 Hz and 19.09 Hz.

Since  $[x]$  is a non-zero matrix, it can be established that [14]:

$$\det |-\omega^2[m]+[k]| = 0 \quad (2.6)$$

The mode shapes  $[X]$  of the system can be found by replacing  $\omega$  with the calculated frequencies. The mode shapes of the system are:

$$[X]^{(1)} = \begin{bmatrix} 1 \\ 1 \\ 1 \end{bmatrix} \quad [X]^{(2)} = \begin{bmatrix} 1 \\ 0 \\ -1 \end{bmatrix} \quad [X]^{(3)} = \begin{bmatrix} 1 \\ -0.4 \\ 1 \end{bmatrix} \quad (2.7)$$

Mode shape  $[X]^{(1)}$  is the rigid body motion the aircraft. Mode shape  $[X]^{(2)}$  denotes the wings moving in opposite directions with no fuselage motion. Mode shape  $[X]^{(3)}$  shows the wings moving the same direction, while the fuselage moves in an opposite direction.

### **Finite Element Modeling and Simulation of the Lumped Mass System**

The lumped mass system is modeled and simulated using ANSYS®. Fig. 5 illustrates the two dimensional lumped mass system modeled in ANSYS®. In this simulation, damping is ignored and no external forces are considered to act on the system.

The model geometry and material properties were chosen such that this model remains identical to the theoretical lumped mass system. To ensure this, the masses of the three bodies, beam stiffness and spring constants are obtained from Table 1. Since the beams connecting the three bodies have negligible mass, they were assigned low density values, in the order of  $1 \times 10^{-8} \text{ kg/m}^3$ . The geometry and modulus of elasticity of these beams were assigned such that their stiffness remains identical to the theoretical lumped mass model. The constants of the springs which suspend the wings are obtained from Table 1 as well.

Spot welds are connections that allow structural loads to be transmitted between connected entities, and are ideal connections in the case of a two dimensional analysis. A modal analysis is conducted to determine the mode shapes and natural frequencies of the system.

Constraints are placed on the fuselage allowing it to move only along the Y-axis, while the wings are constrained using springs, thus allowing them to move only along the Y-axis as well. The ANSYS® simulation results are summarized in Table 2.

Table 2. Summary of ANSYS® modal analysis results

Natural Frequency (Hz)	Mode Shape
5.4841	Rigid body translation
18.704	Wings move in opposite directions; No fuselage motion
19.233	Wings move in same direction; Fuselage moves in opposite direction

The observed mode shapes of the lumped mass system are illustrated in Fig. 7, 8 and 9.

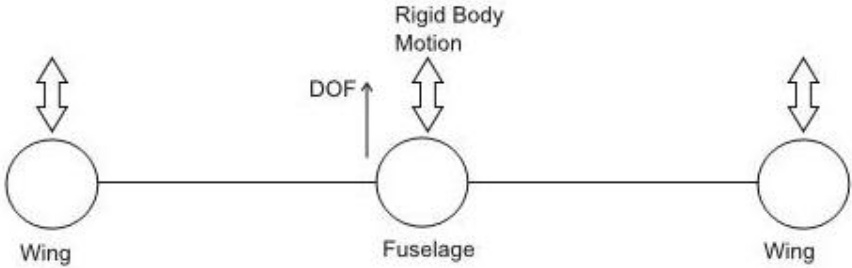


Figure 7. First mode shape of the lumped mass system, 5.48 Hz.

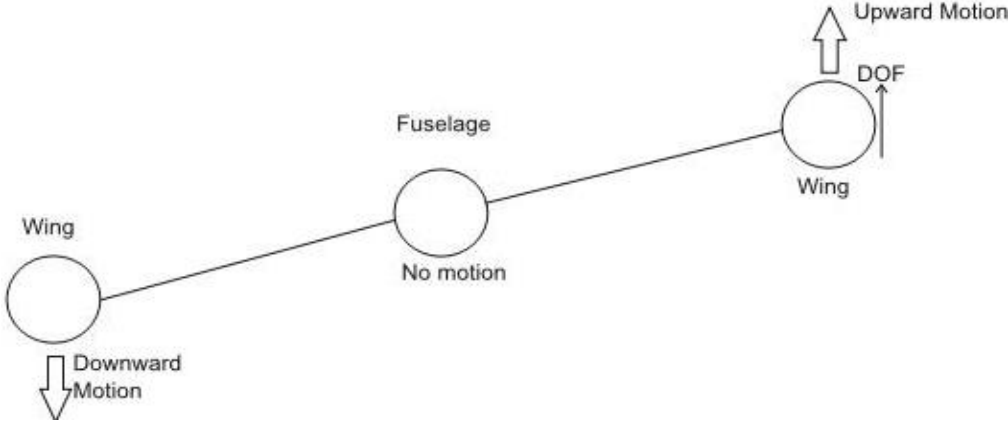


Figure 8. Second mode shape of the lumped mass system, 18.70 Hz.

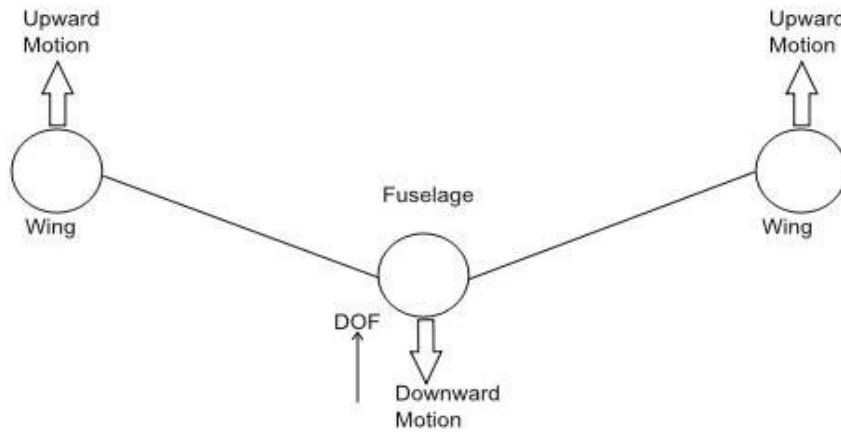


Figure 9. Third mode shape of the lumped mass system, 19.23 Hz.

Table 3 compares the calculated results with the simulation results. This comparison confirms the natural frequencies and mode shapes obtained using the two methods are in very good agreement with one another, thus validating the finite element modal analysis of the lumped mass system.

Table 3. Comparison between calculated results and simulation results

<b>Frequency</b> <b>Approach</b>	<b>1<sup>st</sup> Natural</b> <b>Frequency and</b> <b>Mode Shape</b>	<b>2<sup>nd</sup> Natural</b> <b>Frequency and</b> <b>Mode Shape</b>	<b>3<sup>rd</sup> Natural</b> <b>Frequency and</b> <b>Mode Shape</b>
Theoretical Modal Analysis	$\omega = 5.49 \text{ Hz}$ $X^{(1)} = \begin{bmatrix} 1 \\ 1 \\ 1 \end{bmatrix}$	$\omega = 18.55 \text{ Hz}$ $X^{(2)} = \begin{bmatrix} 1 \\ 0 \\ -1 \end{bmatrix}$	$\omega = 19.09 \text{ Hz}$ $X^{(3)} = \begin{bmatrix} 1 \\ -0.4 \\ 1 \end{bmatrix}$
ANSYS® Simulation Results	$\omega = 5.4841 \text{ Hz}$	$\omega = 18.704 \text{ Hz}$	$\omega = 19.233 \text{ Hz}$

## Forced Vibration Analysis using Modal Superposition Equations

The use of modal superposition equations determines the positions of all three masses with respect to time. This section reviews the modal superposition equations that are used to obtain the position of the masses with respect to time. This theoretical analysis is damped since it is assumed that the system has a 5% natural damping ratio ( $\zeta=0.05$ ). The analysis of the system is conducted for a step input and a sinusoidal input acting on the wings. As can be seen in Fig.6, a force  $u$  is applied to one wing and a force  $v$  is applied to the other wing. Applying these forces on the wings causes them to be displaced, which in turn causes the fuselage to vibrate.

Using Fig. 6, the equations of motion of a damped lumped mass system are:

$$\begin{cases} m_1\ddot{x}_1 + (b_1 + b_2)\dot{x}_1 + (k_1 + k_2)x_1 - b_2\dot{x}_2 - k_2x_2 = u \\ m_2\ddot{x}_2 + (b_2 + b_3)\dot{x}_2 + (k_2 + k_3)x_2 - b_2\dot{x}_1 - k_2x_1 - b_3\dot{x}_3 - k_3x_3 = 0 \\ m_3\ddot{x}_3 + (b_3 + b_4)\dot{x}_3 + (k_3 + k_4)x_3 - b_3\dot{x}_2 - k_3x_2 = v \end{cases} \quad (2.8)$$

where

$m_1, m_3$  = masses of the wings (kg)

$m_2$  = mass of the fuselage (kg)

$x_1, x_3$  = displacements of the wings (m)

$x_2$  = displacement of the fuselage (m)

$k_1, k_4$  = spring stiffness (N/m)

$k_2, k_3$  = beam stiffness (N/m)

$\ddot{x}_2$  = acceleration of the fuselage (m/s<sup>2</sup>)

$\ddot{x}_1, \ddot{x}_3$  = accelerations of the wings (m/s<sup>2</sup>)

$\dot{x}_2$  = velocity of the fuselage (m/s)

$\dot{x}_1, \dot{x}_3$  = velocity of the wings (m/s)

$b_1, b_2, b_3, b_4$  = damping constants (N.s/m)

$u$  = force applied on  $m_1$

$v$  = force applied on  $m_3$

For a step input analysis, it is assumed that a force of -5 N is applied on one wing, while a -10 N force is applied onto the other wing in order to simulate an unsymmetrical loading condition. Hence for a step input,  $u = 2 \times v$ . Considering the sine input simulation, a sinusoidal force of 5 N with an arbitrary frequency of 10 Hz applied to both wings. Hence for a sine input,  $u = v$ .

For a damped multi-degree-of-freedom system, the equation of motion of all its masses is represented as [14]:

$$[m]\ddot{x} + b\dot{x} + [k]x = [F] \quad (2.9)$$

where

$[x]$  = displacement vector of the system or solution vector

$[m]$  = mass matrix of the system

$[b]$  = damping matrix of the system

$[k]$  = stiffness matrix of the system

$[F]$  = external force(s) acting on the system

In accordance with Eq. 2.9, the equations of motion can be represented in matrix form as:

$$[m] = \begin{bmatrix} m_1 & 0 & 0 \\ 0 & m_2 & 0 \\ 0 & 0 & m_3 \end{bmatrix} \quad [k] = \begin{bmatrix} k_1 + k_2 & -k_2 & 0 \\ -k_2 & k_2 + k_3 & -k_3 \\ 0 & -k_3 & k_3 + k_4 \end{bmatrix}$$



$$[b] = \begin{bmatrix} b_1 + b_2 & -b_2 & 0 \\ -b_2 & b_2 + b_3 & -b_3 \\ 0 & -b_3 & b_3 + b_4 \end{bmatrix} \quad F_{step} = u \quad F_{sine} = v$$

The damping coefficient,  $\zeta = 0.05$ . From this value, the damper values can be calculated. Damper values are calculated for each mass using the equation [15]:

$$\zeta = \frac{c}{c_c} \quad (2.10)$$

where

$c$  = actual damping of the system

$c_c$  = critical damping,  $c_c = 2\sqrt{km}$ .

Table 4 summarizes the damping values used in Fig.6, using Eq. 2.10.

Table 4. Summary of calculated damping values

<b>Mass Number</b>	<b>Left Side Damper (N.s/m)</b>	<b>Right Side Damper (N.s/m)</b>
$m_1$	18.5296	14.1436
$m_2$	31.626	31.626
$m_3$	14.1436	18.5296

Plugging in values from Table 2, these matrices can now be expressed as:

$$[m] = \begin{bmatrix} 2 & 0 & 0 \\ 0 & 10 & 0 \\ 0 & 0 & 2 \end{bmatrix} \quad [k] = \begin{bmatrix} 27169.5 & -10002 & 0 \\ -10002 & 20004 & -10002 \\ 0 & -10002 & 27169.5 \end{bmatrix}$$

$$[b] = \begin{bmatrix} 32.6732 & -14.1436 & 0 \\ -31.626 & 63.252 & -31.626 \\ 0 & -14.1436 & 32.6732 \end{bmatrix} \quad F_{step} = -5N \quad F_{sine} = -5 \times (10t)N$$

The solution vector,  $[x]$  can be represented as a linear combination of the natural modes of the undamped system as [14]:

$$[x(t)] = [X][q(t)] \quad (2.11)$$

where

$[X]$  = corresponding normal modes

$[q]$  = generalized displacement of the masses.

$[X]$  is obtained by normalizing each mode shape with respect to  $[m]$ . This is done by solving the equation [14]:

$$[X]^T \cdot [m] \cdot [X] = [I] \quad (2.12)$$

Vector  $[q]$  is defined as [14]:

$$[q_i(t)] = e^{-\zeta_i \omega_i t} \left\{ \cos \omega_{di} t + \frac{\zeta_i}{\sqrt{1-\zeta_i^2}} \sin \omega_{di} t \right\} q_i(0) + \left\{ \frac{1}{\omega_{di}} e^{-\zeta_i \omega_i t} \sin \omega_{di} t \right\} \dot{q}_0(0) + \frac{1}{\omega_{di}} \int_0^t Q_i e^{-\zeta_i \omega_i t} \sin \omega_{di}(t-\tau) d\tau \quad (2.13)$$

where

$[q]$  = generalized displacement of the masses

$[q_i(0)]$  = initial generalized displacement of the masses

$[\dot{q}_i(0)]$  = initial generalized velocities of the masses

$\zeta$  = damping ratio of the system

$\omega$  = natural frequencies of the system

In Eq.2.13, the damped natural frequency,  $\omega_{di}$  is represented as [14]:

$$\omega_{di} = \omega_i \sqrt{1 - \zeta_i^2} \quad (2.14)$$

Also in Eq.2.13, the vector of generalized forces,  $[Q(t)]$  is represented as [14]:

$$[Q(t)] = [X]^T F(t) \quad (2.15)$$

For a step force excitation,  $[Q(t)] = \begin{bmatrix} -1.854 \\ 2.504 \\ -7.268 \end{bmatrix}$

For a sine force excitation,  $[Q(t)] = \begin{bmatrix} -1.236 \times \sin(10t) \\ 0.003 \times \sin(10t) \\ -4.845 \times \sin(10t) \end{bmatrix}$

Since the initial displacements and velocities of the lumped mass system is zero,

Eq.2.13 can now be expressed as [14]:

$$[q_i(t)] = \frac{1}{\omega_{di}} \int_0^t Q_i e^{-\zeta_i \omega_i \tau} \sin \omega_{di}(t - \tau) d\tau \quad (2.16)$$

Plugging in variable values in the above equation, the three generalized displacements of the masses become:

In the case of a step input:

$$[q_1(t)] = -0.0537 \int_0^t e^{-0.6909(t-\tau)} \sin 34.5362(t - \tau) d\tau$$
$$[q_2(t)] = 0.0215 \int_0^t e^{-2.3310(t-\tau)} \sin 16.5279(t - \tau) d\tau$$

$$[q_3(t)] = -0.0606 \int_0^t e^{-2.3994(t-\tau)} \sin 119.9440(t-\tau) d\tau \quad (2.17)$$

In the case of a sine input:

$$\begin{aligned} [q_1(t)] &= -0.0358 \int_0^t \sin(10t) e^{-0.6909(t-\tau)} \sin 34.5362(t-\tau) d\tau \\ [q_2(t)] &= 2.5745 \times 10^{-5} \int_0^t \sin(10t) e^{-2.3310(t-\tau)} \sin 116.5279(t-\tau) d\tau \\ [q_3(t)] &= -0.0404 \int_0^t \sin(10t) e^{-2.3994(t-\tau)} \sin 119.9440(t-\tau) d\tau \end{aligned} \quad (2.18)$$

$[X]$  is obtained from previously calculated mode shapes and normalizing them using Eq. 2.12. Combining all three vectors,  $[X]$  can be represented as:

$$[X] = \begin{bmatrix} 0.1237 & 0.3064 & 0.1236 \\ 0.4997 & 0 & -0.5003 \\ 0.4843 & -0.0782 & 0.4847 \end{bmatrix}$$

The closed form equation for the displacement of the masses can be obtained by using Eq. 2.11. The time period used in the closed form equation is five seconds. The focus is on determining the motion of the fuselage, which is represented by the variable  $x_2(t)$ .

Using the Eq. 2.11, a closed form equation for the motion of the fuselage with respect to time is derived, in the case of an applied step force as well as an applied sinusoidal force.

For the step input case, the closed form equations of the masses are defined as:

$$\begin{aligned} [x_1(t)] &= e^{-1.7271t} (1.9225 \times 10^{-4} \times \cos(34.499t) + 9.6247 \times 10^{-6} \\ &\times \sin(34.499t)) + e^{-5.9984t} (2.4458 \times 10^{-4} \times \cos(119.8178t) \\ &+ 1.2245 \times 10^{-5} \times \sin(119.8178t)) - e^{-5.8275t} (9.1899 \times 10^{-5} \\ &\times \cos(116.5511t) + 4.595 \times 10^{-6} \times \sin(116.5511t)) - 3.449 \times 10^{-4} \end{aligned} \quad (2.19)$$

$$\begin{aligned}
[x_2(t)] = & e^{-1.7271t} (4.762 \times 10^{-4} \times \cos(34.499t) + 2.384 \times 10^{-5} \\
& \times \sin(34.499t)) - e^{-5.9984t} (3.9493 \times 10^{-5} \times \cos(119.8178t) \\
& + 1.9771 \times 10^{-6} \times \sin(119.8178t)) - 4.3671 \times 10^{-4}
\end{aligned} \tag{2.20}$$

$$\begin{aligned}
[x_3(t)] = & e^{-1.7271t} (1.921 \times 10^{-4} \times \cos(34.499t) + 9.6169 \times 10^{-6} \\
& \times \sin(34.499t)) + e^{-5.9984t} (2.4479 \times 10^{-4} \times \cos(119.8178t) \\
& 1.2255 \times 10^{-5} \times \sin(119.8178t)) - e^{-5.8275t} (9.2010 \times 10^{-5} \\
& \times \sin(119.8178t) - e^{-5.8275t} (9.2010 \times 10^{-5} \times \cos(116.5511t) \\
& + 4.6005 \times 10^{-6} \times \sin(116.5511t)) - 5.2889 \times 10^{-4}
\end{aligned} \tag{2.21}$$

For the sine input case, the closed form equations of the masses are defined as:

$$\begin{aligned}
[x_1(t)] = [x_3(t)] = & (\sin(10t)) [e^{-1.7271t} (1.2819 \times 10^{-4} \times \cos(34.499t) + 6.4173 \times \\
& 10^{-6} \times \sin(34.399t)) - 1.2819 \times 10^{-4}] - (\sin(10t)) [e^{-5.827t} (1.1008 \times 10^{-7} \times \\
& \cos(116.5511t) + 5.5041 \times 10^{-9} \times \sin(116.5511t)) - 1.1008 \times 10^{-7}] + \\
& (\sin(10t)) [e^{-5.9984t} (1.6303 \times 10^{-4} \times \cos(119.8178t) + 8.1619 \times 10^{-6} \times \\
& \sin(119.8178t)) - 1.6303 \times 10^{-4}]
\end{aligned} \tag{2.22}$$

$$\begin{aligned}
[x_2(t)] = & (\sin(10t)) [e^{-1.7271t} (3.1751 \times 10^{-4} \times \cos(34.499t) + 1.5895 \\
& \times 10^{-5} \times \sin(34.399t)) - 3.1751 \times 10^{-4}] - (\sin(10t)) [e^{-5.9984t} (2.6325 \\
& \times 10^{-5} \times \cos(119.8178t) + 1.3719 \times 10^{-6} \times \sin(119.8178t)) - 2.6325 \times 10^{-7}]
\end{aligned} \tag{2.23}$$

Since the same sinusoidal forces are applied on both wings, their displacements are the same. It can therefore be said that the displacement of the aircraft is symmetrical. Hence, the displacements both wings can be determined using the same function, as shown in Eq. 2.22.

### **Finite Element Forced Vibration Simulation of the Lumped Mass System**

The model in Fig. 5 will now undergo a transient response analysis to step and sinusoidal forces respectively, using ANSYS®. The resultant fuselage motion observed in this analysis will be compared with mathematical results for comparison.

Similar to the theoretical analysis, while applying a step load to the system, a force of -5 N is applied to one wing while a -10 N force is applied to another wing, to simulate unsymmetrical loading. An application of this load will cause the wings to displace, which in turn causes a vibration in the fuselage. The simulation is run for a period of 5 seconds. While applying a sinusoidal load to the system, the lumped mass model is subjected to a sinusoidal force of 5 N with an arbitrary frequency of 10 Hz applied to both wings. The results of both simulations are compared with the theoretical results for validation. It should be noted that a damped simulation was conducted in both cases, since all materials have an inherent damping property. Hence, a 5% damping ratio ( $\zeta = 0.05$ ) was used.

Fig. 10 compares the calculated response of the fuselage with the simulation results for a step force input. Fig. 11 compares the same results for a sinusoidal force input.

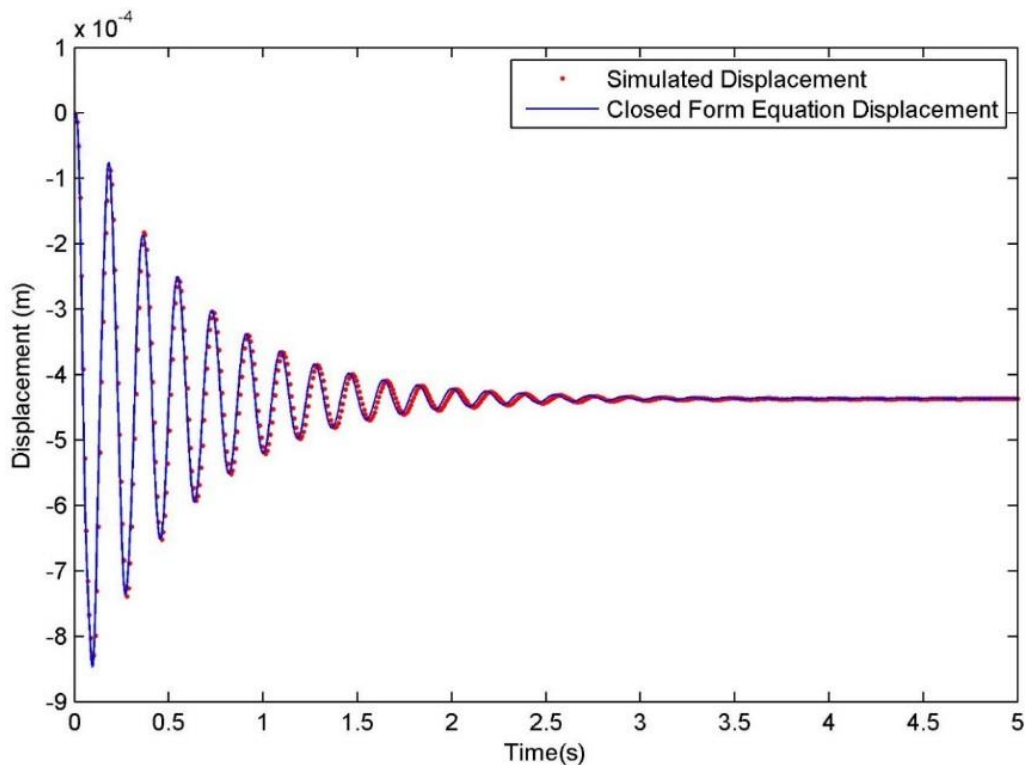


Figure 10. Comparison between calculated and simulation results for a step force input.

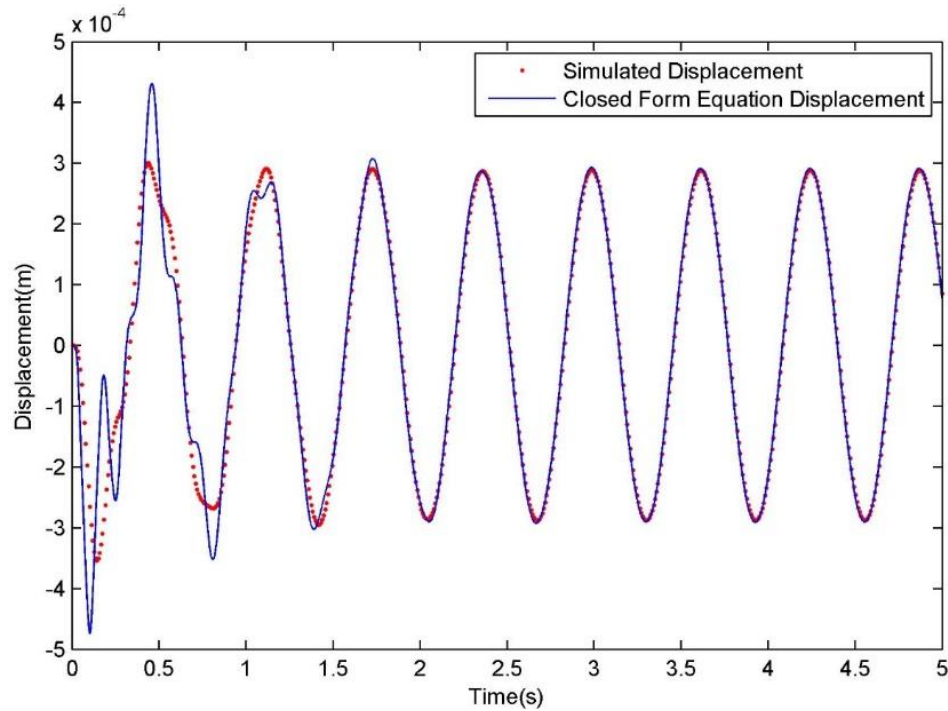


Figure 11. Comparison between calculated and simulation results for a sine force input.

The above graphs indicate that the results are in good agreement with each other. During the sine force excitation analysis, the two results show a slight disagreement in displacement within the first two seconds of the analysis. This is because the closed form equation does not reflect the transient period which is calculated by the ANSYS® simulation. From the results, it can be said that the graphs validate the forced vibration response simulation of the lumped mass model.

### Theoretical State Space Model

The next step in validating the lumped mass model analysis will be to compare the output of the state space representation derived through system identification with the output of the state space model derived through equations of motion. The results obtained using this step are used to validate the state space model obtained using the system identification tool.

To derive a state space model, Fig.6 is used to obtain the equations of motion, which are given by Eq. 2.8. The state space model is derived using the following state space variables:

$$\begin{aligned}
 z_1 &= x_1 \\
 z_2 &= x_2 \\
 z_3 &= x_3 \\
 z_4 &= \dot{z}_1 = \dot{x}_1 \\
 z_5 &= \dot{z}_2 = \dot{x}_2 \\
 z_6 &= \dot{z}_3 = \dot{x}_3
 \end{aligned}$$

Along with the equations of motion in Eq. 2.8, the state space model can be written as:

$$\begin{aligned}
 \dot{z}_1 &= \dot{x}_1 \\
 \dot{z}_2 &= \dot{x}_2 \\
 \dot{z}_3 &= \dot{x}_3 \\
 \dot{z}_4 &= \frac{u}{m_1} + \frac{b_2 z_5}{m_1} + \frac{k_2 z_2}{m_2} - \frac{(k_1 + k_2) z_1}{m_1} - \frac{(b_1 + b_2) z_4}{m_1} \\
 \dot{z}_5 &= \frac{b_2 z_4}{m_2} + \frac{k_2 z_1}{m_2} + \frac{b_3 z_6}{m_2} + \frac{k_3 z_3}{m_2} - \frac{(k_2 + k_3) z_2}{m_2} - \frac{(b_2 + b_3) z_5}{m_2} \\
 \dot{z}_6 &= \frac{v}{m_3} + \frac{b_3 z_5}{m_3} + \frac{k_3 z_2}{m_3} - \frac{(k_3 + k_4) z_3}{m_3} - \frac{(b_3 + b_4) z_6}{m_3}
 \end{aligned} \tag{2.24}$$

The state space representation of a system is written in its matrix form as [15]:

$$\begin{aligned}
 \dot{x} &= Ax + Bu \\
 y &= Cx + Du
 \end{aligned} \tag{2.25}$$

where

$[x]$  = state vector

$[y]$  = output vector

$[u]$  = input vector



$[A]$  = state matrix

$[B]$  = input matrix

$[C]$  = output matrix

$[D]$  = feedthrough matrix

Similar to the forced vibration response calculations, for a step input analysis, it is assumed that a force of -5 N is applied on one wing, while a -10 N force is applied onto the other wing in order to simulate an unsymmetrical loading condition. Hence for a step input,  $u = 2 \times v$ . In this case, the input vector  $u(t)$  is defined as:  $u(t) = -5N$ .

Considering the sine input simulation, equal sinusoidal forces of  $-5 \times \sin(10t)$  N are applied to both wings. Hence for a sine input,  $u = v$ . In this case,  $u(t) = -5 \times \sin(10 \times t) N$ .

The C matrix specifies the output of the state space model. Since the focus of this state space model is the rigid body motion of the fuselage, the C matrix, which is multiplied by the  $x(t)$  matrix, will therefore be defined as:  $C = [0 \ 1 \ 0 \ 0 \ 0 \ 0]$ .

Using Eq. 2.25 and Eq. 2.8, the constituent matrices of the theoretical state space model  $[A]$ ,  $[B]$ ,  $[C]$  and  $[D]$  can be represented in a general form as:

$$A = \begin{bmatrix} 0 & 0 & 0 & 1 & 0 & 0 \\ 0 & 0 & 0 & 0 & 1 & 0 \\ 0 & 0 & 0 & 0 & 0 & 1 \\ -\left(\frac{k_1 + k_2}{m_1}\right) & \frac{k_2}{m_1} & 0 & -\left(\frac{b_1 + b_2}{m_1}\right) & \frac{b_2}{m_1} & 0 \\ \frac{k_2}{m_2} & -\left(\frac{k_2 + k_3}{m_2}\right) & \frac{k_3}{m_2} & \frac{b_2}{m_2} & -\left(\frac{b_2 + b_3}{m_2}\right) & \frac{b_3}{m_2} \\ 0 & \frac{k_3}{m_3} & -\left(\frac{k_3 + k_4}{m_3}\right) & 0 & \frac{b_3}{m_3} & -\left(\frac{b_3 + b_4}{m_3}\right) \end{bmatrix}$$

$$B = \begin{bmatrix} 0 \\ 0 \\ 0 \\ \frac{1}{m_1} \\ 0 \\ \frac{2}{m_3} \end{bmatrix} \quad C = [0 \ 1 \ 0 \ 0 \ 0 \ 0] \quad D = 0 \quad x(t) = \begin{bmatrix} z_1 \\ z_2 \\ z_3 \\ z_4 \\ z_5 \\ z_6 \end{bmatrix}$$

Plugging in values from Table 1 and Table 4, the matrices of the state space model can be rewritten as:

$$A = \begin{bmatrix} 0 & 0 & 0 & 1 & 0 & 0 \\ 0 & 0 & 0 & 0 & 1 & 0 \\ 0 & 0 & 0 & 0 & 0 & 1 \\ -13584.7 & 5001 & 0 & -16.3366 & 7.0718 & 0 \\ 1000.2 & -2000.4 & 1000.2 & 3.1626 & -6.3258 & 3.1626 \\ 0 & 5001 & -13584.7 & 0 & 7.0718 & -16.3366 \end{bmatrix}$$

$$B_{step} = \begin{bmatrix} 0 \\ 0 \\ 0 \\ 0.5 \\ 0 \\ 1 \end{bmatrix} \quad B_{sine} = \begin{bmatrix} 0 \\ 0 \\ 0 \\ 0.5 \\ 0 \\ 0.5 \end{bmatrix} \quad C = [0 \ 1 \ 0 \ 0 \ 0 \ 0]$$

$$D = 0 \quad x(t) = \begin{bmatrix} z_1 \\ z_2 \\ z_3 \\ z_4 \\ z_5 \\ z_6 \end{bmatrix} = \begin{bmatrix} x_1 \\ x_2 \\ x_3 \\ \dot{x}_1 \\ \dot{x}_2 \\ \dot{x}_3 \end{bmatrix} \quad (2.26)$$

It should be noted that the entire state space model does not change as a function of the input. Only the [B] matrix changes as a function of the input.

## System Identification State Space Model

Using the system identification toolbox in MATLAB®, a fitting state space model can be found using the displacements of the wings as inputs, and the position of the fuselage as the output. System identification is to find the dynamic model of a physical object or process by defining a mathematical relation between the inputs and outputs. The resulting dynamic mathematical model can be further used to perform simulation and prediction of systems or processes.

In order to identify the state space model of the system using ANSYS® simulation results, the displacements of both wings are specified as inputs while the displacement of the fuselage along the Y axis is specified as the output. Since this system has multiple inputs (displacements of both wings) and a single output (displacement of the fuselage), it is a MISO (Multiple Input Single Output) system. Once the inputs and outputs have been specified in the data import toolbox, the state space model estimator is chosen in the system identification toolbox, and models between orders 4 and 10 are compared for the best fit with the given data. The toolbox estimated state space models with fits of 99.5% in both cases.

In the case of a step input, the system identification toolbox derived the state space model as:

$$A = \begin{bmatrix} -34.91 & -134.1 & 6.721 & 82.42 \\ 21.82 & 30.33 & 7.237 & 41.23 \\ 202.5 & -38.84 & -1351 & -2.524 \times 10^4 \\ 2.411 & 1.877 & 1410 & -710.3 \end{bmatrix}$$
$$B = \begin{bmatrix} 9.823 \times 10^4 & -4.53 \times 10^4 \\ 4.163 \times 10^4 & -3.103 \times 10^4 \\ -3.012 \times 10^7 & 1.465 \times 10^7 \\ -1.387 \times 10^6 & 7.132 \times 10^5 \end{bmatrix}$$

$$\begin{aligned}
C &= \begin{bmatrix} 0.001084 & 0.000111 & -7.805 \times 10^{-6} & 2.34 \times 10^{-6} \end{bmatrix} \\
D &= 0 \\
K &= \begin{bmatrix} 5.823 \times 10^5 \\ -2.763 \times 10^5 \\ 1.874 \times 10^7 \\ 2.655 \times 10^6 \end{bmatrix}
\end{aligned} \tag{2.27}$$

In the case of a sine input, the system identification toolbox derived the state space model as:

$$\begin{aligned}
A &= \begin{bmatrix} -28.57 & -56.88 \\ 47.23 & 24.63 \end{bmatrix} \\
B &= \begin{bmatrix} 9233 & -7012 \\ -7.686 \times 10^4 & -2.569 \times 10^4 \end{bmatrix} \\
C &= \begin{bmatrix} 0.0003362 & -1.496 \times 10^{-5} \end{bmatrix} \\
D &= 0 \\
K &= \begin{bmatrix} 5.535 \times 10^5 \\ -3.293 \times 10^6 \end{bmatrix}
\end{aligned} \tag{2.28}$$

It should be noted that the equations of the state space model derived with MATLAB® are expressed as [16]:

$$\begin{aligned}
\dot{x} &= Ax + Bu + Ke \\
y &= Cx + Du + e
\end{aligned} \tag{2.29}$$

where

$[x]$  = state vector

$[y]$  = output vector

$[u]$  = input vector

$[A]$  = state matrix

$[B]$  = input matrix

$[C]$  = output matrix

$[D]$  = feedthrough matrix

$[K] = 0$  gives the state space representation of the output – error model

Fig. 12 compares the results between the derived state space model and the MATLAB® model for a step force input. Fig. 13 compares the same results for a sinusoidal force input.

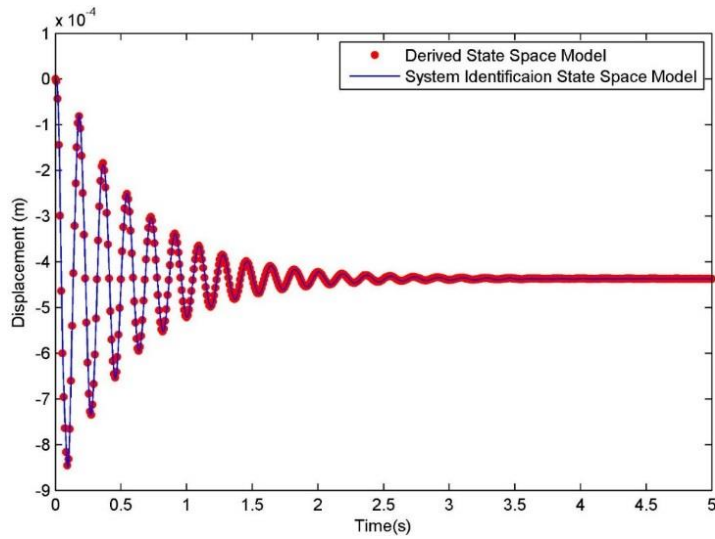


Figure 12. Comparison between derived state space model and MATLAB® model for a step input.

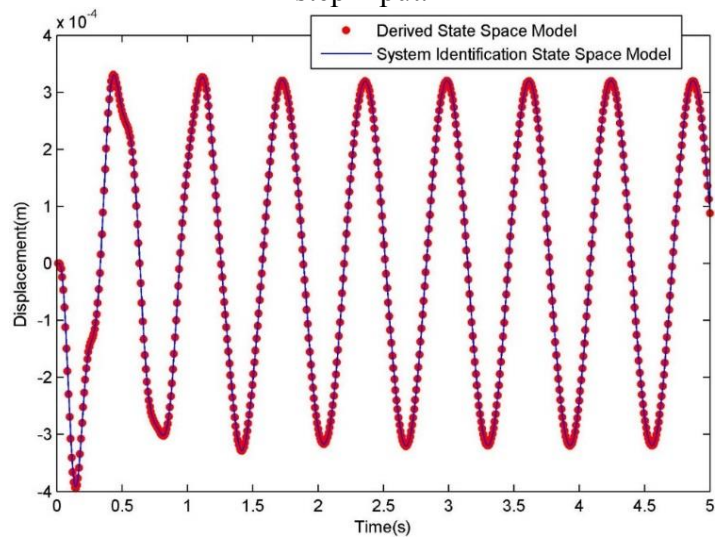


Figure 13. Comparison between derived state space model and MATLAB® model for a sine input.

The comparisons show that the two results given by the two state space models superimpose, indicating a very good agreement between them. This verification also signifies that the MATLAB® system identification toolbox is a valuable tool in modeling suitable state space models to determine the dynamic behavior of the given lumped mass system.

Although two different state space models are used to predict the motion of the fuselage for step and sine inputs acting on the system, the step input state space model is just as capable of predicting the motion of the system when subjected to a sine input. This can be proved by using a sine force as input to this state space model, and comparing its output with the sine input state space model. Fig. 14 compares the two outputs.

This comparison reveals that the step input state space model, which is derived using MATLAB® is indeed capable of predicting the fuselage rigid body motion of the lumped mass system, when it is subjected to both sinusoidal forces and step forces as inputs.

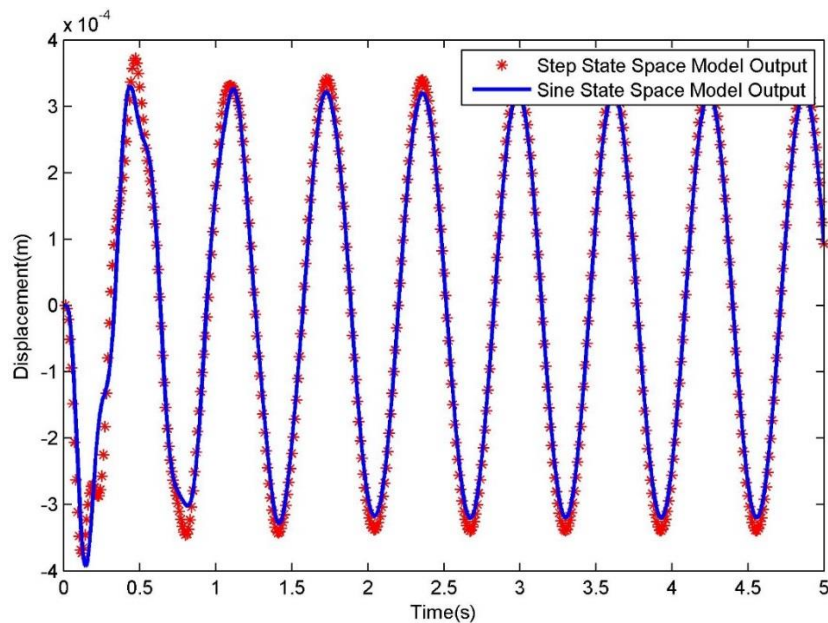


Figure 14. Comparison between the two state space models.

## Frequency Response Function

A Frequency Response Function (FRF) can be defined as the characteristic of a system that describes its response to excitation as the function of frequency [17]. The FRF of a system is expressed by the equation [18]:

$$H(\omega) = \frac{X_j}{F_k} \quad (2.30)$$

where

$H(\omega)$  = Frequency Response Function

$X_j$  = Harmonic response of the system

$F_k$  = Harmonic force applied to the system

Research shows that turbulent loads can impact UAVs with frequencies as high as 25 Hz [11]. In order to ascertain the dynamic characteristics of the lumped mass system, a frequency response function is simulated using ANSYS® between frequencies of 0 Hz and 40 Hz. Although the maximum observed turbulence frequency is 25 Hz, the simulation is conducted up to 40 Hz to ascertain its response characteristics well and over the established limit.

A harmonic response simulation is conducted on the model, with a force of amplitude 1 N applied to the wings, whose frequencies range from 0 to 40 Hz. The displacement of the wings causes a disturbance in the fuselage of the model, which is the focus of this simulation. The amplitude and phase of the fuselage displacement across all frequencies is measured and compared with the frequency response of the theoretical state space model as well as the state space model derived using system identification.

In order to compare the state space model response with the results of the ANSYS®

simulation, a complete state space model of the lumped mass system first needs to be developed – a model which can correctly predict the dynamic characteristics of the entire system. In the previously derived model, the position of the fuselage was determined using the displacement of the wings as input. This state space model may not represent the dynamics of the lumped mass model over a broad band of frequencies. To capture the dynamic characteristics of the entire system, the forces acting on the wings will be used as input, and the displacement of the wings and the fuselage will be used as the output.

The frequency domain model is developed using the system identification toolbox in MATLAB® and is represented as:

$$A = \begin{bmatrix} -3.185 & -35.05 & 0.4014 & 0.3619 & 0.01251 & 0.03344 \\ 33.39 & -0.2711 & -0.1433 & -0.1273 & -0.007432 & -0.01493 \\ 2.468 & -7.582 & -10.3 & 101.6 & -0.9093 & 0.9107 \\ 12.95 & -14.22 & -124.1 & 0.2526 & -1.205 & -0.7821 \\ 1.396 & 7.185 & 20.59 & 22.06 & -10.22 & -94.12 \\ 14.97 & -22.26 & -35.05 & 2.095 & 128.2 & -0.02665 \end{bmatrix}$$

$$B = \begin{bmatrix} -0.2243 & -0.4487 \\ -0.7354 & -1.471 \\ -13.78 & -27.55 \\ -32.78 & -65.57 \\ 114.1 & 228.2 \\ -119.6 & -239.2 \end{bmatrix}$$

$$C = \begin{bmatrix} C_{11} & C_{12} & C_{13} \\ C_{21} & C_{22} & C_{23} \\ C_{31} & C_{32} & C_{33} \end{bmatrix}$$

where



$$\begin{aligned}
C_{11} &= \begin{bmatrix} 0.0003135 & -2.808 \times 10^{-5} \end{bmatrix} & C_{12} &= \begin{bmatrix} -3.525 \times 10^{-5} & -1.597 \times 10^{-5} \end{bmatrix} \\
C_{13} &= \begin{bmatrix} -2.974 \times 10^{-6} & 1.06 \times 10^{-6} \end{bmatrix} & C_{21} &= \begin{bmatrix} 0.0007829 & -6.08 \times 10^{-5} \end{bmatrix} \\
C_{22} &= \begin{bmatrix} 2.461 \times 10^{-6} & 4.097 \times 10^{-6} \end{bmatrix} & C_{23} &= \begin{bmatrix} 2.294 \times 10^{-7} & -8.781 \times 10^{-8} \end{bmatrix} \\
C_{31} &= \begin{bmatrix} 0.0003192 & -3.023 \times 10^{-5} \end{bmatrix} & C_{32} &= \begin{bmatrix} -3.674 \times 10^{-5} & 9.356 \times 10^{-6} \end{bmatrix} \\
C_{33} &= \begin{bmatrix} 3.751 \times 10^{-6} & -3.594 \times 10^{-7} \end{bmatrix} \\
D &= 0 \\
K &= \begin{bmatrix} -6361 & 2.223 \times 10^4 & -4811 \\ -1211 & -390.5 & -576 \\ 1.219 \times 10^5 & 1.576 \times 10^6 & 8.245 \times 10^4 \\ 1.953 \times 10^4 & 1.203 \times 10^6 & 5.228 \times 10^4 \\ -5.657 \times 10^5 & 4.212 \times 10^5 & 1.623 \times 10^6 \\ -5.208 \times 10^5 & -8.075 \times 10^6 & 2.317 \times 10^5 \end{bmatrix}
\end{aligned} \tag{2.31}$$

The frequency response of the derived state space model is obtained by generating its Bode plots in MATLAB®. Figs. 15 and 16 compare the magnitude and phase responses of the lumped mass model using: (1) theoretical approach (2) ANSYS® simulation (3) frequency domain system identification.

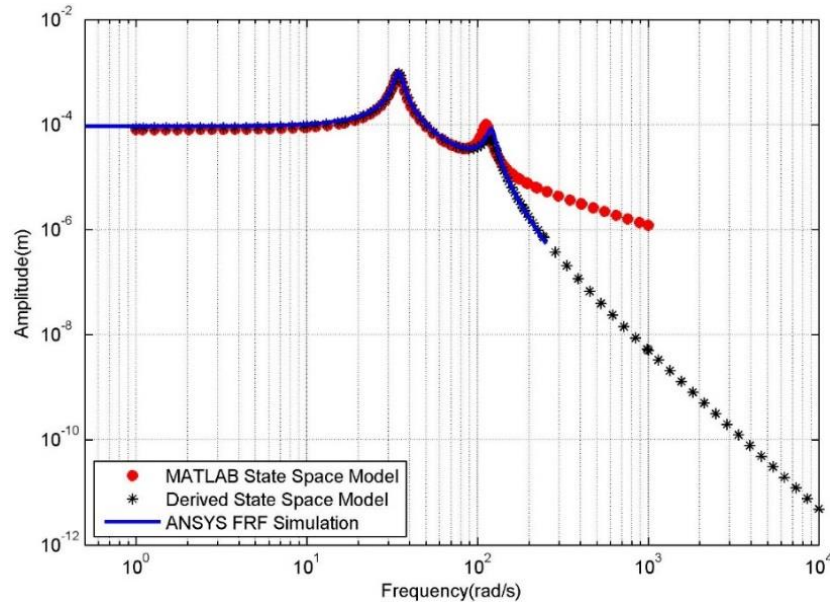


Figure 15. Amplitude comparison between simulation results and state space models.

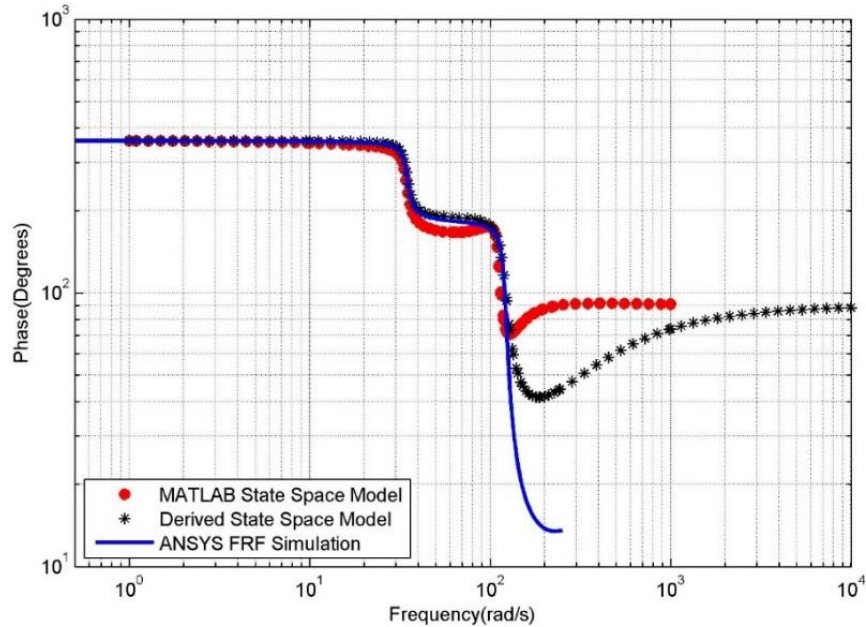


Figure 16. Phase comparison between simulation results and state space models.

The comparisons show the response of the model across different frequencies, which are a close match between the simulation results and the two models. The theoretical state space model, MATLAB® state space model and the ANSYS® frequency response simulation show a good agreement in response till about 40 Hz. Beyond this frequency, the MATLAB® state space model is seen to veer off from the path followed by the theoretical state space model. Since the highest frequency of concern in this part of the simulation is 40 Hz, this discrepancy does not matter as it occurs beyond this limit. This match implies that the state space models can accurately describe the dynamic behavior of the lumped mass system.

## CHAPTER III

### DEVELOPMENT OF A THREE DIMENSIONAL MODEL

Chapter 2 describes the steps used in simulating the lumped mass model using finite element analysis. Simulation results were later compared against mathematical results to validate the boundary conditions used to simulate this finite element model, which showed a good consistency between the two results. A similar three dimensional model of the aircraft is now modeled using SOLIDWORKS® and its response to excitation is simulated in ANSYS®. The results of this simulation are used to derive a state space model which relates the applied force to the fuselage motion.

#### Free Vibration Simulation of the Three Dimensional Aircraft

The three dimensional model of the aircraft was modeled, and is shown in Fig. 17. This model is loosely based on the BTE Super Hauler, designed by Bruce Tharpe Engineering, which is presented in Fig. 18.

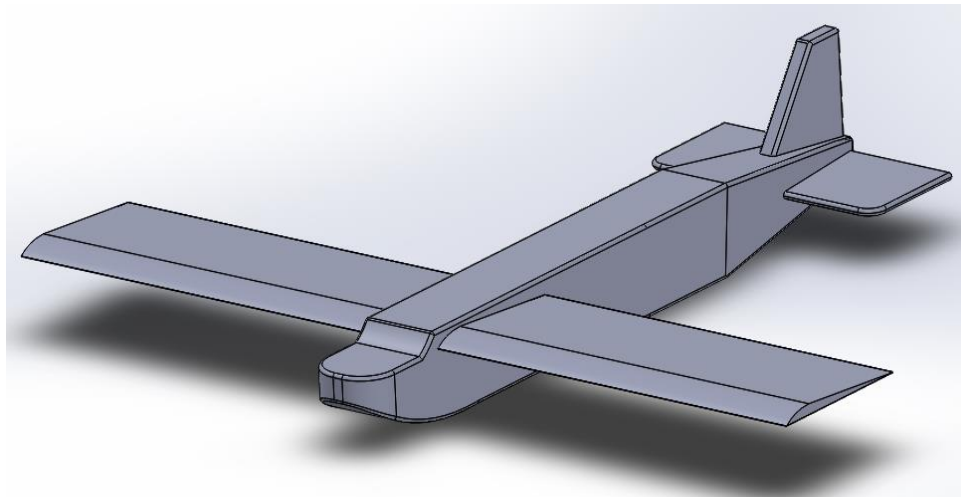


Figure 17. Three Dimensional model of the aircraft used for analysis.



Figure 18. BTE Super Hauler.

Table 5 summarizes the specifications of the BTE which were used to develop the 3D model.

Table 5. Specifications used to develop the 3D model.

<b>Parameter</b>	<b>Value</b>	<b>Unit</b>
Wingspan	3.65	m
Wing Width	0.65	m
Wing Area	2.374	m <sup>2</sup>
Fuselage Length	3.048	m
Maximum Fuselage Width	0.323	m
Standard Empty Weight	14	kg

A modal analysis is conducted on the three dimensional model, by constraining it in a manner similar to the lumped mass model – the fuselage is allowed to move only along the Y-axis while the wings are suspended using springs. These spring constants are obtained from Table 1. The fuselage is constrained by applying a displacement boundary condition on its bottom face. The boundary conditions are made to compare the mode

shapes of the three dimensional model to the mode shapes of the lumped mass model. Fig. 19 shows the constraints placed on the three dimensional plane.

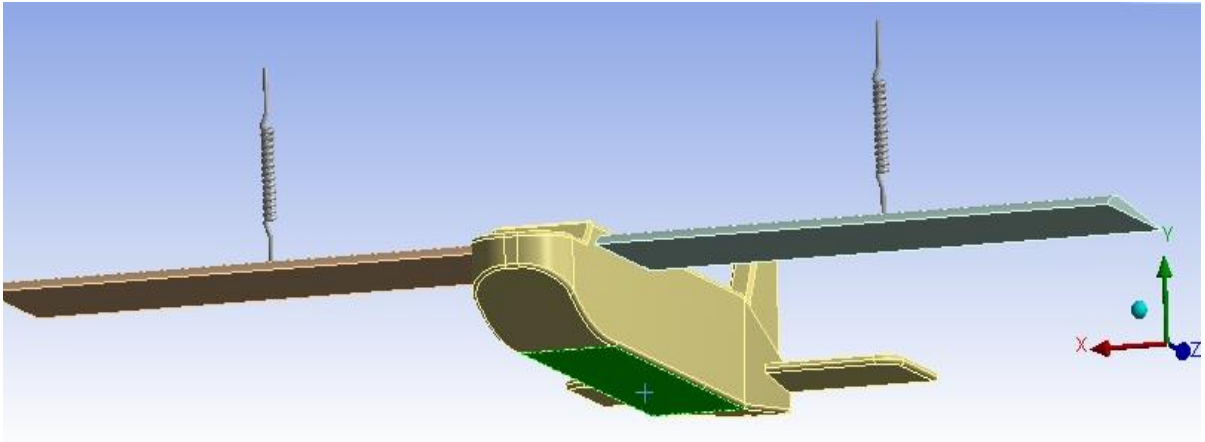


Figure 19. Constraints placed on the three dimensional plane. Area shaded in green shows the constrained face of the fuselage.

The materials used for the system were developed by using structural steel from the ANSYS® material library as the material to begin with, and then changing its densities and modulus of elasticity accordingly. The fuselage is chosen to be comparatively rigid, while the wings show more of an elastic behavior. The material properties are chosen such that the behavior of the aircraft as realistic as possible.

The material properties used while executing the simulation are shown in Table 6. The results of the modal analysis are shown in Table 7.

Table 6. Material specifications used for three dimensional simulation.

<b>Part Name</b>	<b>Density (kg/m<sup>3</sup>)</b>	<b>Modulus of Elasticity (MPa)</b>
Fuselage	36.527	$1 \times 10^{12}$
Wings	90.013	$1 \times 10^9$

Table 7. Summary of the 3D modal analysis results

Natural Frequency (Hz)	Mode Shape
5.6818	Rigid body motion
12.16	Wings move in opposite directions; No fuselage motion
16.804	Wings move in same direction; Fuselage moves in opposite direction

The densities of the materials are chosen such that the masses of the wings and the fuselage are the same as those used during the lumped mass analysis. The mode shapes of the three dimensional model are the same as that of the lumped mass model. The first natural frequency, which is the rigid body motion, is comparable to the lumped mass model result. The other two natural frequencies are different, owing to the differences in wing stiffness between the two models and the distributed weight in the wing.

In this modal analysis, the fuselage was allowed to translate along the Y-axis. In a real life environment, the fuselage can translate and rotate about all three axes. Hence, elastic supports are used to constrain the model. Elastic supports behave similar to springs, but are much better suited for voluminous objects that need to be constrained by more than a couple of springs. Since most of the lift generated by an aircraft is through its wings, it would be ideal to place elastic supports right underneath them.

However, placing constraints on the wings of the aircraft will not allow them to deflect freely and will result in an incorrect analysis. Therefore, elastic supports are placed at the top face of the fuselage and on one side of the fuselage. The analysis involves

studying the rigid body motion of the fuselage, hence placing the elastic supports on the fuselage will be appropriate. Elastic supports allow the movement or deformation of the bodies it is attached to according to a spring behavior [19]. Moreover, elastic supports also act in a direction normal to the selected face of the body [20]. Therefore, applying supports to the top face and on one side of the fuselage will suffice.

During this part of the simulation, the elastic supports on the top face have a stiffness of  $32506 \text{ N/m}^3$  and the supports on the side face have a stiffness of  $29818 \text{ N/m}^3$ . The elastic stiffness values are established by assigning a value for the required displacement for a predetermined force acting on the fuselage. Fig. 20 shows the aircraft with the locations of the elastic supports which are represented in blue.

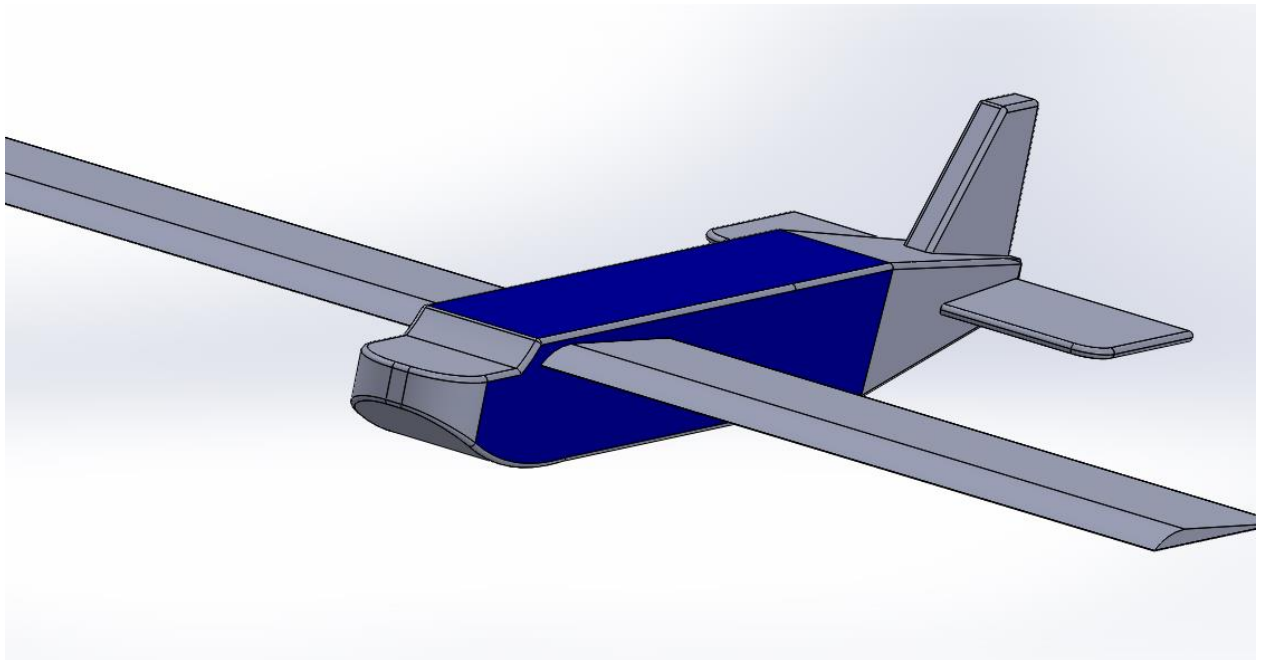


Figure 20. Locations of the elastic supports on the aircraft.

### **Forced Vibration Simulation**

The forced vibration analysis of the three dimensional is simulated using ANSYS®, and the model is subjected to both step and sinusoidal loads. The loads are applied on both

wings. When step loads are being applied, unequal loads are applied on the wings, to simulate an unsymmetrical loading condition. In the case of sinusoidal loads, equal loads are applied on the wings. Fig. 21 shows the faces of the wings where the loads are applied.

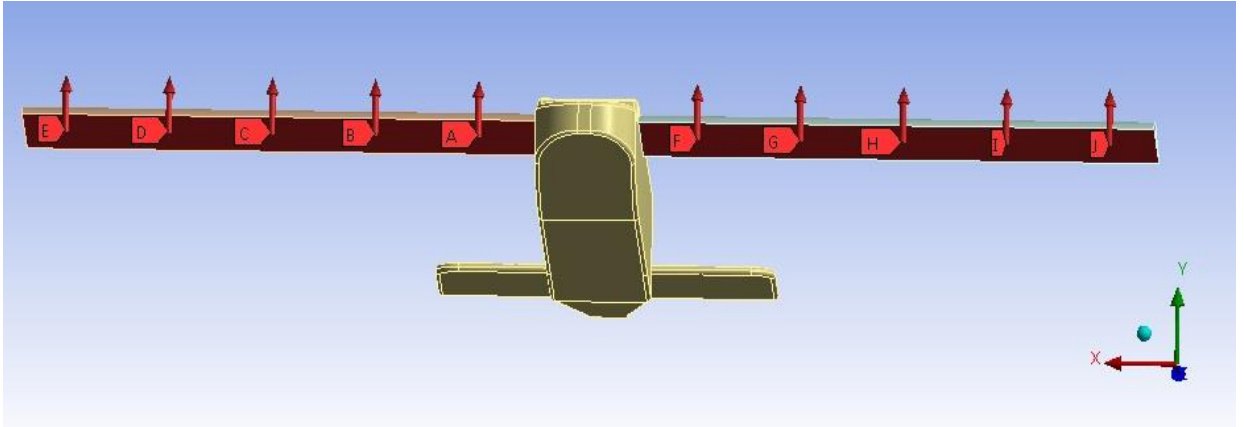


Figure 21. Loads applied on the faces of the wings.

A load of -10 N is applied at five points of one wing, and a load of -20 N is applied at five points of the other wing while simulating a step load. Ten point forces are applied to the wings of the aircraft since this would allow a total of ten inputs to be used to develop the state space model. If a distributed load were used to excite the model, a total of two inputs would be used to develop a state space model with six outputs – a model which would not be able to predict the motion of the fuselage accurately. A sinusoidal load of 10 N with an arbitrary frequency of 10 Hz is applied at five points of both wings while simulating a sinusoidal load. The simulation is run for a period of 5 seconds, and a 5% damping ratio ( $\zeta = 0.05$ ) is used. To record a change in position of the fuselage, a displacement probe can be placed on the fuselage. The position of this probe does not make a difference, since the relative rigid body displacement and rotation are the quantities being measured. Hence the probe was placed on the bottom face of the fuselage. A total of 6 probes are used, each probe to record translation or rotation of the fuselage about a given



axis. The observed data is then imported to MATLAB® for further processing, which is discussed below.

### **Deriving State Space Models using System Identification**

Once the simulation is completed, the data can now be analyzed using system identification to derive suitable state space models. Since the fuselage is free to translate and rotate about all axes, a single state space model, which uses the forces applied on the wings as input and gives the change in position or rotation about an axis as output can be used.

The system has ten inputs which yields six outputs. Systems with more than one input and more than one output can be classified as MIMO (Multiple Input, Multiple Output) systems. State space models are better suited for MIMO systems than transfer functions since it can calculate all the outputs using a single model unlike a transfer function, which needs a transfer function for each and every output of the system. The equations of the state space representation are expressed using Eq. 2.29.

For the step input simulation, the state space model is represented as:

$$A = \begin{bmatrix} A_{11} & A_{12} & A_{13} \\ A_{21} & A_{22} & A_{23} \\ A_{31} & A_{32} & A_{33} \end{bmatrix}$$

where

$$A_{11} = \begin{bmatrix} -0.7400 & -7.0527 & -1.1910 & 1.9905 \\ 6.4541 & 0.2714 & -0.4195 & -2.6524 \\ 2.7388 & -0.3284 & -0.6687 & 23.0023 \\ -2.2671 & 2.4572 & -20.2863 & -1.0330 \end{bmatrix}$$

$$A_{12} = \begin{bmatrix} -0.1892 & -0.2149 & -0.0181 & -0.0276 \\ 0.4934 & 0.2719 & 0.0040 & 0.0461 \\ -2.7542 & -1.2809 & 0.0514 & -0.2209 \\ -0.5941 & -2.4248 & -0.0172 & 0.1160 \end{bmatrix}$$

$$A_{13} = \begin{bmatrix} 0.0143 & -0.0056 & -0.0068 \\ 0.0088 & -0.0148 & -0.0469 \\ 0.1106 & 0.0369 & -0.0471 \\ 0.0299 & 0.1342 & -0.1672 \end{bmatrix}$$

$$A_{21} = \begin{bmatrix} -3.7835 & -2.5559 & 6.2890 & 1.8992 \\ 1.0923 & 2.0455 & -2.2686 & 0.8729 \\ 2.4412 & 0.0841 & -0.9750 & 0.6471 \\ 1.7016 & 0.7045 & -2.4127 & 0.6547 \end{bmatrix}$$

$$A_{22} = \begin{bmatrix} -5.3626 & -30.1040 & -4.8440 & -0.3097 \\ 30.9725 & 2.6644 & -1.5143 & 2.3568 \\ 11.9836 & -2.2879 & -1.4723 & -20.0622 \\ 3.8546 & -2.3308 & 17.1499 & -0.7090 \end{bmatrix}$$

$$A_{23} = \begin{bmatrix} -0.1635 & 0.9906 & -2.4197 \\ 1.6450 & 0.7892 & 0.0441 \\ 6.9916 & -3.9232 & 0.3915 \\ -6.2260 & 6.7063 & 7.6703 \end{bmatrix}$$

$$A_{31} = \begin{bmatrix} -5.1768 & -7.2760 & 11.2847 & 5.0169 \\ -2.0068 & -5.9499 & -0.8529 & 13.5094 \\ -7.8285 & -21.6670 & 9.8303 & 33.2607 \end{bmatrix}$$

$$A_{32} = \begin{bmatrix} -10.3020 & -14.0596 & 8.2898 & 9.3223 \\ -10.2996 & -9.2505 & 12.7804 & -10.9776 \\ -31.1451 & -29.9021 & 36.3790 & -9.6686 \end{bmatrix}$$

$$A_{33} = \begin{bmatrix} 10.5580 & -42.6772 & -9.4060 \\ 58.4963 & -18.9022 & 4.1627 \\ 26.8462 & -33.6095 & -176.0881 \end{bmatrix}$$

$$B = \begin{bmatrix} B_{11} & B_{12} \\ B_{21} & B_{22} \\ B_{31} & B_{32} \end{bmatrix}$$

where

$$B_{11} = \begin{bmatrix} -0.0062 & -0.0062 & -0.0062 & -0.0062 & -0.0062 \\ -0.0112 & 0.0112 & 0.0112 & 0.0112 & 0.0112 \\ -0.0588 & -0.0588 & -0.0588 & -0.0588 & -0.0588 \\ 0.0474 & 0.0474 & 0.0474 & 0.0474 & 0.0474 \end{bmatrix}$$

$$B_{12} = \begin{bmatrix} -0.0124 & -0.0124 & -0.0124 & -0.0124 & -0.0124 \\ 0.0224 & 0.0224 & 0.0224 & 0.0224 & 0.0224 \\ -0.1177 & -0.1177 & -0.1177 & -0.1177 & -0.1177 \\ 0.0948 & 0.0948 & 0.0948 & 0.0948 & 0.0948 \end{bmatrix}$$

$$B_{21} = \begin{bmatrix} 0.2309 & 0.2309 & 0.2309 & 0.2309 & 0.2309 \\ 0.2547 & 0.2547 & 0.2547 & 0.2547 & 0.2547 \\ 0.1122 & 0.1122 & 0.1122 & 0.1122 & 0.1122 \\ -0.0608 & -0.0608 & -0.0608 & -0.0608 & -0.0608 \end{bmatrix}$$

$$B_{22} = \begin{bmatrix} 0.4617 & 0.4617 & 0.4617 & 0.4617 & 0.4617 \\ 0.5094 & 0.5094 & 0.5094 & 0.5094 & 0.5094 \\ 0.2244 & 0.2244 & 0.2244 & 0.2244 & 0.2244 \\ -0.1215 & -0.1215 & -0.1215 & -0.1215 & -0.1215 \end{bmatrix}$$

$$B_{31} = \begin{bmatrix} -0.2458 & -0.2458 & -0.2458 & -0.2458 & -0.2458 \\ -1.0782 & -1.0782 & -1.0782 & -1.0782 & -1.0782 \\ -0.4877 & -0.4877 & -0.4877 & -0.4877 & -0.4877 \end{bmatrix}$$

$$B_{32} = \begin{bmatrix} -0.4917 & -0.4917 & -0.4917 & -0.4917 & -0.4917 \\ -2.1564 & -2.1564 & -2.1564 & -2.1564 & -2.1564 \\ -0.9755 & -0.9755 & -0.9755 & -0.9755 & -0.9755 \end{bmatrix}$$

$$C = [C_{11} \quad C_{12} \quad C_{13}]$$

where

$$C_{11} = \begin{bmatrix} 0.1564 & 0.0501 & -0.0083 & -0.0032 & -2.2577 \times 10^{-4} \\ -2.2584 \times 10^{-4} & 5.8532 \times 10^{-4} & -0.0022 & -0.0019 & 6.6358 \times 10^{-4} \\ -6.6364 \times 10^{-4} & 3.3618 \times 10^{-4} & -0.0014 & -0.0051 & 3.1789 \times 10^{-4} \\ 0.1880 & -0.1016 & 0.3962 & 1.4631 & -0.1052 \\ 0.2281 & 0.0749 & -0.0216 & -0.0118 & 0.0011 \\ 55.5341 & 17.7822 & -2.9398 & -1.1504 & -0.1069 \end{bmatrix}$$

$$C_{12} = \begin{bmatrix} -9.4259 \times 10^{-4} & -1.3364 \times 10^{-4} & 3.5540 \times 10^{-5} & -3.4450 \times 10^{-5} \\ 0.0042 & 7.9749 \times 10^{-4} & -2.9536 \times 10^{-4} & -4.5881 \times 10^{-5} \\ 2.7189 \times 10^{-6} & 1.2010 \times 10^{-6} & 1.0013 \times 10^{-5} & 9.1727 \times 10^{-6} \\ -0.0058 & -0.0063 & 1.0039 \times 10^{-4} & -0.0060 \\ -0.0067 & 0.0064 & 0.0127 & 0.0020 \\ -0.2984 & -0.0486 & -0.0025 & -0.0255 \end{bmatrix}$$

$$C_{13} = \begin{bmatrix} 2.5031 \times 10^{-5} & -7.4530 \times 10^{-5} \\ -17946 \times 10^{-4} & -4.3180 \times 10^{-5} \\ 1.0264 \times 10^{-5} & 7.9196 \times 10^{-5} \\ -3.3557 \times 10^{-4} & 7.1151 \times 10^{-5} \\ -1.8403 \times 10^{-4} & 5.8020 \times 10^{-4} \\ 0.0084 & -0.0031 \end{bmatrix}$$

$$D = 0$$

$$K = \begin{bmatrix} K_{11} & K_{12} \\ K_{21} & K_{22} \end{bmatrix}$$

where

$$K_{11} = \begin{bmatrix} 18.8035 & 68.9592 & -53.7682 \\ -51.5360 & 10.6660 & 675.6058 \\ 25.0669 & -219.5750 & 127.2889 \\ 178.4361 & 325.6582 & -144.8200 \\ 1.8133 \times 10^3 & 3.4500 \times 10^3 & 305.7829 \\ -944.0169 & 2.0634 \times 10^4 & 1.7046 \times 10^4 \end{bmatrix}$$

$$K_{12} = \begin{bmatrix} 19.3244 & 4.8265 & 8.0613 \\ 36.7362 & 21.6261 & 82.0345 \\ -48.7411 & 38.6632 & 64.0151 \\ 437.5257 & 44.4777 & 149.7448 \\ 4.0092 \times 10^3 & 754.3681 & 2.2555 \times 10^3 \\ 721.7027 & 412.6925 & 1.8616 \times 10^3 \end{bmatrix}$$

$$K_{21} = \begin{bmatrix} 2.0725 \times 10^3 & 2.6168 \times 10^4 & -1.4344 \times 10^4 \\ 622.0177 & 2.0950 \times 10^4 & -4.8959 \times 10^4 \\ 7.7210 \times 10^3 & -6.2229 \times 10^4 & -2.6470 \times 10^4 \\ 9.9776 \times 10^3 & 7.8967 \times 10^4 & -8.1637 \times 10^4 \\ -9.8256 \times 10^4 & -3.7888 \times 10^5 & 1.6349 \times 10^6 \end{bmatrix}$$

$$K_{22} = \begin{bmatrix} 1.7345 \times 10^3 & 242.8547 & -763.4168 \\ -7.5758 \times 10^3 & -1.525 \times 10^3 & -8.3769 \times 10^3 \\ 1.4824 \times 10^4 & 1.2564 \times 10^3 & 1.6956 \times 10^3 \\ 7.6461 \times 10^3 & -2.6416 \times 10^3 & -5.5092 \times 10^3 \\ 1.2148 \times 10^5 & 7.6629 \times 10^4 & 2.4382 \times 10^5 \end{bmatrix} \quad (3.1)$$

For the sine input simulation, the state space model the equations of the state space representation are expressed as:

$$A = \begin{bmatrix} A_{11} & A_{12} \\ A_{21} & A_{22} \end{bmatrix}$$

where

$$A_{11} = \begin{bmatrix} -0.7802 & 7.0256 & -0.9588 & -0.9604 \\ -7.2144 & -0.7579 & 1.4372 & -5.1690 \\ 1.1175 & -1.5639 & -0.8619 & -19.0777 \\ -2.8630 & 10.8787 & 24.0707 & -1.4621 \end{bmatrix}$$

$$A_{12} = \begin{bmatrix} -0.2714 & -0.4769 & -0.2698 & 0.0323 \\ -0.6179 & -3.2443 & -1.8580 & 0.8845 \\ -0.1346 & 0.7611 & 1.9826 & -0.8108 \\ -2.4338 & -1.6438 & 0.1816 & -1.6617 \end{bmatrix}$$

$$A_{21} = \begin{bmatrix} -7.2180 & 6.0040 & -1.9932 & 18.4320 \\ -3.6161 & 10.4249 & 3.8184 & 6.5007 \\ 16.8407 & -49.5775 & -27.3607 & 10.0827 \\ -50.9875 & 155.3144 & 205.2008 & -321.1068 \end{bmatrix}$$

$$A_{22} = \begin{bmatrix} -3.8576 & -34.9197 & -13.6565 & 20.0587 \\ 28.8693 & -6.6866 & 1.3046 & 5.6773 \\ 21.8791 & -56.3064 & -60.6198 & -6.2766 \\ -0.9569 & 298.2713 & 395.5523 & -422.9850 \end{bmatrix}$$

$$B = \begin{bmatrix} B_{11} & B_{12} \\ B_{21} & B_{22} \end{bmatrix}$$

where

$$\begin{aligned}
B_{11} &= \begin{bmatrix} 0.0122 & 0.0122 & 0.0122 & 0.0122 & 0.0122 \\ 0.1507 & 0.1507 & 0.1507 & 0.1507 & 0.1507 \\ -0.0882 & -0.0882 & -0.0882 & -0.0882 & -0.0882 \\ -0.1566 & -0.1566 & -0.1566 & -0.1566 & -0.1566 \end{bmatrix} \\
B_{12} &= \begin{bmatrix} 0.0122 & 0.0122 & 0.0122 & 0.0122 & 0.0122 \\ 0.1507 & 0.1507 & 0.1507 & 0.1507 & 0.1507 \\ -0.0882 & -0.0882 & -0.0882 & -0.0882 & -0.0882 \\ -0.1566 & -0.1566 & -0.1566 & -0.1566 & -0.1566 \end{bmatrix} \\
B_{21} &= \begin{bmatrix} 1.2431 & 1.2431 & 1.2431 & 1.2431 & 1.2431 \\ 0.1459 & 0.1459 & 0.1459 & 0.1459 & 0.1459 \\ 4.2234 & 4.2234 & 4.2234 & 4.2234 & 4.2234 \\ -24.9081 & -24.9081 & -24.9081 & -24.9081 & -24.9081 \end{bmatrix} \\
B_{22} &= \begin{bmatrix} 1.2431 & 1.2431 & 1.2431 & 1.2431 & 1.2431 \\ 0.1459 & 0.1459 & 0.1459 & 0.1459 & 0.1459 \\ 4.2234 & 4.2234 & 4.2234 & 4.2234 & 4.2234 \\ -24.9081 & -24.9081 & -24.9081 & -24.9081 & -24.9081 \end{bmatrix}
\end{aligned}$$

$$C = [C_{11} \quad C_{12}]$$

where

$$C_{11} = \begin{bmatrix} 0.0048 & -0.0017 & 5.2764 \times 10^{-4} & -7.8802 \times 10^{-5} \\ 5.3413 \times 10^{-4} & -0.0010 & -0.0015 & -2.7983 \times 10^{-4} \\ 3.0360 \times 10^{-4} & -0.0014 & -0.0028 & -2.9032 \times 10^{-4} \\ -0.880 & 0.3935 & 0.8065 & 0.0835 \\ 0.0071 & -0.0026 & 8.4158 \times 10^{-4} & -1.4826 \times 10^{-4} \\ 1.6920 & -0.6186 & 0.1862 & -0.0285 \end{bmatrix}$$

$$C_{12} = \begin{bmatrix} 3.2419 \times 10^{-5} & -7.8013 \times 10^{-5} & 2.4027 \times 10^{-5} & -6.9927 \times 10^{-6} \\ 4.0205 \times 10^{-4} & 0.0019 & 4.5503 \times 10^{-4} & 1.5491 \times 10^{-4} \\ 1.3336 \times 10^{-4} & -1.9056 \times 10^{-4} & -1.6124 \times 10^{-5} & 1.2165 \times 10^{-5} \\ -0.0380 & 0.0514 & 0.0040 & -0.0040 \\ 3.2143 \times 10^{-5} & 2.0498 \times 10^{-5} & -1.7117 \times 10^{-4} & -4.0147 \times 10^{-4} \\ 0.0114 & -0.0277 & 0.0091 & -0.0014 \end{bmatrix}$$

$$D = 0$$

$$K = \begin{bmatrix} K_{11} & K_{12} \\ K_{21} & K_{22} \end{bmatrix}$$

where

$$K_{11} = \begin{bmatrix} 3.6263 \times 10^3 & 150.9438 & -4.9480 \times 10^3 \\ 9.9590 \times 10^4 & -977.7570 & -6.5853 \times 10^3 \\ -9.4825 \times 10^4 & -107.9249 & 9.1892 \times 10^3 \\ -6.5536 \times 10^4 & 844.0414 & -1.3057 \times 10^4 \end{bmatrix}$$

$$K_{12} = \begin{bmatrix} -15.7773 & -88.8714 & 12.2753 \\ 18.2991 & -2.4248 \times 10^3 & -145.9323 \\ 66.7170 & 664.5984 & 77.8070 \\ -178.2089 & -1.0470 \times 10^3 & -179.0455 \end{bmatrix}$$

$$K_{21} = \begin{bmatrix} 6.7139 \times 10^5 & -6.0246 \times 10^3 & -1.4616 \times 10^5 \\ -1.8391 \times 10^5 & 1.5479 \times 10^4 & -2.5563 \times 10^5 \\ 3.1470 \times 10^6 & -2.5053 \times 10^3 & -2.6935 \times 10^5 \\ -2.5918 \times 10^7 & 2.1306 \times 10^5 & 8.9231 \times 10^5 \end{bmatrix}$$

$$K_{22} = \begin{bmatrix} 74.5036 & 539.7744 & 1.5859 \times 10^3 \\ -583.2421 & 2.0943 \times 10^4 & 1.8788 \times 10^3 \\ -792.7002 & -8.5663 \times 10^4 & -1.0412 \times 10^3 \\ -6.7627 \times 10^3 & 1.4413 \times 10^5 & -6.9938 \times 10^3 \end{bmatrix} \quad (3.2)$$

### Validation of Derived State Space Models

In order to validate the derived state space model, the output of the state space model is compared against simulation results. This is done by exciting the model with a different set of step and sinusoidal forces, and comparing the fuselage motion obtained with the state space model output.

For this comparison, a force of -6 N was applied at five points on one wings, and a force of -12 N was applied at five points on the other wing. For the sinusoidal comparison, a force of -6 N with a frequency of 10 Hz was applied at five points on each wing. Fig. 22-33 compare these two results.

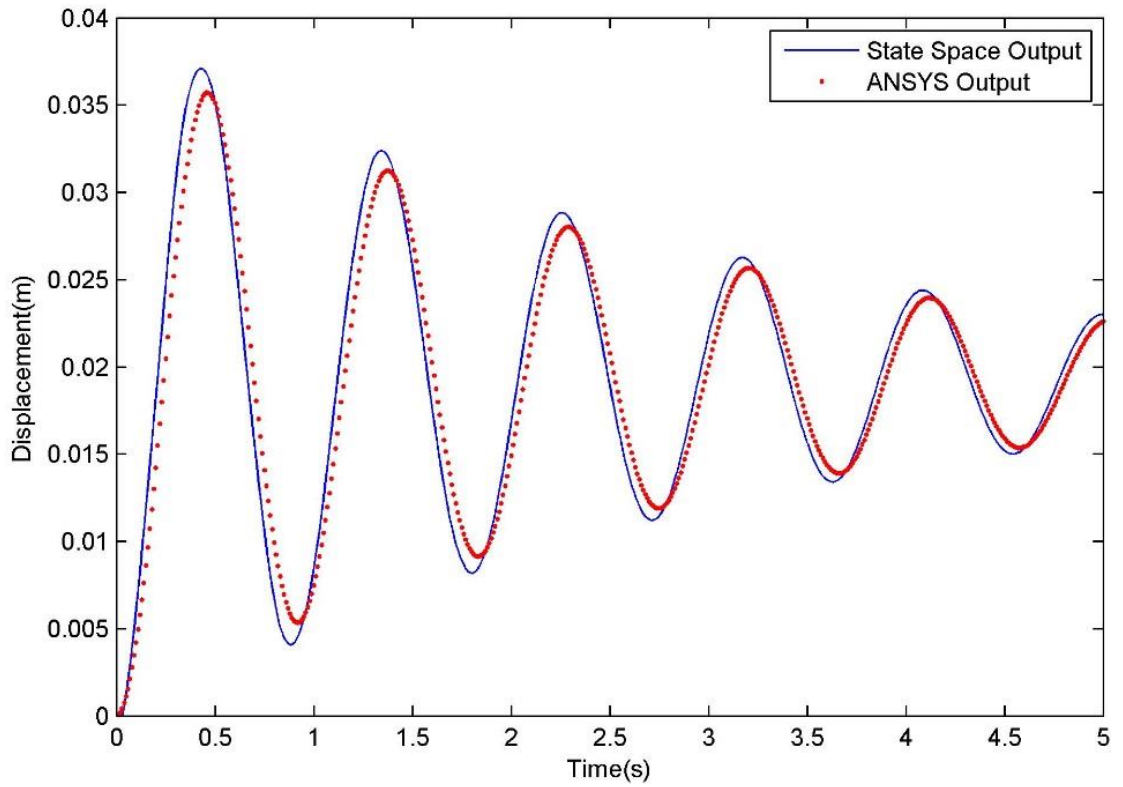


Figure 22. Comparison between simulation results and state space output for fuselage motion in the X direction. The force applied is a step input.

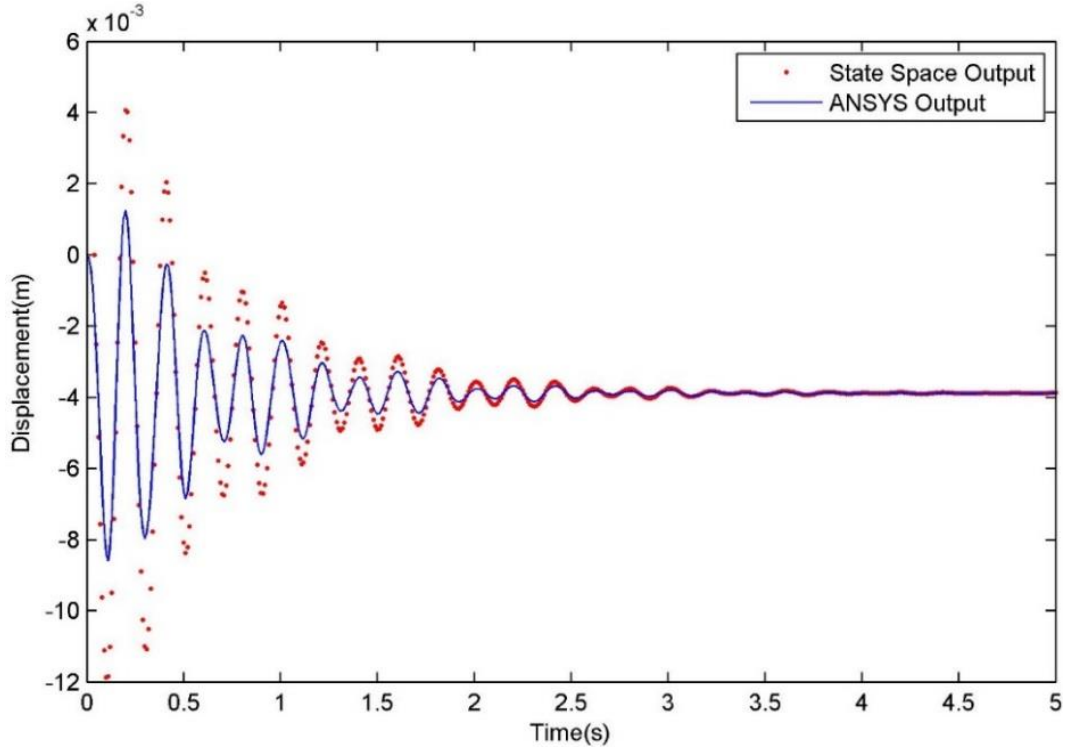


Figure 23. Comparison between simulation results and state space output for fuselage motion in the Y direction. The force applied is a step input.



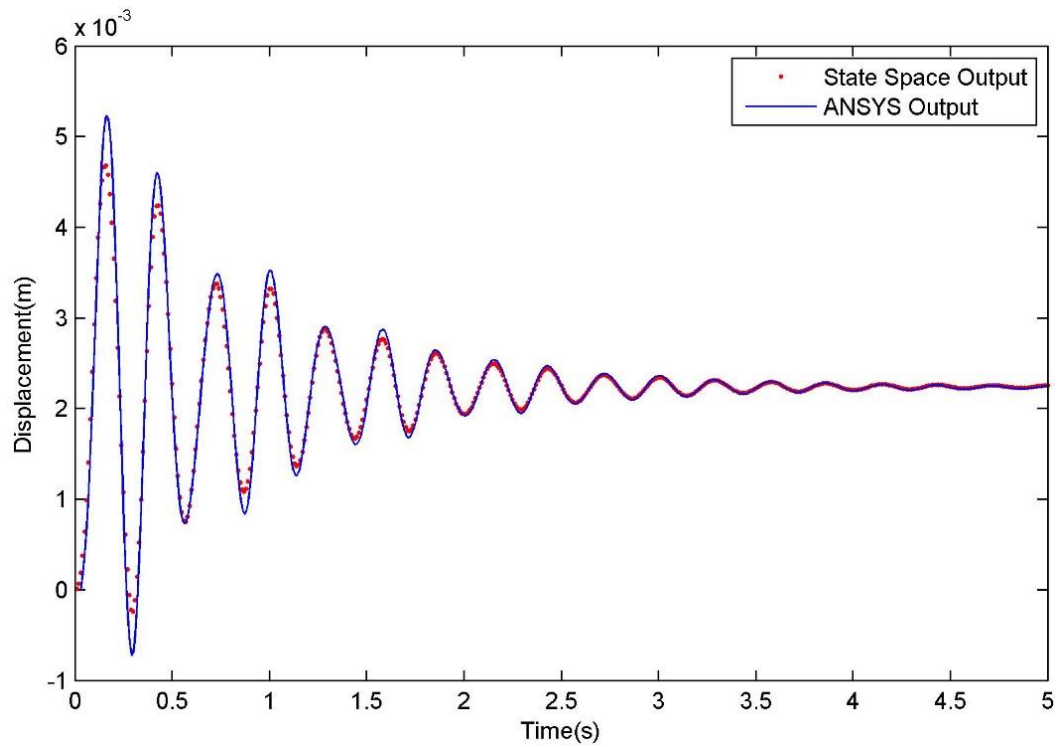


Figure 24. Comparison between simulation results and state space output for fuselage motion in the Z direction. The force applied is a step input.

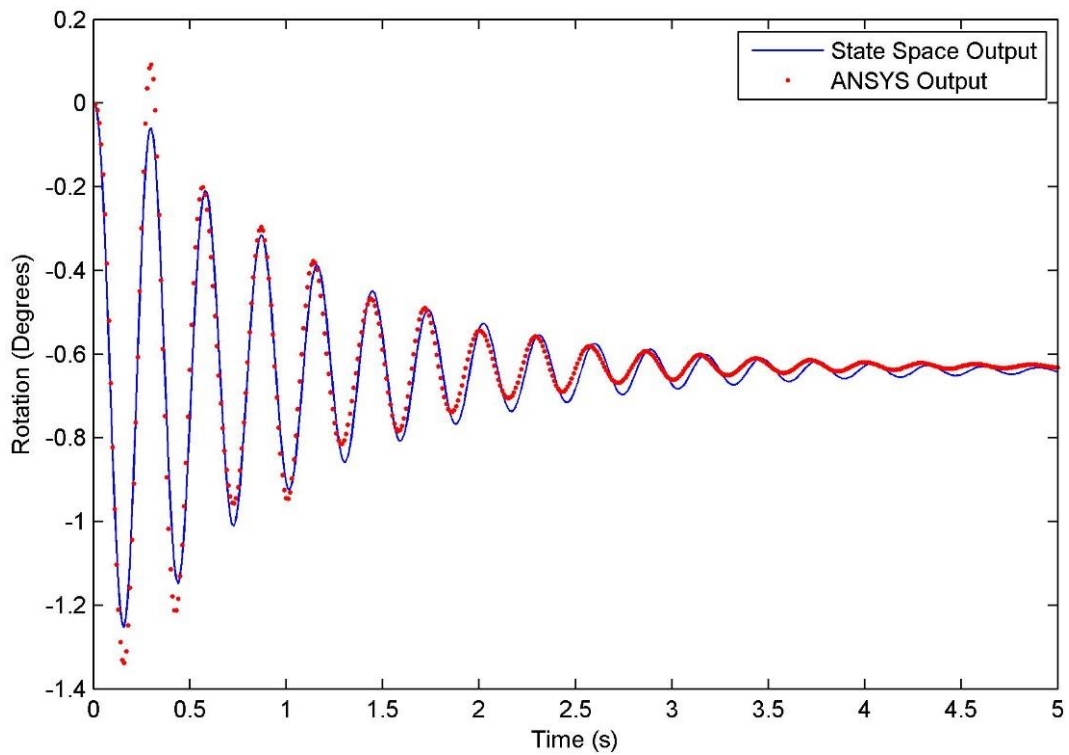


Figure 25. Comparison between simulation results and state space output for fuselage rotation about the X direction. The force applied is a step input.

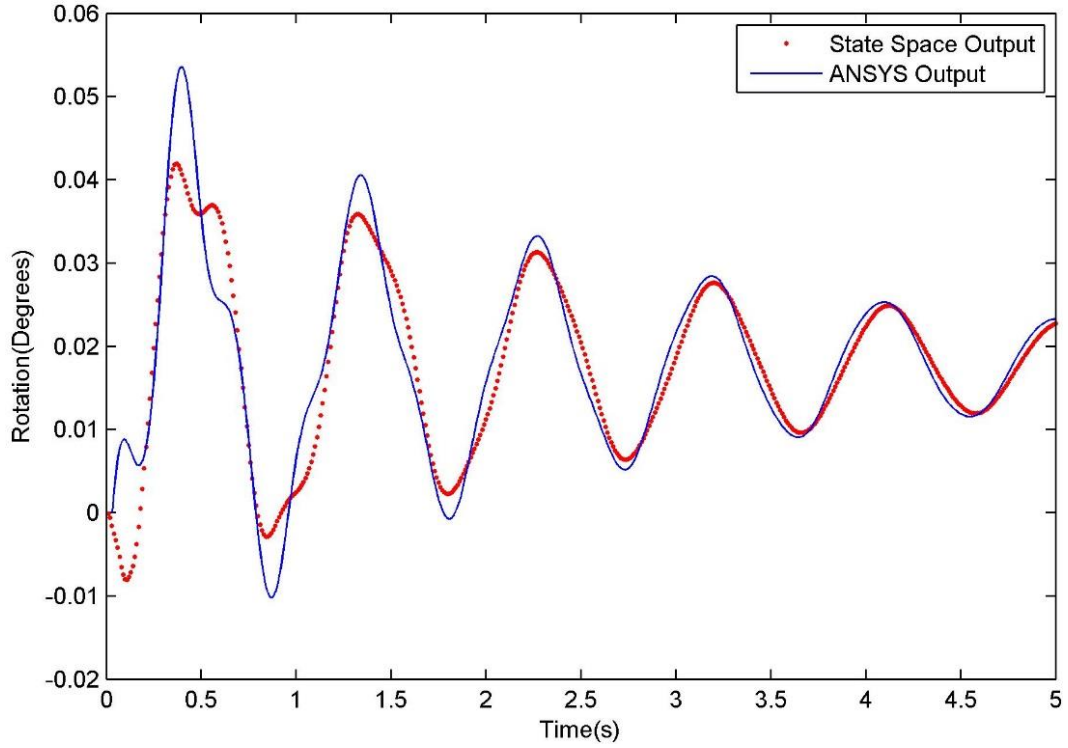


Figure 26. Comparison between simulation results and state space output for fuselage rotation about the Y direction. The force applied is a step input.

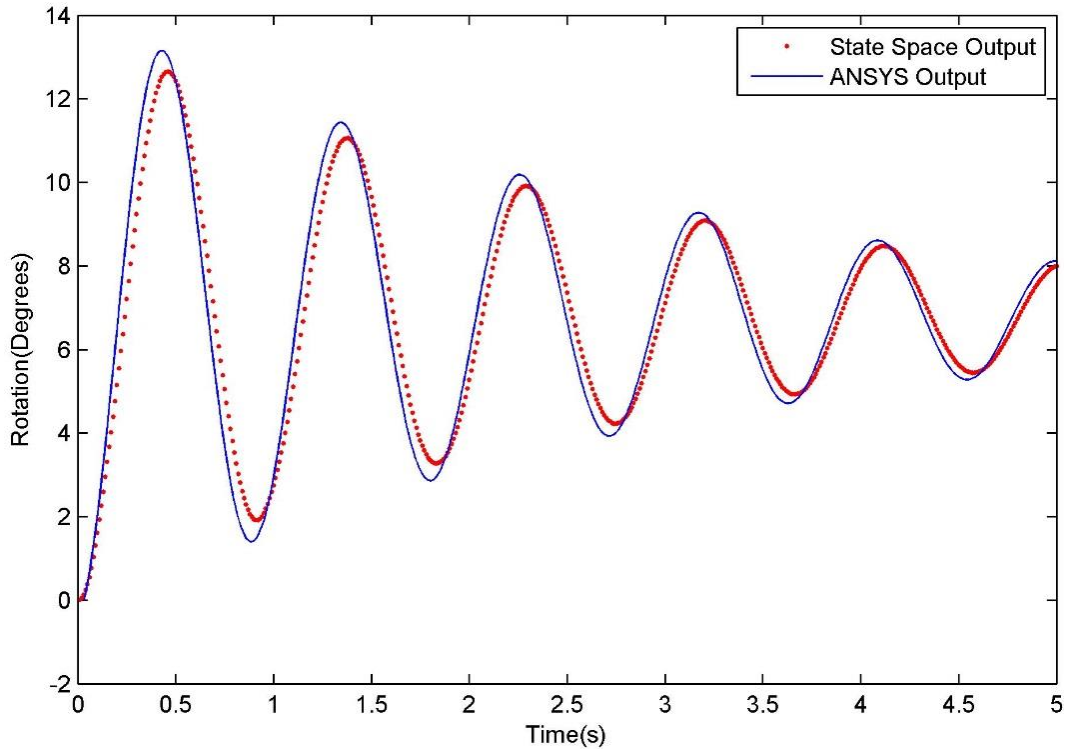


Figure 27. Comparison between simulation results and state space output for fuselage rotation about the Z direction. The force applied is a step input.

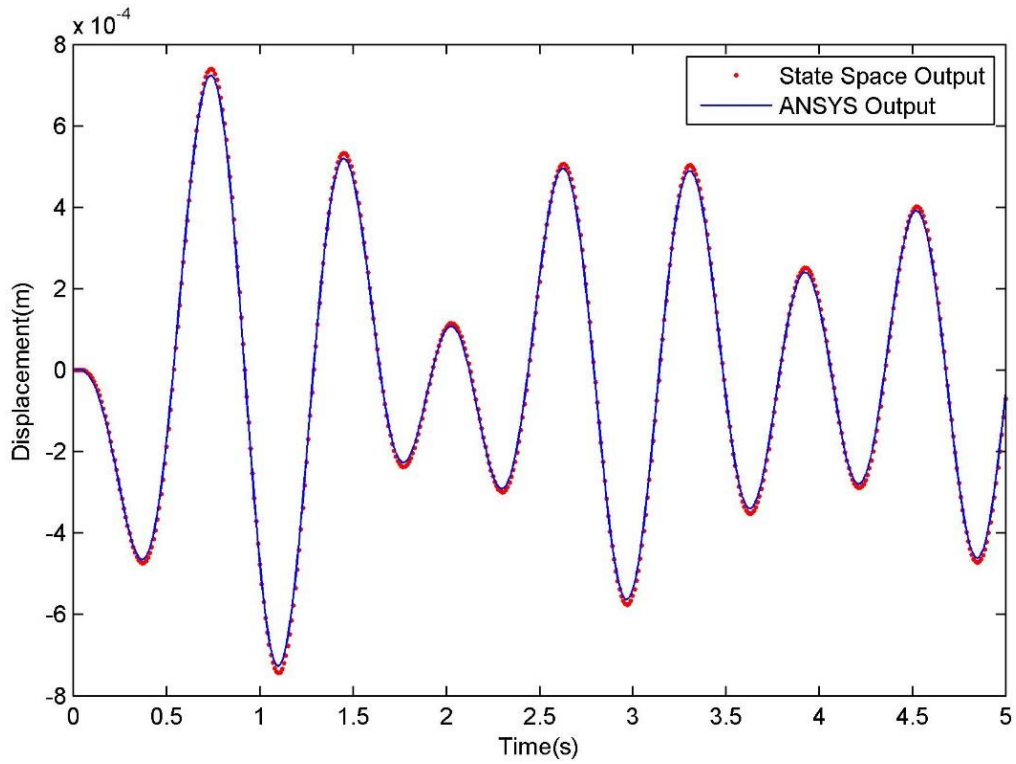


Figure 28. Comparison between simulation results and state space output for fuselage motion in the X direction. The force applied is a sine input.

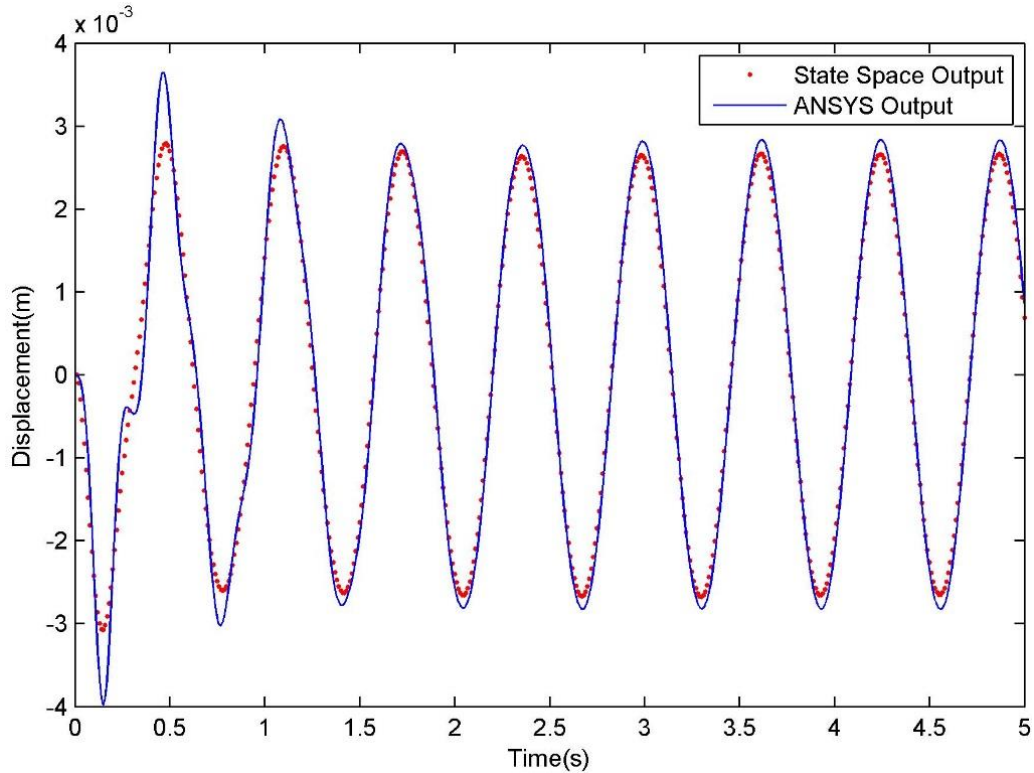


Figure 29. Comparison between simulation results and state space output for fuselage motion in the Y direction. The force applied is a sine input.

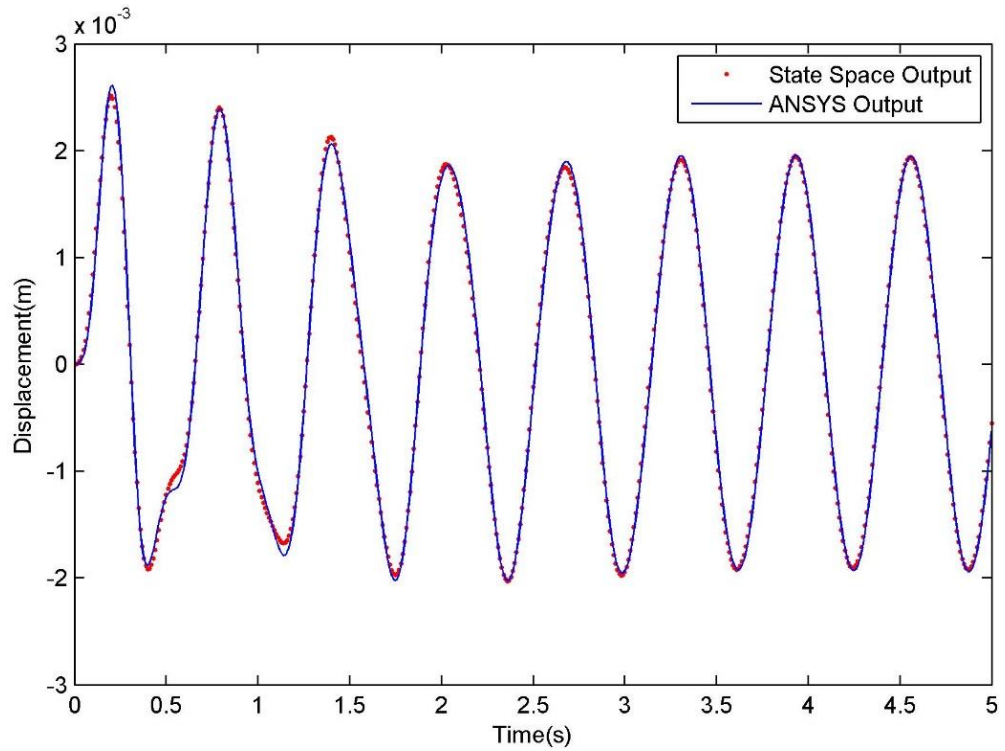


Figure 30. Comparison between simulation results and state space output for fuselage motion in the Z direction. The force applied is a sine input.

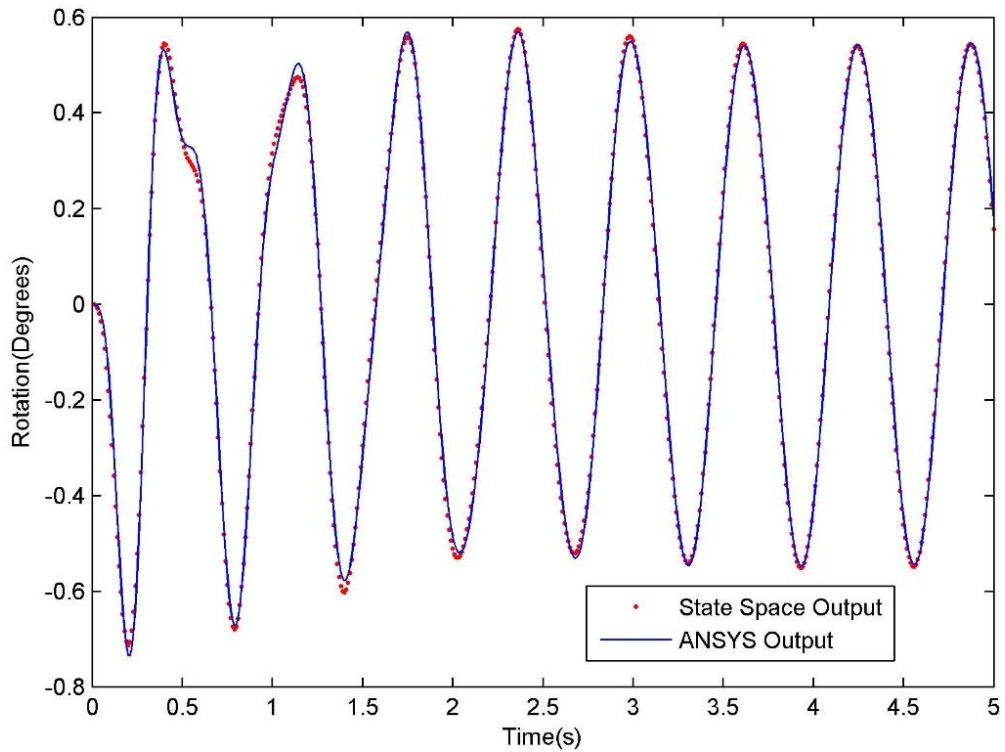


Figure 31. Comparison between simulation results and state space output for fuselage rotation about the X direction. The force applied is a sine input.

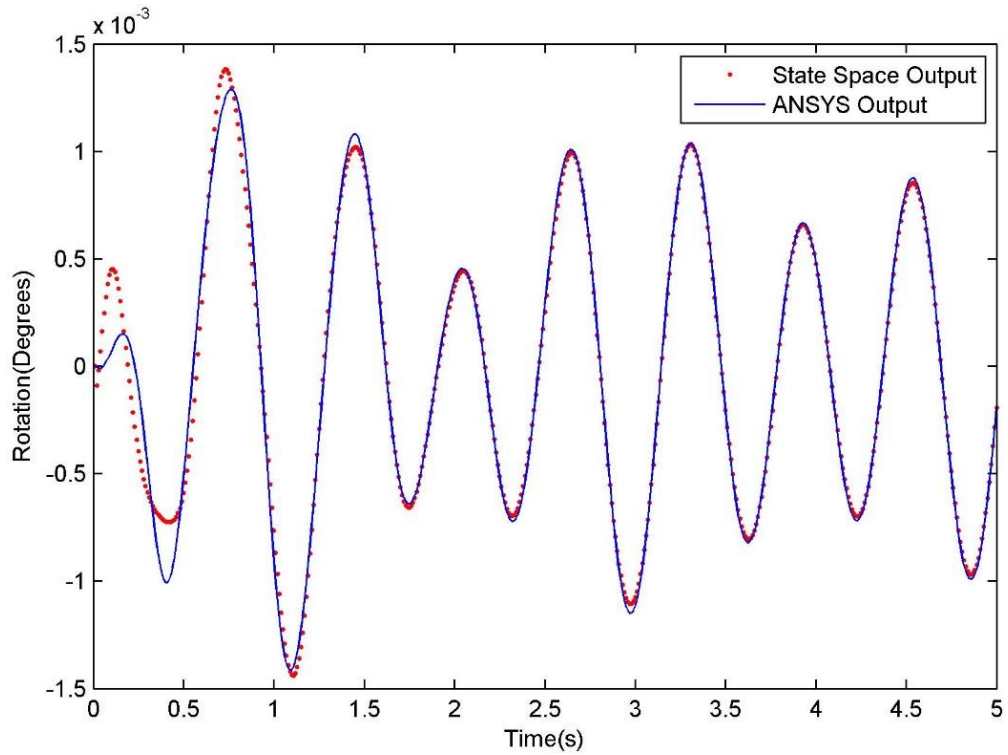


Figure 32. Comparison between simulation results and state space output for fuselage rotation about the Y direction. The force applied is a sine input.

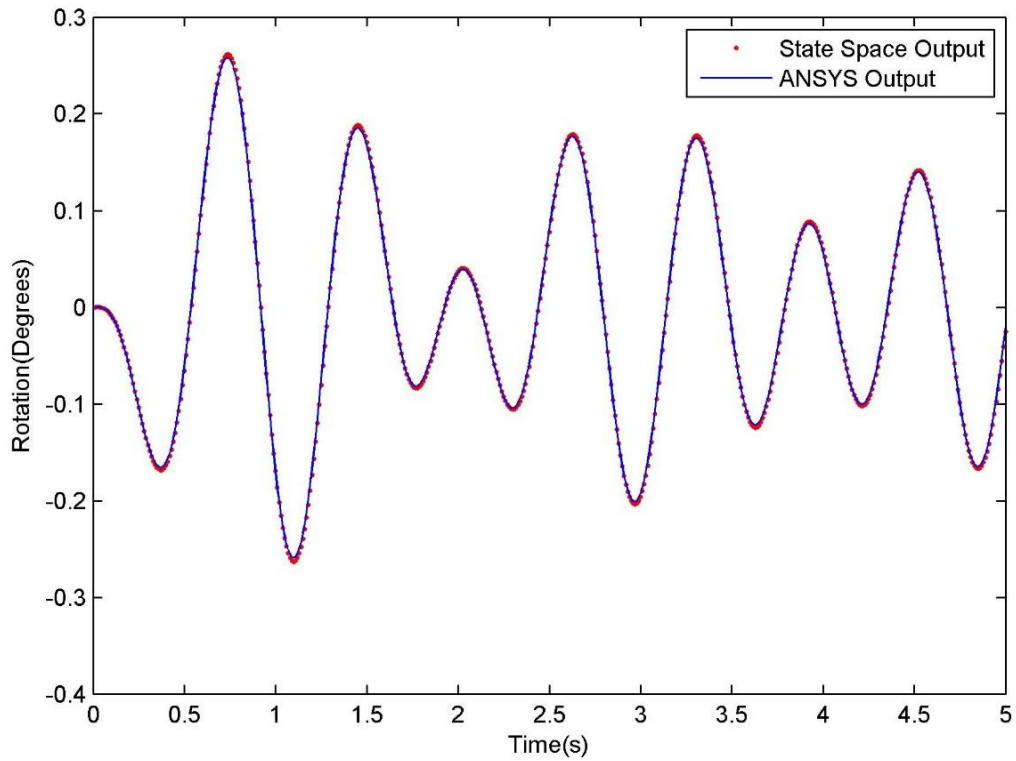


Figure 33. Comparison between simulation results and state space output for fuselage rotation about the Z direction. The force applied is a sine input.

The results show that the derived MATLAB® state space model is able to predict the motion of the fuselage when the forces acting on the wings are provided to it as input. The graphs show discrepancies between the two results within the first few seconds. This is the transient period, and small differences between the two plots during this period of time is not significant.

### **Frequency Response Function**

The Frequency Response Function of the 3D model is simulated using ANSYS® to study the dynamic characteristics of the aircraft across a range of frequencies. As previously described in Chapter 2, a frequency response simulation is performed to determine the response of the aircraft model over a broad range of frequencies.

The analysis is conducted using the same parameters that were used to determine the Frequency Response Function of the lumped mass model. The forcing function used in the simulation has an amplitude of 1 N and frequencies ranging from 0 to 40 Hz, to determine the response of the system well and over the established turbulence frequency. This force is applied to both wings of the aircraft in the Y-axis and the displacement of the fuselage across all frequencies are observed. A 5% damping ratio ( $\zeta = 0.05$ ) was used while conducting the analysis.

Since equal forces are applied to the wings, the displacements and rotations of the aircraft about all other axes is almost zero or negligible. The motion of the fuselage and the wings are mostly along the Y-axis and therefore the motion of the fuselage along this axis is the focal point of the analysis. Although this analysis is restricted to motion about one axis, the displacements about other axes can be observed, and suitable state space models can be derived. Figs. 34 and 35 compare the amplitude and phase response of the

MATLAB® state space model with the ANSYS® results.

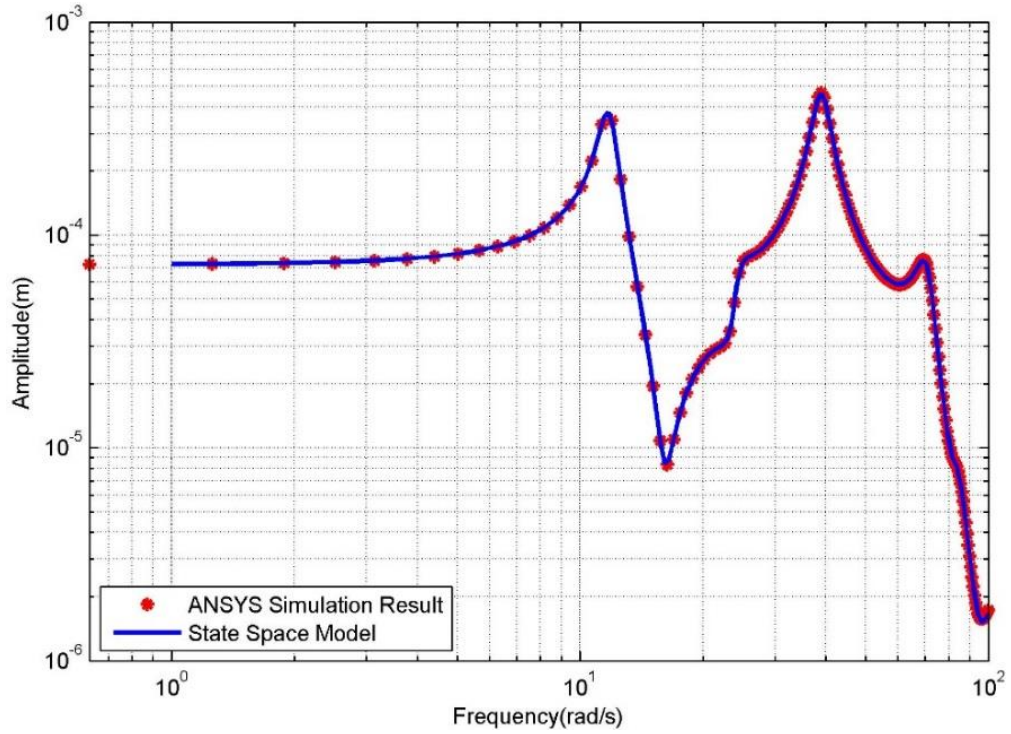


Figure 34. Amplitude comparison between simulation results and state space model.

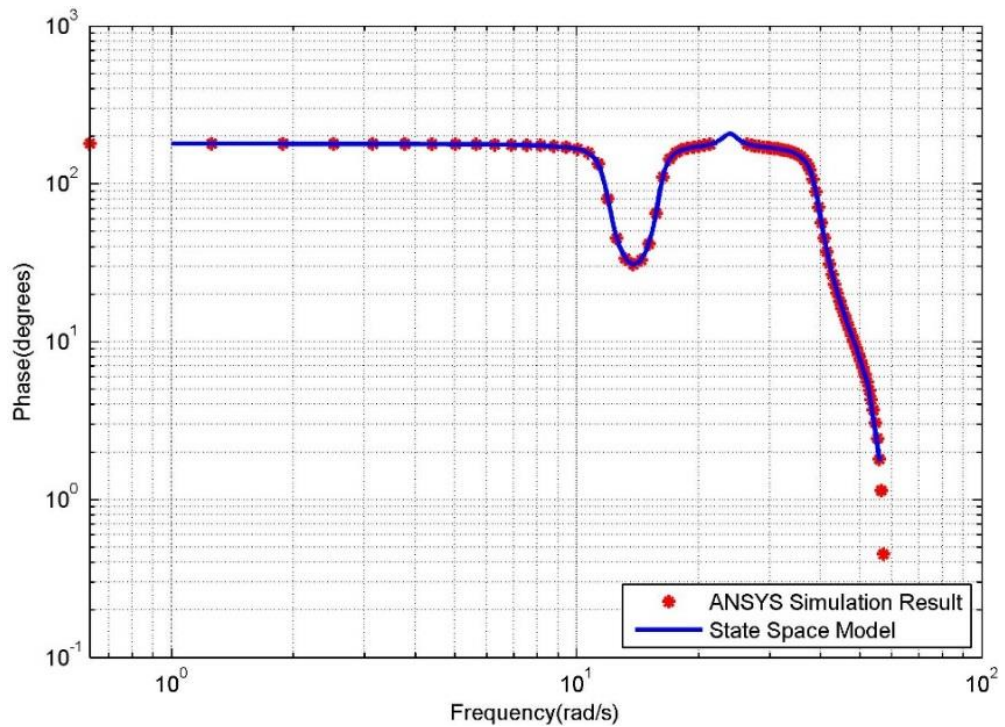


Figure 35. Phase comparison between simulation results and state space model.

Using the frequency response characteristics of the model, a suitable state space model is derived using MATLAB®. This state space model is expressed in Eq. 2.29.

$$A = \begin{bmatrix} A_{11} & A_{12} & A_{13} & A_{14} & A_{15} & A_{16} \\ A_{21} & A_{22} & A_{23} & A_{24} & A_{25} & A_{26} \\ A_{31} & A_{32} & A_{33} & A_{34} & A_{35} & A_{36} \\ A_{41} & A_{42} & A_{43} & A_{44} & A_{45} & A_{46} \\ A_{51} & A_{52} & A_{53} & A_{54} & A_{55} & A_{56} \\ A_{61} & A_{62} & A_{63} & A_{64} & A_{65} & A_{66} \end{bmatrix}$$

where

$$A_{11} = \begin{bmatrix} -2.519 & -40.52 \\ 36.94 & -1.14 \end{bmatrix}$$

$$A_{12} = \begin{bmatrix} -1.883 & -11.12 \\ -4.043 & -7.339 \end{bmatrix}$$

$$A_{13} = \begin{bmatrix} -10.69 & -4.956 \\ -7.654 & -4.851 \end{bmatrix}$$

$$A_{14} = \begin{bmatrix} -4.873 & -5.288 \\ -2.352 & -4.889 \end{bmatrix}$$

$$A_{15} = \begin{bmatrix} -13.97 & -11.53 \\ -12.77 & -8.298 \end{bmatrix}$$

$$A_{16} = \begin{bmatrix} 7.154 & -9.459 \\ 5.345 & -8.479 \end{bmatrix}$$

$$A_{21} = \begin{bmatrix} -0.6344 & 2.539 \\ 3.584 & 0.4783 \end{bmatrix}$$

$$A_{22} = \begin{bmatrix} -0.4742 & -14.77 \\ 9.366 & -1.201 \end{bmatrix}$$

$$A_{23} = \begin{bmatrix} -7.789 & -2.451 \\ -3.833 & -10.66 \end{bmatrix}$$

$$A_{24} = \begin{bmatrix} -1.502 & -3.566 \\ -12.19 & -3.444 \end{bmatrix}$$

$$A_{25} = \begin{bmatrix} -9.899 & -6.093 \\ -5.647 & -15.28 \end{bmatrix}$$

$$A_{26} = \begin{bmatrix} 3.94 & -6.577 \\ 8.693 & -4.418 \end{bmatrix}$$

$$A_{31} = \begin{bmatrix} 1.334 & -0.5454 \\ -0.7437 & 0.7257 \end{bmatrix}$$

$$A_{32} = \begin{bmatrix} 1.422 & -1.2 \\ -0.4816 & 2.5845 \end{bmatrix}$$

$$A_{33} = \begin{bmatrix} -4.083 & -75.026 \\ 63.894 & -3.213 \end{bmatrix}$$

$$A_{34} = \begin{bmatrix} -14.641 & -6.843 \\ -7.9366 & -5.0235 \end{bmatrix}$$

$$A_{35} = \begin{bmatrix} -10.899 & -18.659 \\ -14.366 & -13.746 \end{bmatrix}$$

$$A_{36} = \begin{bmatrix} 10.967 & -7.819 \\ 8.299 & -9.998 \end{bmatrix}$$

$$A_{41} = \begin{bmatrix} 0.1586 & -0.0991 \\ -0.1654 & 0.1407 \end{bmatrix}$$

$$A_{42} = \begin{bmatrix} 0.1224 & -0.0364 \\ -0.1107 & 0.3286 \end{bmatrix}$$

$$A_{43} = \begin{bmatrix} 0.5624 & 2.339 \\ 1.897 & -0.889 \end{bmatrix}$$

$$A_{44} = \begin{bmatrix} -0.667 & -28.658 \\ 20.558 & -1.494 \end{bmatrix}$$



$$\begin{aligned}
A_{45} &= \begin{bmatrix} -24.237 & -10.82 \\ -4.802 & -13.98 \end{bmatrix} & A_{46} &= \begin{bmatrix} 7.4623 & -15.228 \\ 7.47 & -4.0469 \end{bmatrix} \\
A_{51} &= \begin{bmatrix} -0.092 & 0.0779 \\ 0.121 & -0.0815 \end{bmatrix} & A_{52} &= \begin{bmatrix} -0.0679 & 0.1676 \\ 0.0912 & -0.183 \end{bmatrix} \\
A_{53} &= \begin{bmatrix} 0.7699 & -0.7609 \\ -0.8849 & 0.9207 \end{bmatrix} & A_{54} &= \begin{bmatrix} 1.8266 & -1.425 \\ -0.801 & 2.5621 \end{bmatrix} \\
A_{55} &= \begin{bmatrix} 5.749 & -193.066 \\ 164.06 & -12.768 \end{bmatrix} & A_{56} &= \begin{bmatrix} 33.41 & -2.482 \\ 8.505 & -40.594 \end{bmatrix} \\
A_{61} &= \begin{bmatrix} -0.0426 & 0.0309 \\ -0.368 & 0.0254 \end{bmatrix} & A_{62} &= \begin{bmatrix} -0.323 & 0.0683 \\ -0.027 & 0.0595 \end{bmatrix} \\
A_{63} &= \begin{bmatrix} 0.3163 & -0.348 \\ 0.3029 & -0.2473 \end{bmatrix} & A_{64} &= \begin{bmatrix} 0.305 & -0.8547 \\ 0.4912 & -0.5389 \end{bmatrix} \\
A_{65} &= \begin{bmatrix} -16.8944 & 7.254 \\ -6.457 & 20.893 \end{bmatrix} & A_{66} &= \begin{bmatrix} -4.8187 & 97.2695 \\ -85.9781 & -3.39 \end{bmatrix}
\end{aligned}$$

$$B = \begin{bmatrix} -0.0003125 \\ 0.0004454 \\ -0.000117 \\ 0.0001638 \\ 1.556 \times 10^{-5} \\ -0.0001261 \\ 1.464 \times 10^{-5} \\ -2.301 \times 10^{-5} \\ 5.533 \times 10^{-6} \\ -4.352 \times 10^{-6} \\ 4.3 \times 10^{-6} \\ -5.985 \times 10^{-6} \end{bmatrix}$$

$$C = [2.469 \quad 1.989 \quad 1.49 \quad 2.338 \quad 3.194 \quad 2.726 \quad 3.116 \quad 1.89 \quad 4.477 \quad 5.344 \quad -3.195 \quad 3.125]$$

$$\begin{aligned}
D &= 0 \\
K &= 0
\end{aligned} \tag{3.3}$$

Using this MATLAB® derived state space model, the transient behavior of the fuselage about the Y-axis can be predicted. The output of the model can be compared

with the results of a transient analysis simulated in ANSYS®.

The transient analysis is conducted by applying a single force of 1 N on the wings of the aircraft, and then observing the motion of the fuselage in the Y-axis. The output of the state space model also refers to the motion of the fuselage in the Y-axis. The output of this derived model is generated by applying a step load input to it, using MATLAB®. The comparison between these two results are shown in Fig. 36.

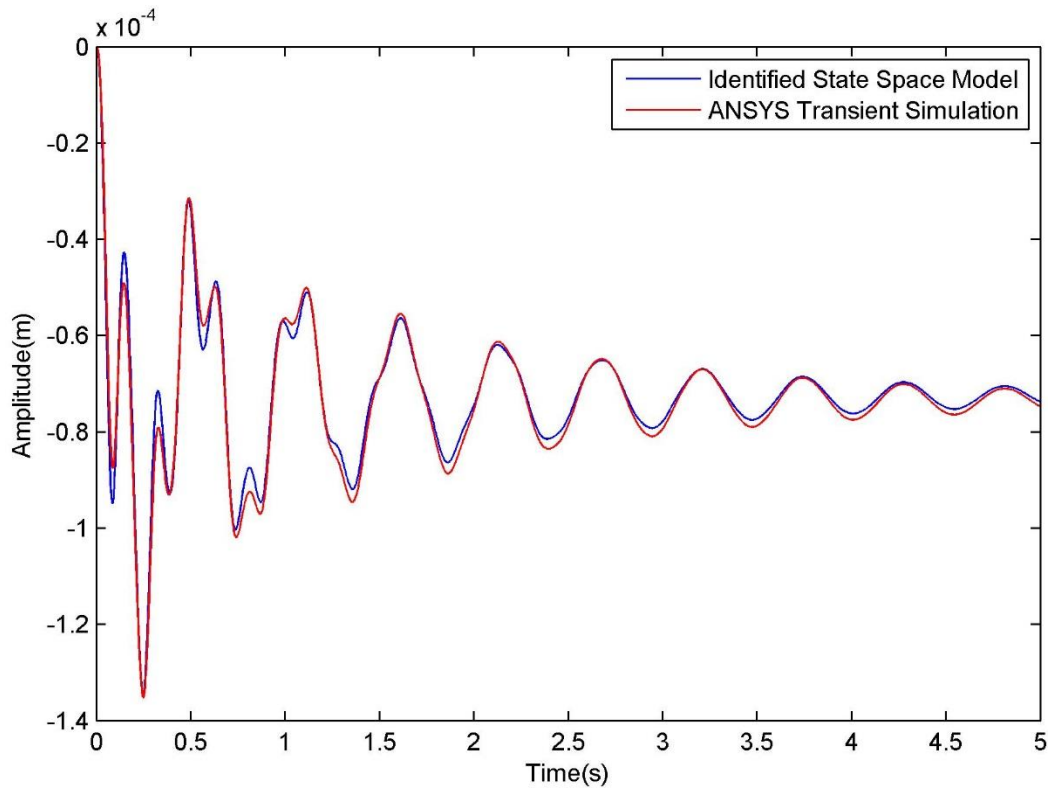


Figure 36. Comparison between FRF state space model and transient analysis.

The comparison shows the derived state space model can also be used to determine the motion of the fuselage about any given axis. The limitation of using a frequency domain state space model to predict the motion of the fuselage is that ANSYS® only provides the displacements of the fuselage as output, its rotations about various axes cannot be determined. Therefore this frequency domain state space model cannot be used to predict

the rotations of the fuselage, although it can be used to predict the translations of the fuselage.

## CHAPTER IV

### VIBRATION SENSOR DESIGN

In order to make measurements such as forces applied to wings or displacement of the wings, a suitable sensor which can actively monitor the system needs to be employed. This measurement can be made by bonding patches of piezoelectric displacement sensors onto the wings of the aircraft. This chapter looks at using piezoelectric materials as displacement sensors for airplane wings.

#### Development of a Theoretical Sensor

Piezoelectric materials can be used as displacement sensors by bonding patches of film along the length of a structure. To demonstrate this theory, a cantilever beam is covered with distributed piezoelectric films along its length. This beam is illustrated in Fig. 37.

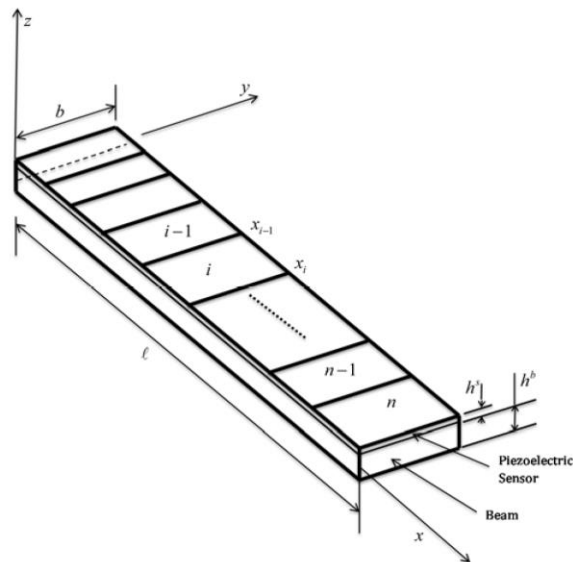


Figure 37. Cantilever Beam covered with piezoelectric patches [13].

A number of assumptions have been made while theoretically developing this sensor. It is assumed that the strains in the film are equal to the outer surface strains of the beam. The film is perfectly bonded to the beam but does not change its dynamic properties. It is also assumed that the piezoelectric patches are of equal length and thickness.

A modified form of a one dimensional piezoelectric equation earlier presented by Tzou is extended to patches bonded onto the beam [13]. This equation can be represented as [13]:

$$\Phi_s = -\frac{bh^s}{S^e} \int h_{31} r_x^s \frac{\partial^2 z}{\partial x^2} dx \quad (4.1)$$

where

$\phi^s$  = output voltage

$b$  = beam width

$h^s$  = piezoelectric sensor layer thickness

$S^e$  = electrode surface area

$h_{31}$  = piezoelectric film strain charge coefficient

$r_x^s$  = distance from beam neutral axis to the mid-plane of sensor layer

$z$  = beam lateral displacement

$x$  = sensor length in x direction

If the beam has  $n$  number of patches bonded on its surface, the output voltage of the  $i^{th}$  patch is [13]:

$$\Phi_i^s = -\frac{bh_i^s}{S_i^e} \int_{x_{i-1}}^{x_i} h_{31} r_{x_i}^s \frac{\partial^2 z_i}{\partial x^2} dx \quad (4.2)$$

On integrating this equation [13]:

$$\Phi_i^s = -\frac{bh_i^s}{S_i^e} \int_{x_{i-1}}^{x_i} h_{31} r_{x_i}^s \left[ \frac{\partial z_i}{\partial x} \right]_{x_{i-1}}^{x_i} \quad (4.3)$$

If the slope  $a_i$  is assumed to be constant, Eq. 4.3 can be rewritten as [13]:

$$\Phi_i^s = -\frac{bh_i^s}{S_i^e} \int_{x_{i-1}}^{x_i} h_{31} r_{x_i}^s a_i (x_i - x_{i-1}) \quad (4.4)$$

Therefore, the slope of the  $i^{th}$  patch on the beam can be expressed as [13]:

$$a_i = \frac{\Phi_i^s S_i^e}{bh_i^s h_{31} r_{x_i}^s (x_i - x_{i-1})} \quad (4.5)$$

Since it is assumed that the patches are of equal length and thickness, Eq. 4.5 can be simplified as [13]:

$$a_i = -2 \frac{\Phi_i^s}{h_s^2 + h^s h^b h_{31}} \quad (4.6)$$

With Eq. 4.6, the slopes of all the patches can be determined. With the slope  $a_i$  of the  $i^{th}$  linear approximation segment on a curve, the ordinate  $z_i$  can be found as [13]:

$$z_i = a_i (x_i - x_{i-1}) + z_{i-1} \quad (4.7)$$

where

$z_i$  = lateral displacement of the  $i^{th}$  segment of the beam

$z_{i-1}$  = lateral displacement of the  $(i-1)^{th}$  segment of the beam

$a_i$  = slope of the  $i^{th}$  segment of the beam

$x_i$  = location of the  $i^{th}$  segment of the beam along its length

$x_{i-1}$  = location of the  $(i-1)^{th}$  segment of the beam along its length

Using Eq. 4.7, the displacement curve of the entire beam can be found. For a cantilever beam, a boundary condition  $z_0 = 0$  can be assumed. This boundary condition states that the displacement of the beam at the support is equal to zero. Since Eq. 4.7 approximates the displacement of the beam, the accuracy of this displacement is dependent on the number of patches bonded on to the beam surface.

### MATLAB® Simulation of the Theoretical Sensor

To evaluate the performance of the sensor patches, a force of 1 N is applied on the third node of the beam. The output of the displacement sensors is compared with the displacement results calculated using a modal superposition equation which is expressed as:

$$(x) \cong \sum_{k=1}^m \hat{W}_k \Psi_k(x) \quad (4.8)$$

where

$x$  = sensor length in the  $x$  direction

$\hat{W}_k$  = modal coordinates of the beam

$\psi_k$  = mass-normalized modal displacement functions

The Frequency Response Function (FRF) of the displacement of the beam, when excited by a force vector  $\{f\}$  is expressed in discretized form as:

$$\{z\} \cong \sum_{k=1}^m \frac{\{\Psi_k\} \{\Psi_k\}^T \{f\}}{\omega_k^2 - \omega^2 + j\eta_k \omega_k^2} \quad (4.9)$$

where

$z$  = beam lateral displacement

$\psi_k$  = mass-normalized modal displacement functions

$\{f\}$  = harmonic excitation force vector

$\omega$  = excitation frequency

$$j = \sqrt{-1}$$

$\omega_k$  = beam  $k_{th}$  natural frequency

$\eta_k$  = modal damping loss factors

Table 8 summarizes the beam and sensor parameters used while evaluating the performance of the sensor.

Table 8. Summary of beam and sensor parameters used during simulation.

<b>Aluminum Beam</b>	<b>PVDF</b>
$l = 0.2 \text{ (m)}$	$h^s = 50 \times 10^{-6} \text{ (m)}$
$b = 0.025 \text{ (m)}$	$h_{31} = 0.4 \times 10^9 \text{ (V/m/m/m)}$
$h^b = 0.95 \times 10^{-3}$	
$\rho = 2770 \text{ (kg/m}^3\text{)}$	
$E = 71 \times 10^9 \text{ (N/m}^2\text{)}$	

The sensor used in this simulation is PolyVinylidene Fluoride (PVDF). The evaluation procedure involves first discretizing the beam and calculating its mode shapes in discretized form. Next, the discretized lateral displacement harmonic response of the beam is found for frequencies ranging from 0 to 800 Hz using Eq. 4.9. Its displacement is also found for an arbitrary excitation force frequency of 298 Hz using Eq. 4.8. Using this response, the voltage output is calculated for all patches using Eq. 4.4. The lateral displacement curve of the beam is determined using Eq. 4.7, and the two results are compared.



Fig. 38 compares the displacement curves of the two results. Fig. 39 compares the cantilever beam admittance of the two results.

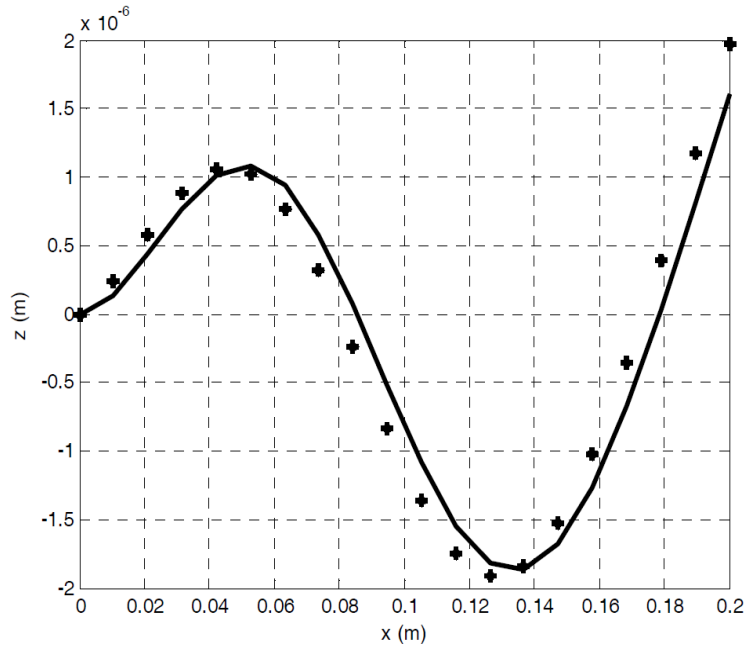


Figure 38. Comparison between results for a cantilever beam displacement for an arbitrary force excitation frequency of 298 Hz. The continuous line represents the actual displacement of the beam, the dots represent the sensor output.

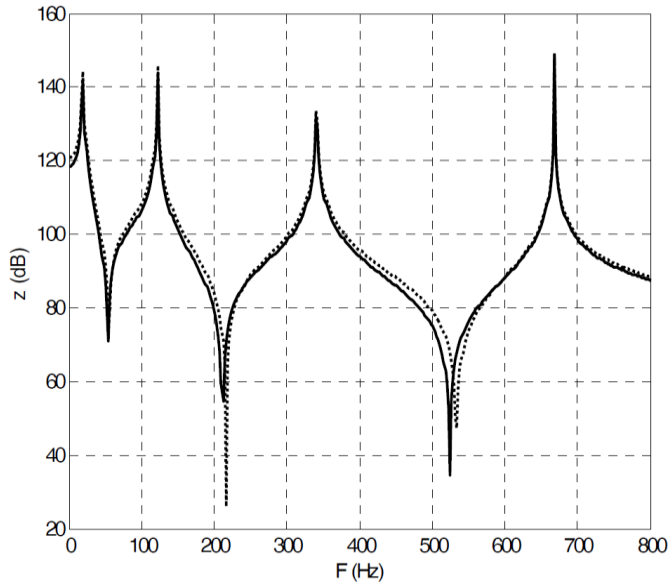


Figure 39. Comparison between results for the Frequency Response Function of displacement of a cantilever beam. The continuous line represents the actual displacement of the beam, the dots represent the sensor output.

### ANSYS® Simulation

To simulate this theory, an analysis is first conducted on a clamped-clamped prismatic steel beam with 25 piezoelectric sensors placed along its length. This simulation is conducted by using a transient analysis with ANSYS®, with a 2% damping ratio ( $\zeta = 0.02$ ). PolyVinylideneFluoride (PVDF) patches are bonded on one side of the beam.

These patches are bonded on to the surface of the beam after placing fixed supports at both ends of the steel beam. The polarization axis of the sensors is along the length of the beam. A vertical force of 5000 N is applied at the center of the beam. The beam and piezoelectric patches are shown in Fig. 40.

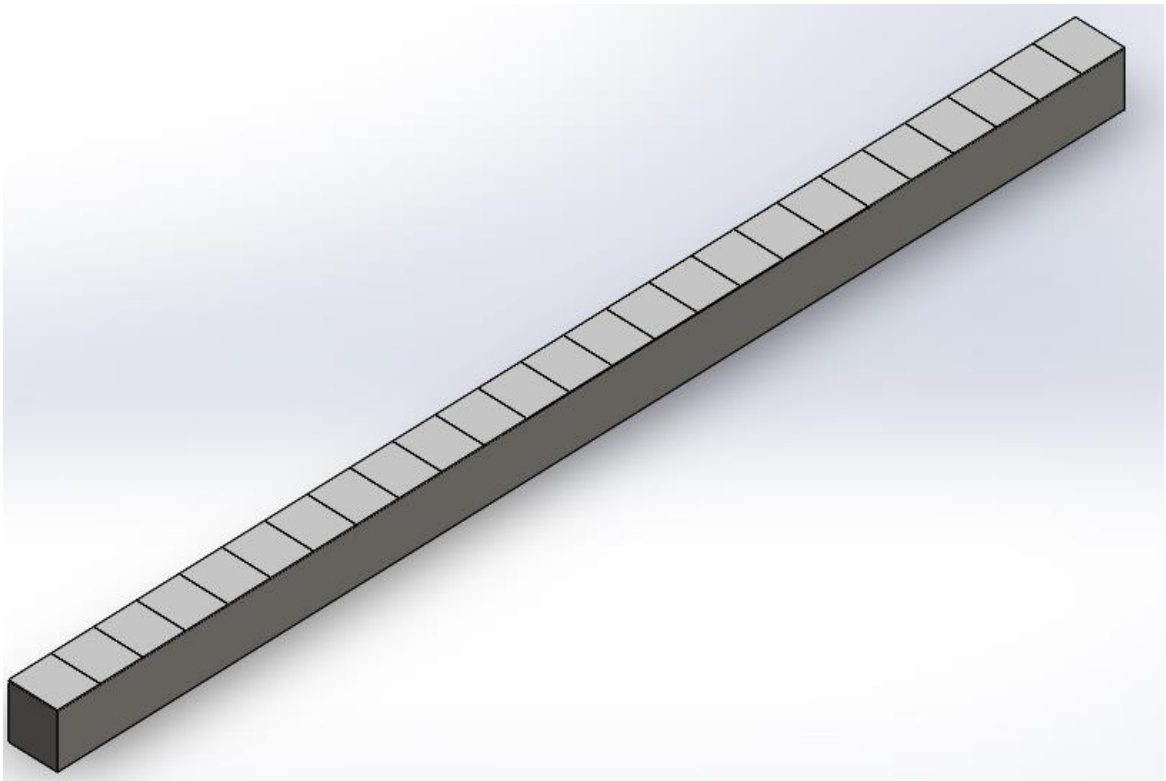


Figure 40. Prismatic beam with piezoelectric patches.

Table 9 describes the parameter values used for the simulation. Table 10 summarizes the parameters used to specify the properties of the PVDF displacement

sensor [21].

Table 9. Parameter values used to simulate a clamped-clamped beam

<b>Beam</b>	<b>Sensor</b>
$l = 2.5(m)$	$h^s = 2 \times 10^{-3} (m)$
$b = 0.115(m)$	$h_{31} = 0.4 \times 10^9 (V/m/m/m)$
$h = 0.115(m)$	$\rho = 1789 (kg/m^3)$
$\rho = 7850 (kg/m^3)$	$E = 8.4 \times 10^9 Pa$
$E = 2 \times 10^{11} Pa$	$\nu = 0.18$

Table 10. Parameters used for the PVDF displacement sensor.

<b>Parameter</b>	<b>Value</b>
$e_{31}$	$0.024 [A \text{ sec}/m^2]$
$e_{33}$	$-0.0270 [A \text{ sec}/m^2]$
$e_{15}$	$0 [A \text{ sec}/m^2]$
$ep_{11}$	$7.4$
$ep_{33}$	$7.6$

Application of the force will cause the beam to deform symmetrically along its length. This kind of deformation also causes symmetrical strains on the sensors, which in turn will exhibit symmetrical voltage readings along the length of the beam. The voltage reading from each sensor patch will be the sum of the voltages across its surface. Each node on the sensor patch surface yields a different voltage depending on its state of strain. While calculating the beam displacement from the sensor output, the sum of the voltages

at every node of a sensor patch gives the open circuit voltage of that patch. The displacement of the entire beam is calculated using Eq. 4.6 and 4.7. Since the beam is clamped at both ends, a boundary condition is used, which sets the displacements of the patches at both clamped ends to zero.

Fig. 41 shows the different voltage outputs present on a single sensor patch, due to the variations in strain that it experiences. Fig. 42 shows the comparison between the measured displacement of the beam and the displacement of the beam obtained from the sensor voltage readings.

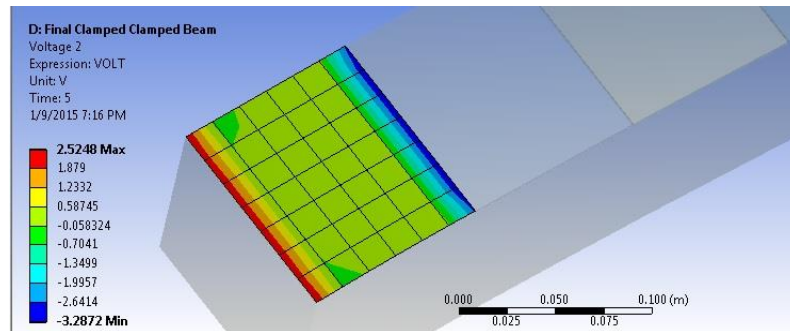


Figure 41. Voltages on a single sensor patch.

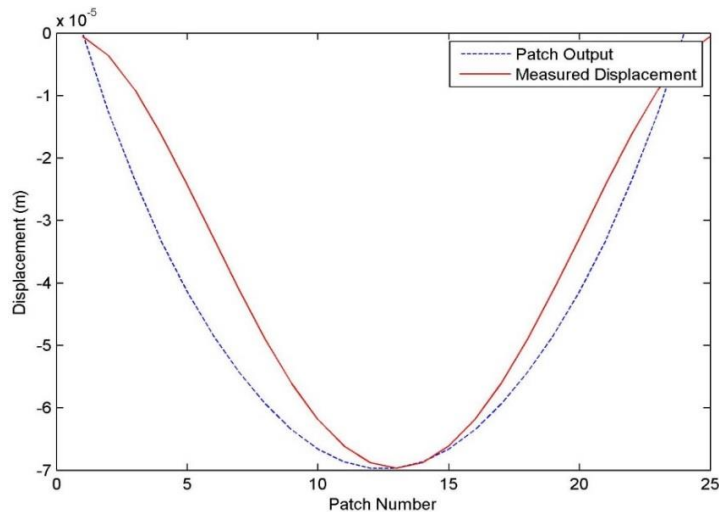


Figure 42. Comparison between measured displacement and patch output for a clamped-clamped beam.

This comparison shows that the displacement of the beam obtained from the

voltage readings of the piezoelectric sensors are in good agreement with the measured displacement of the beam.

### **Displacement Sensors on an Airplane Wing**

The next step will be to place these displacement sensors on an airplane wing to measure its displacement. This simulation involves fixing one end of an airplane wing while applying a vertical force to its bottom face, like a cantilever beam. To ensure that the results are accurate, 30 PVDF patches are placed along the length of the wing, on its bottom face. The parameters used for the sensors are obtained from Tables 9 and 10. The parameters used for the wing are obtained from Table 6.

Fig. 43 shows the placement of the sensors on the airplane wing. Fig. 44 shows the face on which the force is applied.

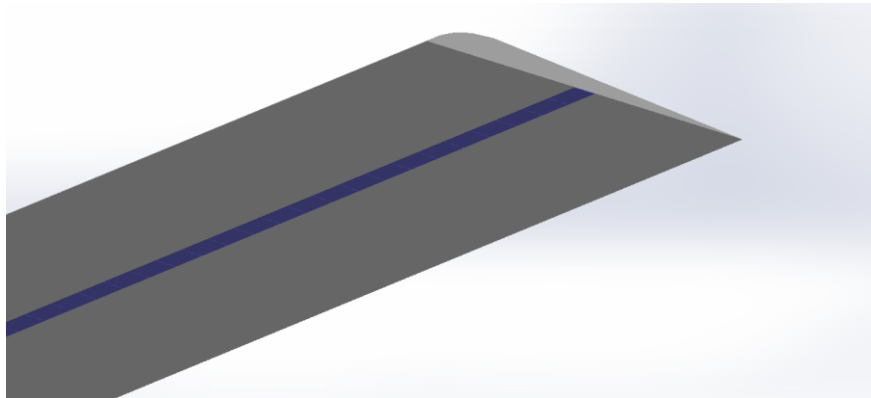


Figure 43. Piezoelectric displacement sensors on an airplane wing.

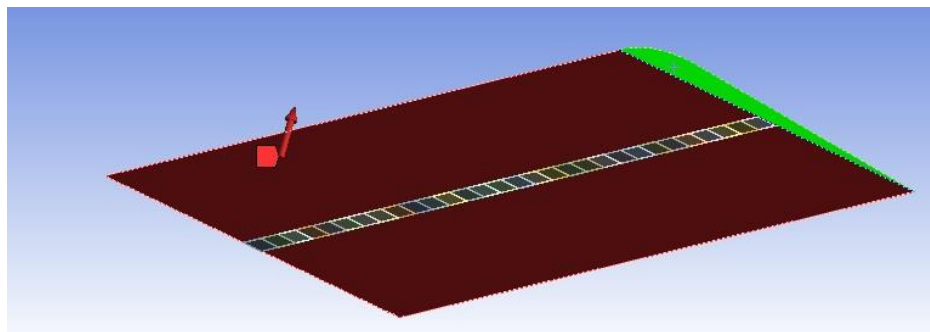


Figure 44. Force applied to the airplane wing. The green face shows the fixed end.

An arbitrary force of 750 N is applied to the bottom face of the wing. The polarization axis of the sensors is along the length of the wing. The wing is fixed at one end, and a boundary condition is applied such that the displacement of the patch closest to this fixed support is equal to zero. Fig. 45 compares the measured displacement of the wing to the displacement of the wing calculated from the displacement sensor output.

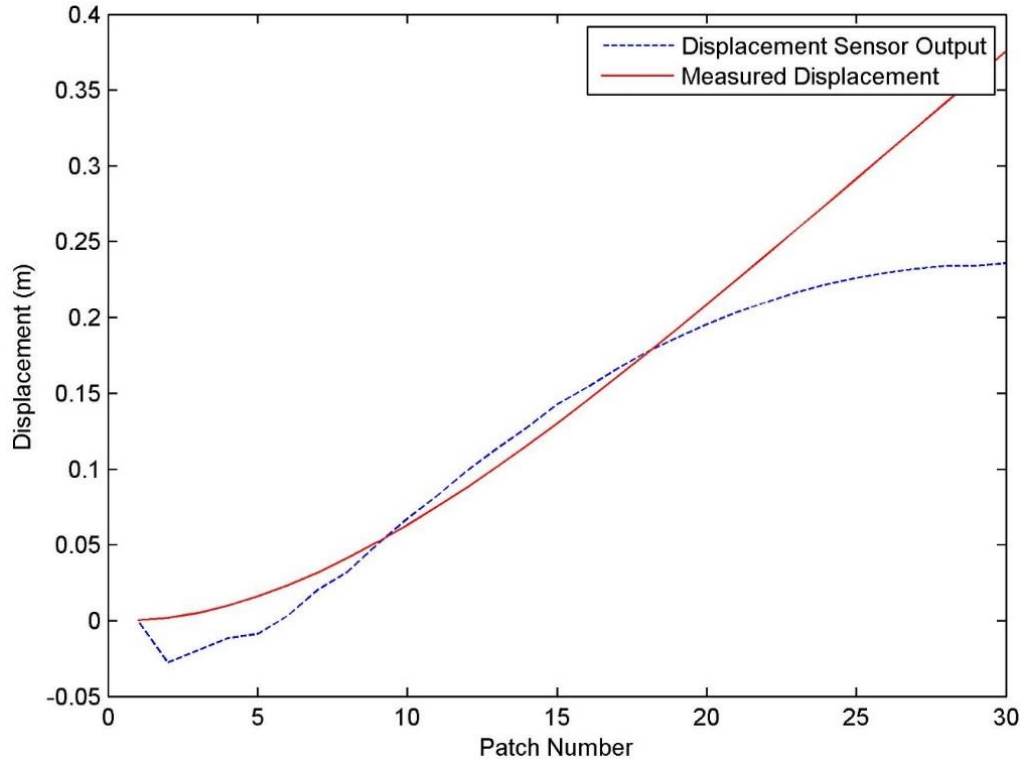


Figure 45. Comparison between measured displacement and patch output for a fixed airplane wing.

It can be clearly seen that there is a clear disagreement between the two results towards the last 11 patches. This is because the strains at the unconstrained end of a cantilever beam, are very small. When a cantilever beam is deformed, a section of the beam that is close to the fixed support experiences high strain. A certain section of the beam that is further away from the fixed support does not undergo much strain. This is illustrated in Fig. 46.

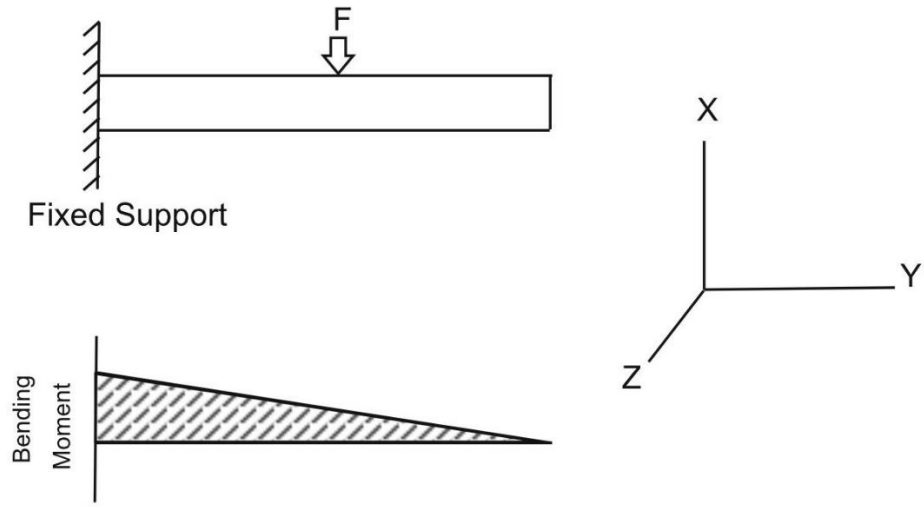


Figure 46. Cantilever beam.

As can be seen from the Fig.46, the strain of the cantilever of the cantilever beam steadily approaches zero towards the free end. Therefore the displacement sensors cannot measure any strain in this region, which prevents it from measuring the displacement curve of the entire beam. Therefore, to compensate for this, a correction factor must be introduced into the calculated slopes, so that the displacement curve of the entire cantilever beam can be calculated.

### Slope Correction

This discrepancy between the two displacements can be rectified by using a correction factor. The correction factor will be used with the patches which show a deviation from the measured value, due to low strain values. The value of the correction factor depends on parameters such as the stiffness of the beam, the length of the beam, and the force applied on the beam.

Fig. 47 shows the comparison between the measured displacements of the wing with the displacement of the wing calculated from the displacement sensor output, with a correction factor being applied.

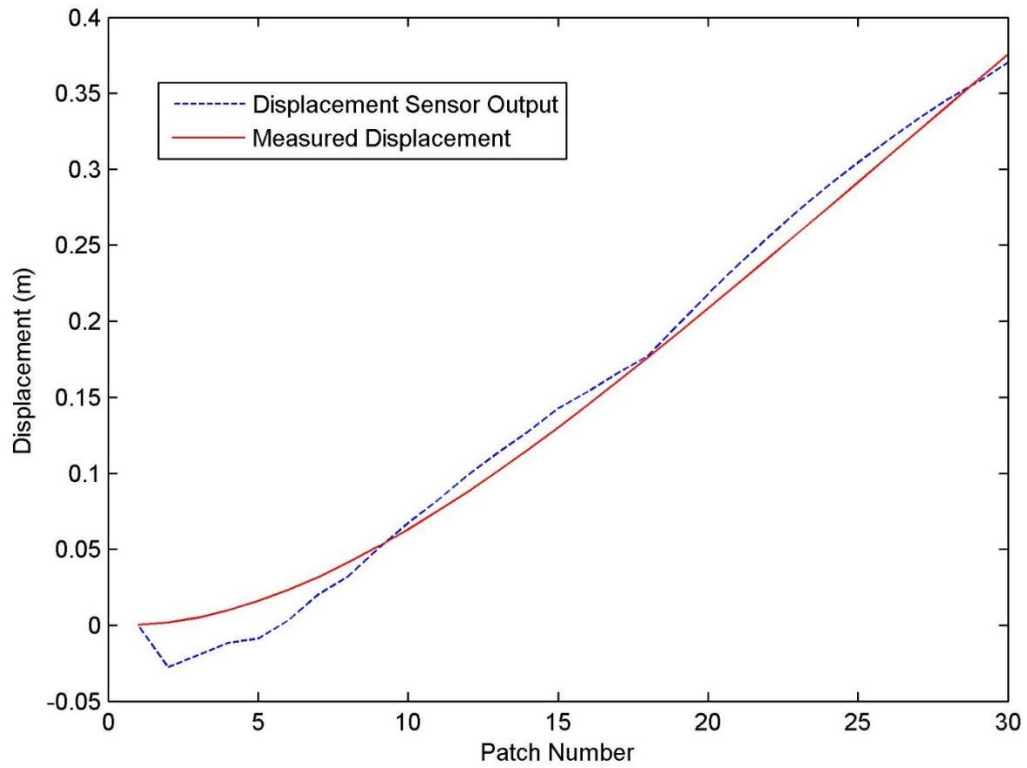


Figure 47. Comparison between measured displacement and patch output for a fixed airplane wing with an applied correction factor.

The above figure shows a much better agreement between the two results, after applying the correction factor. These simulations validate the developed theoretical equations. It also implies that the piezoelectric displacement sensor can effectively be used to measure the displacement of an airplane wing.



## **CHAPTER V**

### **VIBRATION SENSORS ON AN AIRPLANE**

Results so far have shown that piezoelectric materials are very capable of measuring the displacements of structures to which they are bonded. The next objective is to use displacement sensors on wings which are attached to an airplane fuselage. The output from the sensors will be later used as the input to predict the vibration of the fuselage. In the following, wing displacement calculated from the PVDF output will be referred to as measured displacement.

#### **Fixed Fuselage Simulation**

For this simulation, the airplane fuselage is fixed so that the deflection of the wings can be measured. This simulation is conducted because a cantilever wing behaves differently from a wing that is attached to the fuselage using bonded connections. Elastic supports on the fuselage will enable both the wings and the fuselage to exhibit rigid body motion, because of which measurements of wing deflections cannot be made for comparison. Similar to previous simulations, unequal loads are applied to the wings of the aircraft.

The voltage readings from the sensor patches are used to calculate the displacement curve of the two wings. Correction factors will be used while calculating the displacement of the wings. Fig. 48 shows the model of the aircraft with distributed displacement sensors bonded on to its wings. This model is developed by attaching displacement sensors on both wings of the aircraft using bonded connections. In creating such a model, the

displacements of both wings can be calculated and thereby used as inputs in creating a suitable state space prediction model. The faces shaded in blue represent the areas where fixed supports are used. The simulation is run for a period of 20 seconds using a 2% damping ratio ( $\zeta = 0.02$ ).

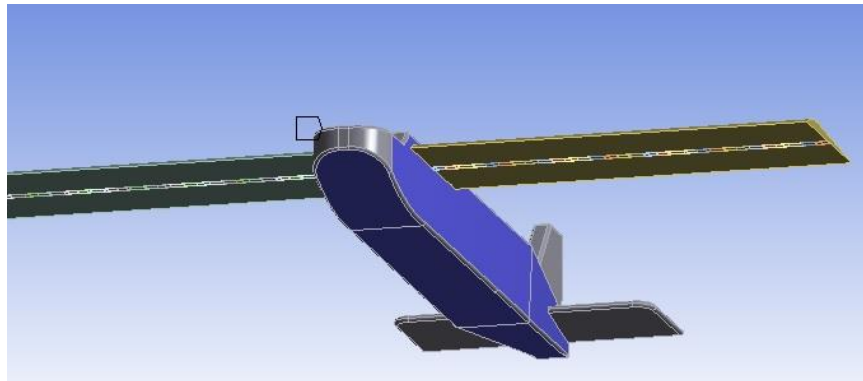


Figure 48. Aircraft with distributed displacement sensors on it wings.

Figs. 49 and 50 compare the results obtained from the simulation.

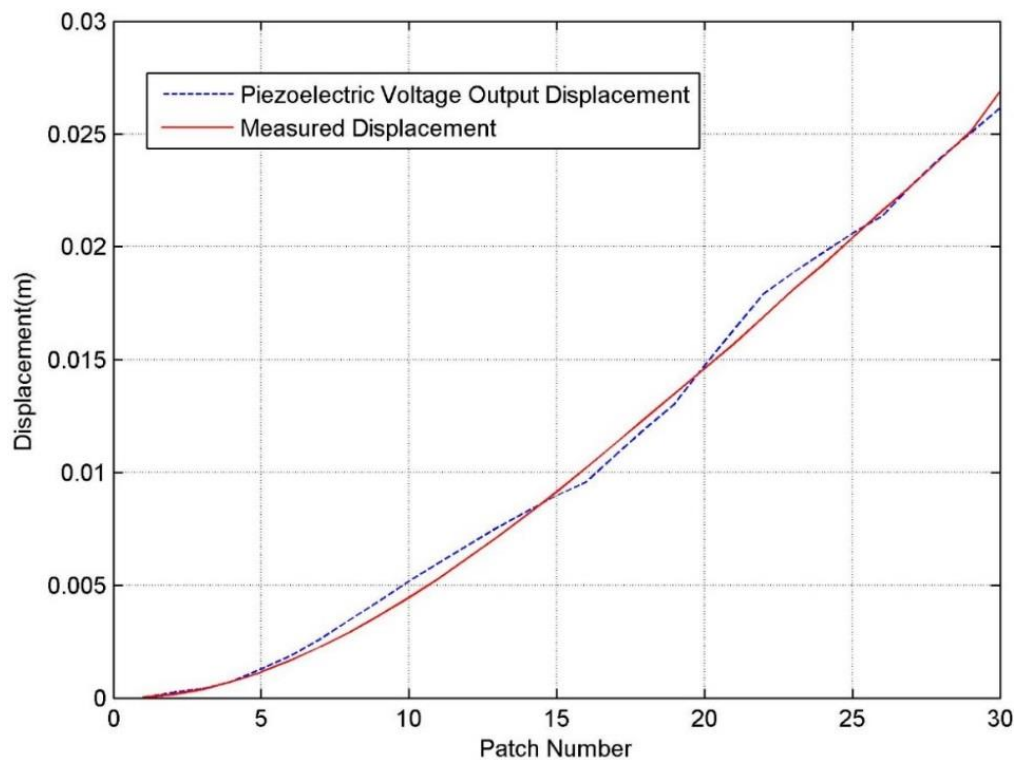


Figure 49. Comparison between the measured displacement and calculated displacement of wing 1. A force of 50 N was applied to this wing.

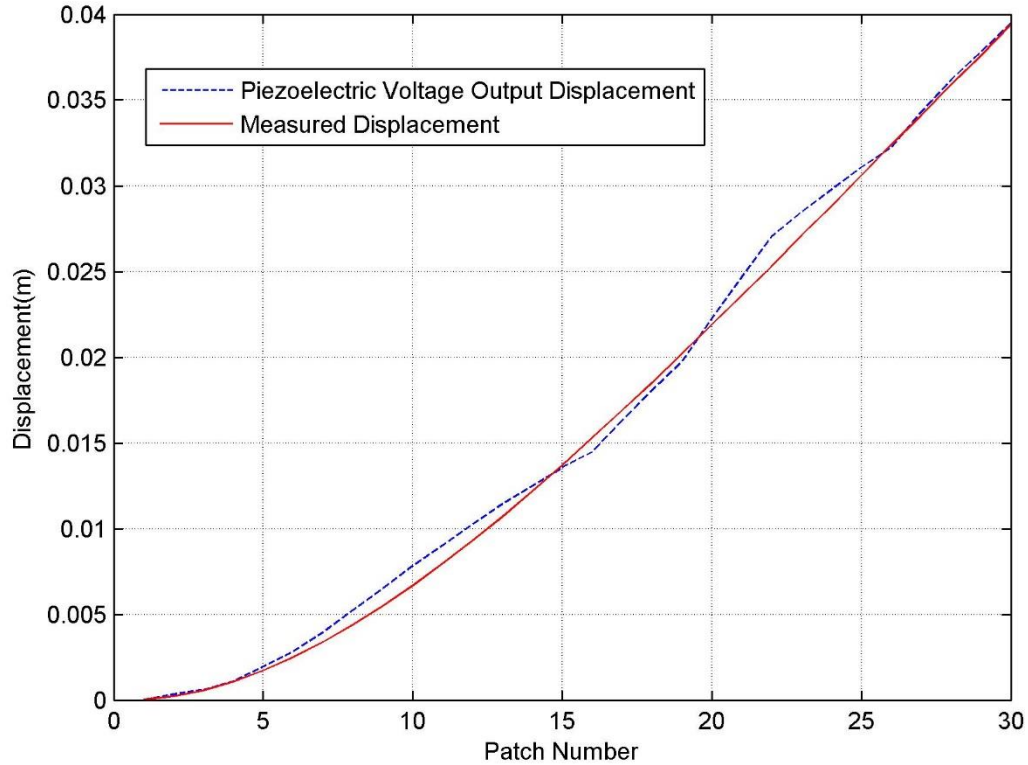


Figure 50. Comparison between the measured displacement and calculated displacement of wing 2. A force of 75 N was applied to this wing.

The graphs show that the calculated displacements of the wings are in close agreement with the measured displacements of the wings.

### **Elastically Supported Fuselage Simulation**

In the next simulation, elastic supports are used on the fuselage, which would allow it to translate and rotate about all three axes. Even though the forces applied on to the wings are the same as in the previous case, it will not deflect as in the previous simulation since the fuselage is not fixed. This implies that the voltage readings from the sensor patches would be different, and the displacement curve of the wings would have to be calculated. This calculated displacement cannot be compared against a measured wing displacement in ANSYS® because this result also accounts for the rigid body motion of the wing.

A displacement and rotation probe is placed on the fuselage to measure its translation and rotation about all three axes. These measurements will be used as the output, and the voltage readings from the sensors as the input to derive the state space model. Figs. 51 and 52 show the calculated displacement curve of the two wings.

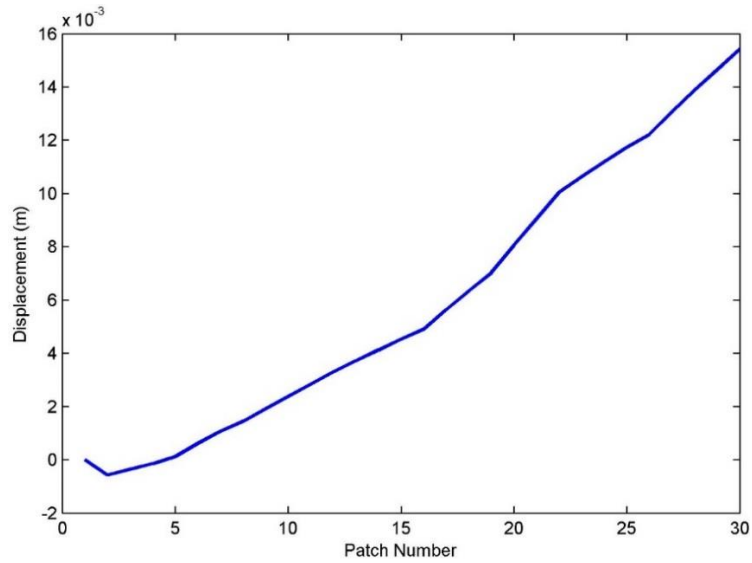


Figure 51. Calculated displacement of wing 1. A force of 50 N was applied to this wing.

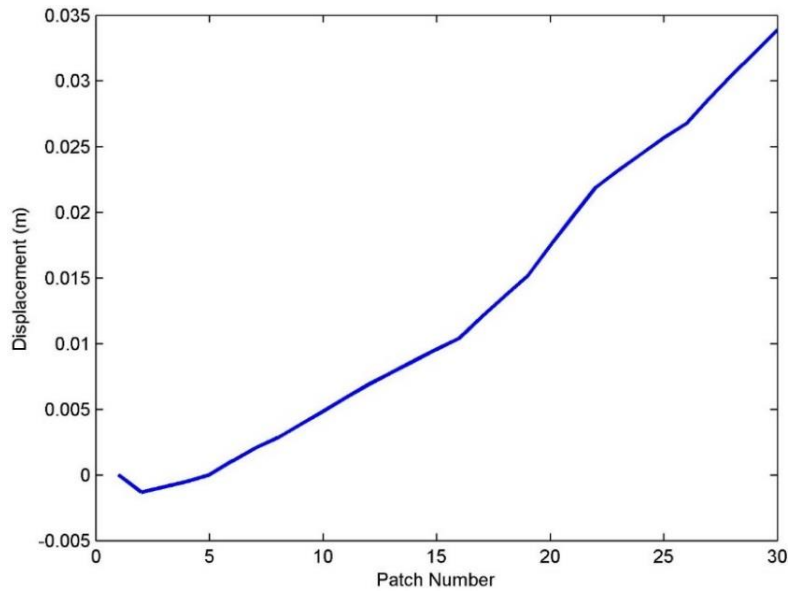


Figure 52. Calculated displacement of wing 2. A force of 100 N was applied to this wing.

A total of 60 displacement sensors are placed underneath both wings of the aircraft. The displacements of the wings will be used as inputs, the rotation and translation of the fuselage about all three axes will be used as outputs in developing a suitable state space model that will be able to predict the motion of the fuselage based on the output of the displacement sensors.

Using the system identification toolbox in MATLAB®, a fitting state space model was found for the Multiple Input-Multiple Output (MIMO) system. The state space model is represented in Eq. 2.29.

$$\begin{aligned}
 A &= \begin{bmatrix} A_{11} & A_{12} \\ A_{21} & A_{22} \end{bmatrix} \\
 B &= \begin{bmatrix} B_{11} & B_{12} & B_{13} & B_{14} & B_{15} & B_{16} & B_{17} & B_{18} & B_{19} & B_{110} & B_{111} & B_{112} & B_{113} & B_{114} & B_{115} \\ B_{21} & B_{22} & B_{23} & B_{24} & B_{25} & B_{26} & B_{27} & B_{28} & B_{29} & B_{210} & B_{211} & B_{212} & B_{213} & B_{214} & B_{215} \end{bmatrix} \\
 C &= \begin{bmatrix} C_{11} & C_{12} \\ C_{21} & C_{22} \end{bmatrix} \\
 D &= 0 \quad K = \begin{bmatrix} K_{11} & K_{12} \\ K_{21} & K_{22} \end{bmatrix}
 \end{aligned}$$

where

$$\begin{aligned}
 A_{11} &= \begin{bmatrix} -0.0206 & 0.3148 & -0.5381 & 1.2466 \\ -1.2233 & -2.4717 & -0.2340 & -0.2170 \\ 0.0166 & -1.5192 & -0.2352 & 5.8055 \\ -2.4962 & -3.1075 & -5.5810 & -0.3468 \end{bmatrix} \\
 A_{12} &= \begin{bmatrix} -0.1848 & -3.6463 & 2.4958 & 1.3444 \\ -1.9229 & 7.9822 & -9.3215 & -7.2591 \\ -3.0912 & 19.6388 & -0.2262 & 12.1523 \\ -2.9305 & 0.9070 & -1.2500 & -12.2633 \end{bmatrix} \\
 A_{13} &= \begin{bmatrix} 37.6331 & 117.2797 & 9.5273 & 22.2241 \\ 14.3602 & 48.5542 & -49.8713 & -13.8708 \\ 9.9469 & 96.1161 & -60.8595 & -37.5270 \\ -7.5462 & -29.8754 & 7.6183 & 26.0594 \end{bmatrix}
 \end{aligned}$$

$$A_{14} = \begin{bmatrix} -1.4539 & -9.3919 & -4.1513 & -31.1907 \\ -0.7760 & 0.5996 & -1.5829 & -3.5475 \\ -1.4008 & 6.3747 & -1.8525 & 1.2121 \\ 2.1593 & -5.3080 & 1.6321 & 2.2474 \end{bmatrix}$$

$$B_{11} = \begin{bmatrix} -3.6983 \times 10^{-11} & -0.3011 & -0.1869 & -0.0770 \\ 2.2872 \times 10^{-13} & 0.6024 & 0.3740 & 0.1540 \\ -1.5170 \times 10^{-14} & 4.3578 & 2.7055 & 1.1138 \\ -4.5786 \times 10^{-13} & -0.8944 & -0.5553 & -0.2286 \end{bmatrix}$$

$$B_{12} = \begin{bmatrix} 0.0597 & 0.3153 & 0.5526 & 0.7430 \\ -0.1195 & -0.6309 & -1.1058 & -1.4867 \\ -0.8644 & -4.5641 & -7.9992 & -10.7552 \\ 0.1774 & 0.9368 & 1.6418 & 2.2075 \end{bmatrix}$$

$$B_{13} = \begin{bmatrix} 0.9885 & 1.2286 & 1.4715 & 1.7092 \\ -1.9778 & -2.4583 & -2.9444 & -3.4198 \\ -14.3079 & -17.7838 & -21.300 & -24.7394 \\ 2.9367 & 3.6501 & 4.3718 & 5.0777 \end{bmatrix}$$

$$B_{14} = \begin{bmatrix} 1.9241 & 2.1365 & 2.3447 & 2.5374 \\ -3.8499 & -4.2750 & -4.6916 & -5.0771 \\ -27.8509 & -30.9257 & -33.9393 & -36.7280 \\ 5.7163 & 6.3474 & 6.9660 & 7.5383 \end{bmatrix}$$

$$B_{15} = \begin{bmatrix} 2.9201 & 3.2852 & 3.6377 & 4.1775 \\ -5.8427 & -6.5733 & -7.2786 & -8.3587 \\ -42.2670 & -47.5518 & -52.6539 & -60.4679 \\ 8.6752 & 9.7599 & 10.8071 & 12.4109 \end{bmatrix}$$

$$B_{16} = \begin{bmatrix} 4.6920 & 5.2044 & 5.5092 & 5.7972 \\ -9.3882 & -10.4134 & -11.0232 & -11.5996 \\ -67.9153 & -75.3317 & -79.7430 & -83.9130 \\ 13.9394 & 15.4616 & 16.3670 & 17.2229 \end{bmatrix}$$

$$B_{17} = \begin{bmatrix} 6.0830 & 6.3339 & 6.7742 & 7.1945 \\ -12.1714 & -12.6735 & -13.5544 & -14.3953 \\ -88.0493 & -91.6813 & -98.0541 & -104.1371 \\ 18.0719 & 18.8173 & 20.1253 & 21.3739 \end{bmatrix}$$

$$\begin{aligned}
B_{18} &= \begin{bmatrix} 7.5931 & 7.9946 & 0 & -0.6819 \\ -15.1929 & 15.9964 & 0 & 1.3644 \\ -109.9071 & -115.7195 & 0 & 9.8705 \\ 22.5581 & 23.7511 & 0 & -2.0259 \end{bmatrix} \\
B_{19} &= \begin{bmatrix} -0.4784 & -0.2680 & 0.0023 & 0.5421 \\ 0.9571 & 0.5362 & -0.0046 & -1.0846 \\ 6.9241 & 3.8791 & -0.0331 & -7.8463 \\ -1.4212 & -0.7962 & 0.0068 & 1.6104 \end{bmatrix} \\
B_{110} &= \begin{bmatrix} 1.0445 & 1.4528 & 1.9831 & 2.5019 \\ -2.0899 & -2.9070 & -3.9679 & -5.0059 \\ -15.1185 & -21.0292 & -28.7044 & -36.2136 \\ 3.1030 & 4.3162 & 5.8915 & 7.4327 \end{bmatrix} \\
B_{111} &= \begin{bmatrix} 3.0339 & 3.5547 & 4.0281 & 4.4975 \\ -6.0704 & -7.1125 & -8.0598 & -8.9990 \\ -43.9139 & -51.4527 & -58.3056 & -65.0995 \\ 9.0132 & 10.5605 & 11.9671 & 13.3615 \end{bmatrix} \\
B_{112} &= \begin{bmatrix} 4.9576 & 5.3866 & 6.2388 & 7.0524 \\ -9.9195 & -10.7780 & -12.4830 & -14.1111 \\ -71.7589 & -77.9691 & -90.3037 & -102.0810 \\ 14.7283 & 16.0029 & 18.5346 & 20.9519 \end{bmatrix} \\
B_{113} &= \begin{bmatrix} 7.8389 & 9.0427 & 10.1914 & 11.3351 \\ -15.6849 & -18.0935 & -20.3919 & -22.6802 \\ -13.4659 & -130.8901 & -147.5170 & -164.0712 \\ 23.2886 & 26.8648 & 30.2775 & 33.6752 \end{bmatrix} \\
B_{114} &= \begin{bmatrix} 12.0160 & 12.6601 & 13.2991 & 13.8600 \\ -24.0427 & -25.3314 & -26.6100 & -27.7323 \\ -173.9271 & -183.2501 & -192.4993 & -200.6181 \\ 35.6981 & 37.6116 & 39.5099 & 41.1763 \end{bmatrix} \\
B_{115} &= \begin{bmatrix} 14.8423 & 15.7790 & 16.6662 & 17.5603 \\ -29.6977 & -31.5720 & -33.3471 & -35.1361 \\ -214.8364 & -228.3951 & -241.2367 & -254.1783 \\ 44.0946 & 46.8775 & 49.5132 & 52.1694 \end{bmatrix} \\
B_{21} &= \begin{bmatrix} 7.0212 \times 10^{-12} & 1.0155 & 0.6305 & 0.2596 \\ 2.6672 \times 10^{-12} & -4.6811 & -2.9062 & -1.1965 \\ 1.8442 \times 10^{-12} & -6.4418 & -3.9993 & -1.6465 \\ -1.3884 \times 10^{-12} & 2.5500 & 1.5832 & 0.6518 \end{bmatrix}
\end{aligned}$$

$$\begin{aligned}
B_{22} &= \begin{bmatrix} -0.2014 & -1.0636 & -1.8641 & -2.5064 \\ 0.9286 & 4.9026 & 8.5925 & 11.5529 \\ 1.2778 & 6.7468 & 11.8246 & 15.8986 \\ -0.5058 & -2.6707 & -4.6808 & -6.2935 \end{bmatrix} \\
B_{23} &= \begin{bmatrix} -3.3343 & -4.1443 & -4.9638 & -5.7653 \\ 15.3692 & 19.1029 & 22.8799 & 26.5744 \\ 21.1503 & 26.2884 & 31.4861 & 36.5703 \\ -8.3725 & -10.4064 & -12.4640 & -14.4766 \end{bmatrix} \\
B_{24} &= \begin{bmatrix} -6.4904 & -7.2069 & -7.9092 & -8.5591 \\ 29.9167 & 33.2195 & 36.4567 & 39.4523 \\ 41.1699 & 45.7150 & 50.1699 & 54.2923 \\ -16.2973 & -18.0965 & -19.8600 & -21.4919 \end{bmatrix} \\
B_{25} &= \begin{bmatrix} -9.8499 & -11.0815 & -12.2705 & -14.0915 \\ 45.4021 & 51.0789 & 56.5595 & 64.9530 \\ 62.4801 & 70.2922 & 77.8343 & 89.3851 \\ -24.7331 & -27.8256 & -30.8111 & -35.3836 \end{bmatrix} \\
B_{26} &= \begin{bmatrix} -15.8270 & -17.5554 & -18.5834 & -19.5551 \\ 72.9528 & 80.9194 & 85.6579 & 90.1372 \\ 100.3940 & 111.3572 & 117.8781 & 124.0423 \\ -39.7415 & -44.0813 & -46.6627 & -49.1028 \end{bmatrix} \\
B_{27} &= \begin{bmatrix} -20.5191 & -21.3655 & -22.8506 & -24.2682 \\ 94.5802 & 98.4816 & 105.3272 & 111.8614 \\ 130.1566 & 135.5255 & 144.9460 & 153.9380 \\ -51.5232 & -53.6485 & -57.3776 & -60.9372 \end{bmatrix} \\
B_{28} &= \begin{bmatrix} -25.6128 & -26.9673 & 0 & 2.3002 \\ 118.0594 & 124.3029 & 0 & -10.6027 \\ 162.4674 & 171.0594 & 0 & -14.5908 \\ -64.3136 & -67.7148 & 0 & 5.7759 \end{bmatrix} \\
B_{29} &= \begin{bmatrix} 1.6136 & 0.9040 & -0.0077 & -1.8285 \\ -7.4377 & -4.1668 & 0.0355 & 8.4283 \\ -10.2354 & -5.7342 & 0.0489 & 11.5986 \\ 4.0517 & 2.2699 & -0.0194 & -4.5913 \end{bmatrix} \\
B_{210} &= \begin{bmatrix} -3.5232 & -4.9007 & -6.6893 & -8.4392 \\ 16.2399 & 22.5890 & 30.8335 & 38.8997 \\ 22.3485 & 31.0859 & 42.4315 & 53.5318 \\ -8.8468 & -12.3055 & -16.7968 & -21.1908 \end{bmatrix}
\end{aligned}$$



$$\begin{aligned}
B_{211} &= \begin{bmatrix} -10.2337 & -11.9906 & -13.8576 & -15.1708 \\ 47.1712 & 55.2692 & 62.6304 & 69.9282 \\ 64.9146 & 76.0587 & 86.1888 & 96.2317 \\ -25.6968 & -30.1082 & -34.1183 & -38.0938 \end{bmatrix} \\
B_{212} &= \begin{bmatrix} -16.7227 & -18.1700 & -21.0444 & -23.7890 \\ 77.0815 & 83.7523 & 97.0018 & 109.6528 \\ 106.0758 & 115.2558 & 133.4891 & 150.8987 \\ -41.9906 & -45.6246 & -52.8424 & -59.7340 \end{bmatrix} \\
B_{213} &= \begin{bmatrix} -26.4422 & -30.5027 & -34.3775 & -38.2352 \\ 121.8821 & 140.5988 & 158.4589 & 176.2410 \\ 167.7281 & 193.4850 & 218.0633 & 242.5340 \\ -66.3960 & -76.5921 & -86.3215 & -96.0084 \end{bmatrix} \\
B_{214} &= \begin{bmatrix} -40.5321 & -42.7047 & -44.8601 & -46.7522 \\ 186.8279 & 196.8425 & 206.7777 & 215.4987 \\ 257.1032 & 270.8848 & 284.5571 & 296.5585 \\ -101.7757 & -107.2312 & -112.6434 & -117.3943 \end{bmatrix} \\
B_{215} &= \begin{bmatrix} -50.656 & -53.2253 & -56.2179 & -59.2339 \\ 230.7716 & 245.3360 & 259.1302 & 273.0317 \\ 317.5763 & 337.6192 & 356.6020 & 375.7325 \\ -125.7143 & -133.6483 & -141.1628 & -148.7357 \end{bmatrix} \\
C_{11} &= \begin{bmatrix} -0.1451 & -0.0027 & -0.0055 & 0.0047 \\ 1.7305 \times 10^{-4} & 0.0036 & -0.0044 & -3.0109 \times 10^{-4} \\ -2.3353 \times 10^{-4} & 0.0060 & 7.2168 \times 10^{-4} & 3.0156 \times 10^{-4} \end{bmatrix} \\
C_{12} &= \begin{bmatrix} 3.4055 \times 10^{-4} & 0.0040 & -0.0035 & -0.0034 \\ 7.4117 \times 10^{-5} & -6.0337 \times 10^{-4} & -3.1823 \times 10^{-4} & -8.0022 \times 10^{-4} \\ -1.6283 \times 10^{-4} & 6.3690 \times 10^{-4} & -5.8428 \times 10^{-4} & -4.1873 \times 10^{-4} \end{bmatrix} \\
C_{21} &= \begin{bmatrix} 0.0653 & -1.7057 & -0.1949 & -0.0909 \\ -0.2180 & 0.0114 & -0.0029 & -0.0094 \\ -51.5160 & -0.9871 & -1.9648 & 1.7089 \end{bmatrix} \\
C_{22} &= \begin{bmatrix} 0.0188 & -0.1800 & 0.1667 & 0.1205 \\ 4.7844 \times 10^{-4} & 0.0080 & -0.0065 & -0.0035 \\ 0.1213 & 1.3920 & -1.2630 & -1.2018 \end{bmatrix} \\
K_{11} &= \begin{bmatrix} 255.5143 & 505.9206 & -53.9191 \\ -130.8322 & 736.4786 & 90.4383 \\ -1.1296 \times 10^3 & -1.1603 \times 10^4 & 59.4599 \\ 4.3630 \times 10^3 & -2.2555 \times 10^3 & -985.8026 \end{bmatrix}
\end{aligned}$$

$$\begin{aligned}
K_{12} &= \begin{bmatrix} -0.0733 & -132.7676 & -1.1927 \\ -42.5669 & 2.9547 & -1.9619 \\ -41.5373 & -33.1619 & 2.0021 \\ -55.0306 & -3.3168 \times 10^3 & -1.8927 \end{bmatrix} \\
K_{21} &= \begin{bmatrix} 4.6030 \times 10^3 & 5.3864 \times 10^4 & -4.0080 \times 10^3 \\ 1.9654 \times 10^3 & -1.0933 \times 10^5 & 293.5151 \\ 5.3402 \times 10^3 & -1.6175 \times 10^5 & 3.1254 \times 10^3 \\ -5.6876 \times 10^3 & 4.2291 \times 10^4 & -2.6128 \times 10^3 \end{bmatrix} \\
K_{22} &= \begin{bmatrix} 1.5370 \times 10^3 & 1.1123 \times 10^4 & 129.6085 \\ 177.0743 & -1.2910 \times 10^4 & 103.1746 \\ 482.6644 & -3.1909 \times 10^4 & 160.6948 \\ -119.3118 & 2.0716 \times 10^4 & -114.0318 \end{bmatrix}
\end{aligned} \tag{5.1}$$

This state space model uses the measured displacements of the wings as input, and gives the displacements of the fuselage about the X, Y and Z axes and then the rotations of the fuselage about the X, Y and Z axes. The output of the state space model, which is in a matrix form, is given in this particular order.

To ensure that this state space model can predict the motion of the fuselage, a transient analysis is performed by applying a different set of forces to excite the model, using ANSYS®. In this part of the simulation, a 40 N force is applied to one wing, and a 60 N force is applied to the other wing. The graphs are generated by comparing the rigid body motion of the fuselage from the simulation with the output of the state space model when the measured displacement of the wing is provided to it as its input.

Figs. 53-58 compare the state space output to the ANSYS® simulation results. Some graphs such as Y rotation, can be seen to show slightly different displacements, since these outputs are noisy owing to the fact that there is not much motion in these directions. The figures show a good agreement between the state space model results and the simulation results, thus validating the derived state space model.

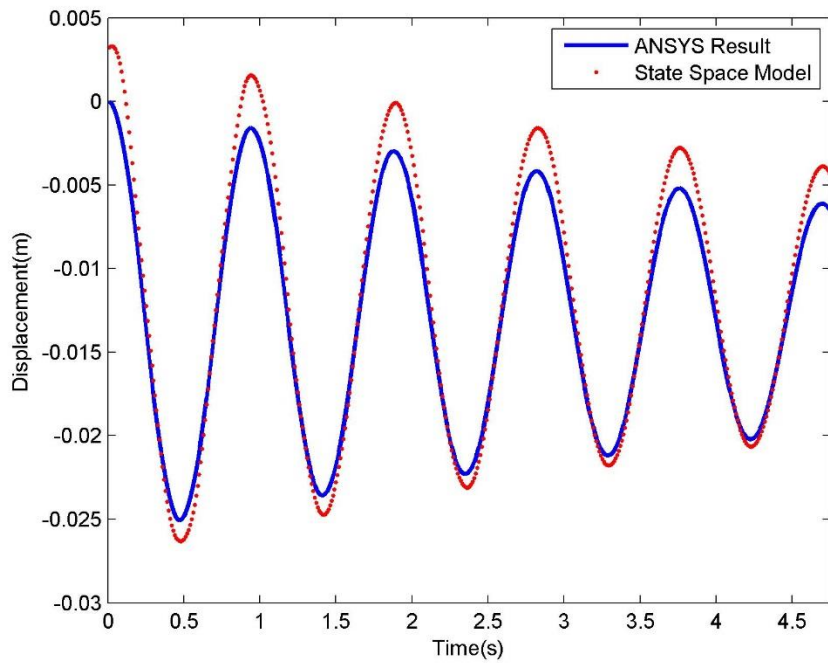


Figure 53. Comparison between state space outputs and simulation results for fuselage motion about the X-axis.

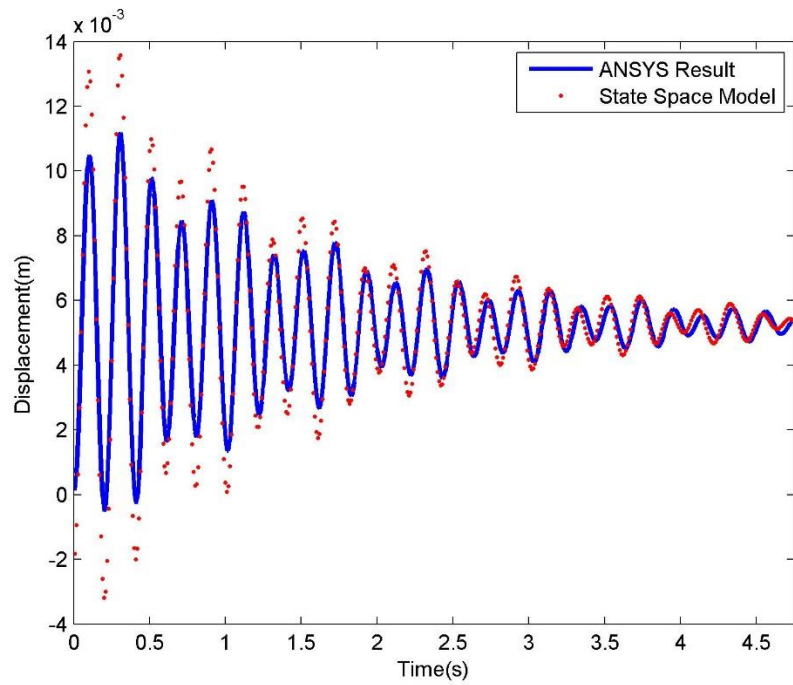


Figure 54. Comparison between state space outputs and simulation results for fuselage motion about the Y-axis.

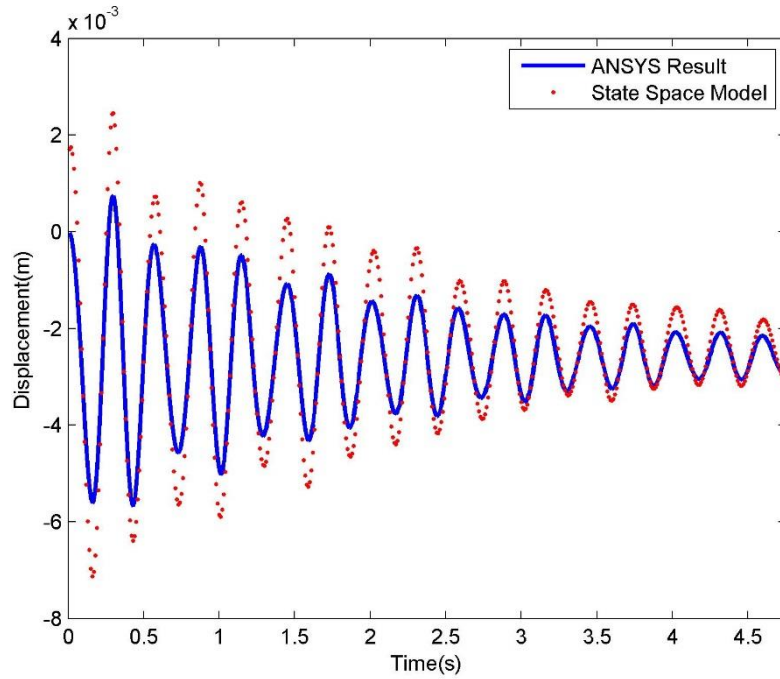


Figure 55. Comparison between state space outputs and simulation results for fuselage motion about the Z-axis.

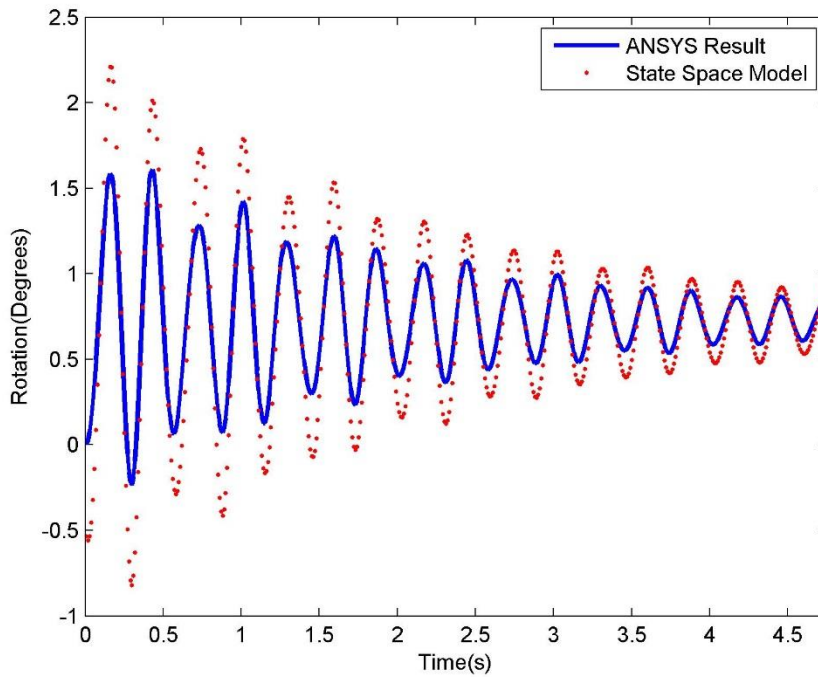


Figure 56. Comparison between state space outputs and simulation results for fuselage rotation about the X-axis.

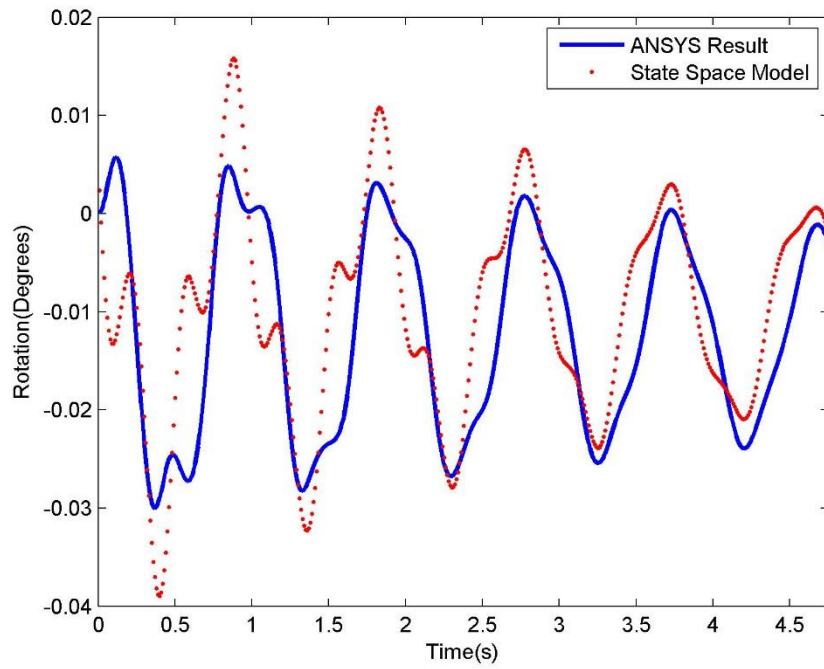


Figure 57. Comparison between state space outputs and simulation results for fuselage rotation about the Y-axis.

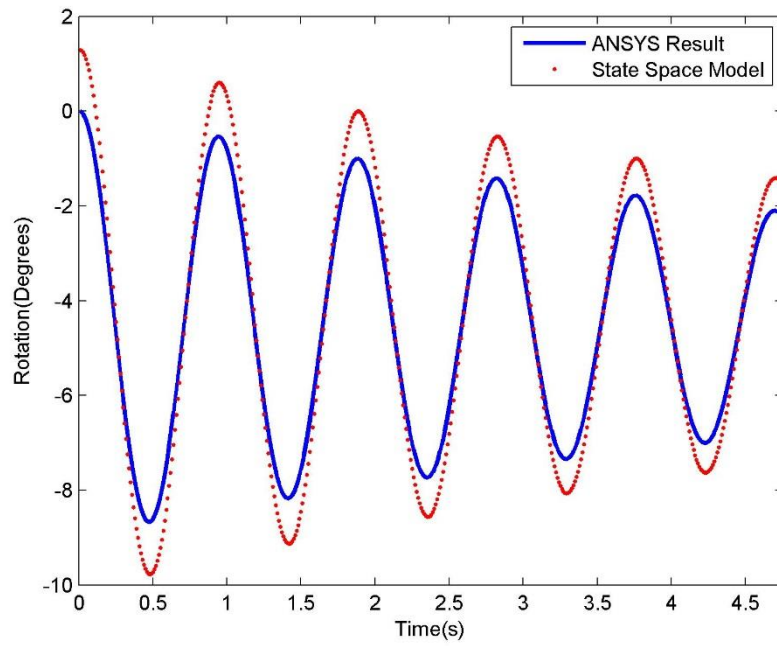


Figure 58. Comparison between state space outputs and simulation results for fuselage rotation about the Z-axis.

## CHAPTER VI

### CONCLUSIONS AND RECOMMENDATIONS

Vibration control systems are used in larger aircraft, but miniaturizing such a system for use with unmanned aerial vehicles brings with it many complexities. Aircraft are especially very flexible since they are large in size and have structurally light damping [22]. Therefore there is a need for a method to predict the motion of the aircraft in turbulent conditions, and provide suitable countermeasures to a payload mounted on active mounts by means of a system that is computationally inexpensive as well as cost effective. Another approach to this problem is to incorporate this system into the avionics of the aircraft to damp out the fuselage vibrations. To introduce said vibration control system, the first step is to develop a sensor that will be able to measure some effect of turbulent loads on the aircraft structure.

This research first began by analyzing a lumped mass model, which was later expanded to a full three dimensional aircraft model. This aircraft was excited by applying forces on its wings, and state space models were derived that could satisfactorily predict the motion and rotation of the fuselage in three dimensional space.

The next phase of this research involved developing a suitable sensor for the aircraft. It is found that the PolyVinylDene Fluoride (PVDF) displacement sensors can be used on the aircraft wings to measure the displacements of its wings. By deriving a fitting state space model that uses the displacement of the wings as the input, and the displacements and rotations of the fuselage as output, the motion of the fuselage was

predicted about all three axes.

To ensure accuracy and fast response time, commonly used sensors are not ideally adapted because of their sizes and limited measurements of degrees of freedom [23]. Piezoelectric sensors are analog sensors and the number of measurements that can be made per second is purely limited by the ability of the processors that will be used with this system. Steady improvements in processor technology over the last decade have made available fast and powerful processors that are cost effective as well.

The development of such a system can lead to the development of a robust, accurate, lightweight and cost effective Active/Passive Vibration Control system, which can actively dissipate the effects of turbulent wind load on the aircraft or payload. An Active/Passive Vibration Control system can help in protecting any sensitive payloads carried by the aircraft, and can prove to be very useful in missions where the stability of the aircraft is of the utmost importance.

Opportunities for future work include to first derive a method to identify equations that would serve as correction factors on the unconstrained ends of a cantilever beam. Such a readymade method would leave no room for error, and will aid in further increasing the accuracy of the measured displacements. Next would be to build an aircraft model and bond the piezoelectric displacement sensors onto its wings and to observe the output of the sensors in a laboratory environment. Conducting an experimental procedure on this model will allow for proper calibration of the sensors. The results for load conditions such as sinusoidal loads are time consuming processes by simulation, and hence it would be easier to measure the output of the sensors through an experimental procedure. The data obtained in an experimental set up could be used in the development of a state space model as well.

The end goal is to create a state space model that can predict the motion of the fuselage in all sorts of environments and under all sorts of conditions.



## APPENDICES

## APPENDIX A

### MATLAB® Codes for a Lumped Mass Model

All of the mathematical analysis done in this research is with the help of MATLAB®. This part of the appendix contains all the codes that were used in developing the lumped mass model.

Below is the MATLAB® code used to derive the motion of the fuselage and wings due to a step force excitation, using modal superposition equations.

```
clear all
close all
clc

%Mass Matrix
m = [2 0 0; 0 10 0; 0 0 2];

%Stiffness Matrix
k = [27169.5 -10002 0; -10002 20004 -10002; 0 -10002 27169.5];

%Natural Frequencies
w1 = 34.5431;
w2 = 116.5512;
w3 = 119.968;
wd1 = 34.4999;
wd2 = 116.5512;
wd3 = 119.8179;

%Eigenvalue Matrix
x = [0.1237 0.4997 0.4843; 0.3064 0 -0.0782; 0.1236 -0.5003 0.4847];

%Force Matrix
f = [-5;0;-10];

%Vector of generalized forces
q = x'*f;

%Principal Coordinates
syms t tau

%Generalized mass displacement
q1 = (q(1)/wd1)*exp(-0.05*w1*(t-tau))*sin(wd1*(t-tau));
```

```

q1 = int(q1,tau,0,t);
t = [0.0005:0.0005:5];
q1 = eval(q1);

syms t
q2 = (q(2)/wd2)*exp(-0.05*w2*(t-tau))*sin(wd2*(t-tau));
q2 = int(q2,tau,0,t);
t = [0.0005:0.0005:5];
q2 = eval(q2);

syms t
q3 = (q(3)/wd3)*exp(-0.05*w3*(t-tau))*sin(wd3*(t-tau));
q3 = int(q3,tau,0,t);
t = [0.0005:0.0005:5];
q3 = eval(q3);

%Solution Vector
sol = x*[q1;q2;q3];

x1 = sol(1,:);

x2 = sol(2,:);

x3 = sol(3,:);

%%Derived State Space Model for comparison

A = [0,0,0,1,0,0;0,0,0,0,1,0;0,0,0,0,0,1;-13584.7 5001 0 -16.3366
7.07175 0; 1000.2 -2000.4 1000.2 3.16259 -6.32578 3.16259; 0 5001 -
13584.7 0 7.07175 -16.3366];
B = [0;0;0;0.5;0;1];
C = [0,1,0,0,0,0];
D = 0;
sys = ss(A,B,C,D)

```

Below is the MATLAB® code used to derive the motion of the fuselage and wings due to a sinusoidal force excitation, using modal superposition equations.

```

clear all
close all
clc
syms t;

%Mass Matrix
m = [2 0 0; 0 10 0; 0 0 2];

%Stiffness Matrix
k = [27169.5 -10002 0; -10002 20004 -10002; 0 -10002 27169.5];

%Natural Frequencies
w1 = 34.5431;

```

```

w2 = 116.5512;
w3 = 119.968;
wd1 = 34.4999;
wd2 = 116.5512;
wd3 = 119.8179;

%Eigenvalue Matrix
x = [0.1237 0.4997 0.4843; 0.3064 0 -0.0782; 0.1236 -0.5003 0.4847];

%Force Matrix
f = [-5*sin(10*t);0;-5*sin(10*t)];

%Vector of generalized forces
q = x'*f;

%Principal Coordinates
syms tau

q1 = (q(1)/wd1)*exp(-0.05*w1*(t-tau))*sin(wd1*(t-tau));
q1 = int(q1,tau,0,t);

q2= (q(2)/wd2)*exp(-0.05*w2*(t-tau))*sin(wd2*(t-tau));
q2 = int(q2,tau,0,t);

q3 = (q(3)/wd3)*exp(-0.05*w3*(t-tau))*sin(wd3*(t-tau));
q3 = int(q3,tau,0,t);

%Solution Vector
sol = x*[q1;q2;q3];

x1 = sol(1,:);
x2 = sol(2,:);
x3 = sol(3,:);

t = [1e-3:1e-3:5];
x1 = eval(x1);
x2 = eval(x2);
x3 = eval(x3);

%%Derived State Space Model for comparison
talt = [8e-3:8e-3:5];
input = [-5*sin(10*talt)];
A = [0,0,0,1,0,0;0,0,0,0,1,0;0,0,0,0,0,1;-13584.7 5001 0 -16.3366
7.07175 0; 1000.2 -2000.4 1000.2 3.16259 -6.32578 3.16259; 0 5001 -
13584.7 0 7.07175 -16.3366];
B = [0;0;0;0.5;0;0.5];
C = [0,1,0,0,0,0];
D = 0;
sys = ss(A,B,C,D)

```

The derived state space models in this research are done using MATLAB® system identification toolbox. This toolbox is relatively user friendly, and the processing time is small. To access this toolbox, the user first needs to have the system identification toolbox license installed. The toolbox can then be accessed by entering the keyword “ident” into the MATLAB® workspace. Fig. 59 illustrates the options available to enter the data into the identification toolbox.

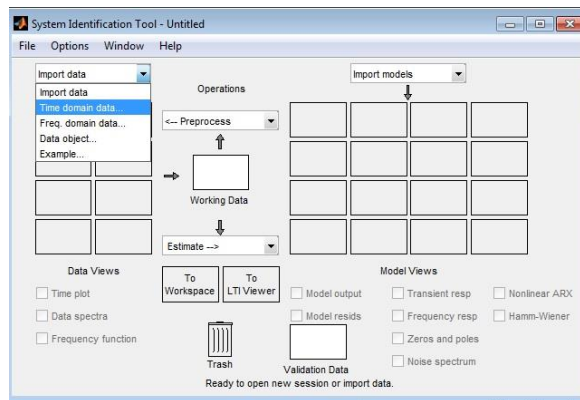


Figure 59. Data input options in the system identification toolbox.

Following this, the data that exists on the MATLAB® workspace need to be entered into the data box. Fig. 60 shows a time domain data example.

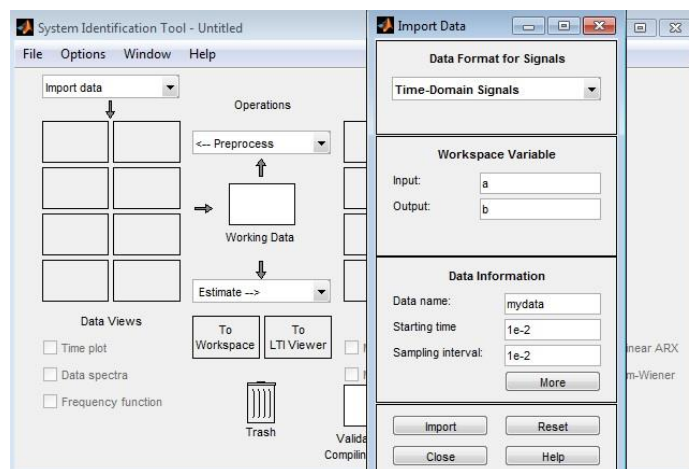


Figure 60. Data being imported into the toolbox.

The state space estimation option can be selected from Estimate-State Space

Models. When this is done, the user has a choice between entering a model order and comparing between specified model orders for the best fit, which is shown in Fig. 61.

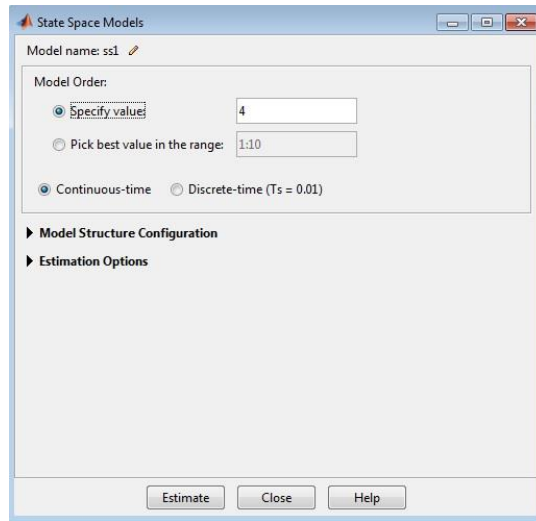


Figure 61. State Space Model window.

If the user chooses to compare state space models of different orders, the following window pops up, allowing the user to find a state space model that has a good balance between model order and fit.

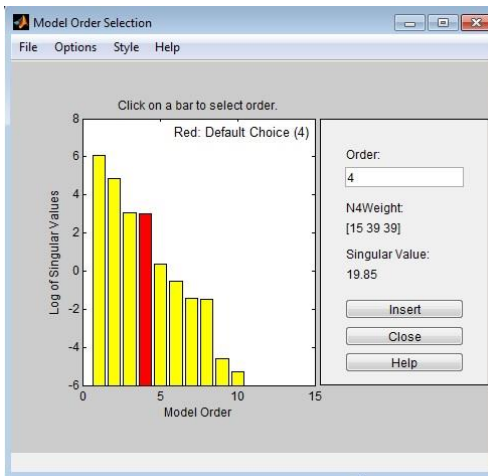


Figure 62. Model order selection window.

Once a suitable model order has been selected, the model can be checked with the output data for its fit. This is done by clicking the model order check box.

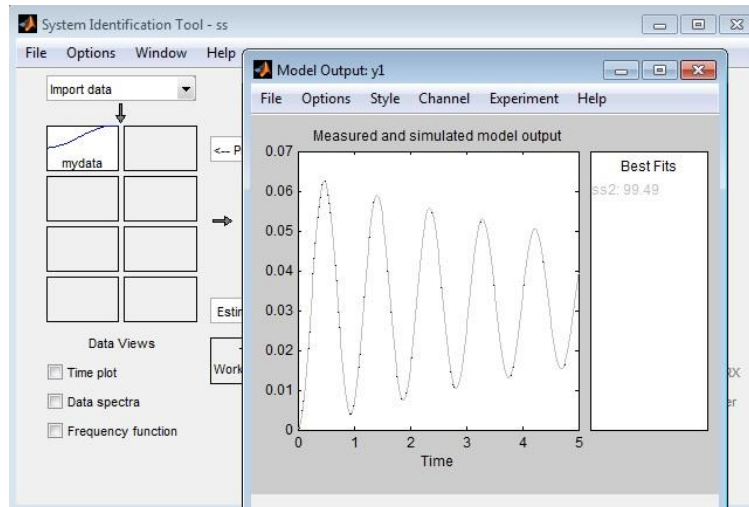


Figure 63. Model output.

## APPENDIX B

### MATLAB® Codes for Piezoelectric Displacement Sensors

To calculate the displacements of the wings from the patch voltage, a code is run

in MATLAB®. This code is shown below:

```
clear all
close all
clc
format long

%%Sensor constants
h31 = 0.4e9;
hs = 1e-3;
hb = 20.6961e-3;

%%Read the ANSYS voltage files
voltage1 = xlsread('Voltage1.xlsx');
voltage2 = xlsread('Voltage2.xlsx');
voltage3 = xlsread('Voltage3.xlsx');
voltage4 = xlsread('Voltage4.xlsx');
voltage5 = xlsread('Voltage5.xlsx');
voltage6 = xlsread('Voltage6.xlsx');
voltage7 = xlsread('Voltage7.xlsx');
voltage8 = xlsread('Voltage8.xlsx');
voltage9 = xlsread('Voltage9.xlsx');
voltage10 = xlsread('Voltage10.xlsx');
voltage11 = xlsread('Voltage11.xlsx');
voltage12 = xlsread('Voltage12.xlsx');
voltage13 = xlsread('Voltage13.xlsx');
voltage14 = xlsread('Voltage14.xlsx');
voltage15 = xlsread('Voltage15.xlsx');
voltage16 = xlsread('Voltage16.xlsx');
voltage17 = xlsread('Voltage17.xlsx');
voltage18 = xlsread('Voltage18.xlsx');
voltage19 = xlsread('Voltage19.xlsx');
voltage20 = xlsread('Voltage20.xlsx');
voltage21 = xlsread('Voltage21.xlsx');
voltage22 = xlsread('Voltage22.xlsx');
voltage23 = xlsread('Voltage23.xlsx');
voltage24 = xlsread('Voltage24.xlsx');
voltage25 = xlsread('Voltage25.xlsx');
voltage26 = xlsread('Voltage26.xlsx');
voltage27 = xlsread('Voltage27.xlsx');
voltage28 = xlsread('Voltage28.xlsx');
voltage29 = xlsread('Voltage29.xlsx');
```



```

voltage30 = xlsread('Voltage30.xlsx');

%%Sum up all the voltages
v1 = sum(voltage1);
v2 = sum(voltage2);
v3 = sum(voltage3);
v4 = sum(voltage4);
v5 = sum(voltage5);
v6 = sum(voltage6);
v7 = sum(voltage7);
v8 = sum(voltage8);
v9 = sum(voltage9);
v10 = sum(voltage10);
v11 = sum(voltage11);
v12 = sum(voltage12);
v13 = sum(voltage13);
v14 = sum(voltage14);
v15 = sum(voltage15);
v16 = sum(voltage16);
v17 = sum(voltage17);
v18 = sum(voltage18);
v19 = sum(voltage19);
v20 = sum(voltage20);
v21 = sum(voltage21);
v22 = sum(voltage22);
v23 = sum(voltage23);
v24 = sum(voltage24);
v25 = sum(voltage25);
v26 = sum(voltage26);
v27 = sum(voltage27);
v28 = sum(voltage28);
v29 = sum(voltage29);
v30 = sum(voltage30);

%%Calculated slopes
a(1) = ((-2*v1(2))/(hs^2 + (hs*hb*h31)));
a(2) = ((-2*v2(2))/(hs^2 + (hs*hb*h31)));
a(3) = ((-2*v3(2))/(hs^2 + (hs*hb*h31)));
a(4) = ((-2*v4(2))/(hs^2 + (hs*hb*h31)));
a(5) = ((-2*v5(2))/(hs^2 + (hs*hb*h31)));
a(6) = ((-2*v6(2))/(hs^2 + (hs*hb*h31)));
a(7) = ((-2*v7(2))/(hs^2 + (hs*hb*h31)));
a(8) = ((-2*v8(2))/(hs^2 + (hs*hb*h31)));
a(9) = ((-2*v9(2))/(hs^2 + (hs*hb*h31)));
a(10) = ((-2*v10(2))/(hs^2 + (hs*hb*h31)));
a(11) = ((-2*v11(2))/(hs^2 + (hs*hb*h31)));
a(12) = ((-2*v12(2))/(hs^2 + (hs*hb*h31)));
a(13) = ((-2*v13(2))/(hs^2 + (hs*hb*h31)));
a(14) = ((-2*v14(2))/(hs^2 + (hs*hb*h31)));
a(15) = ((-2*v15(2))/(hs^2 + (hs*hb*h31)));
a(16) = ((-2*v16(2))/(hs^2 + (hs*hb*h31)));
a(17) = ((-2*v17(2))/(hs^2 + (hs*hb*h31)))+a(16); //correction factor
a(18) = ((-2*v18(2))/(hs^2 + (hs*hb*h31)))+a(16); //correction factor
a(19) = ((-2*v19(2))/(hs^2 + (hs*hb*h31)))+a(16); //correction factor
a(20) = ((-2*v20(2))/(hs^2 + (hs*hb*h31)))+a(17); //correction factor
a(21) = ((-2*v21(2))/(hs^2 + (hs*hb*h31)))+a(17); //correction factor

```

```

a(22) = ((-2*v22(2))/(hs^2 + (hs*hb*h31)))+a(17); //correction factor
a(23) = ((-2*v23(2))/(hs^2 + (hs*hb*h31)))+a(16); //correction factor
a(24) = ((-2*v24(2))/(hs^2 + (hs*hb*h31)))+a(16); //correction factor
a(25) = ((-2*v25(2))/(hs^2 + (hs*hb*h31)))+a(16); //correction factor
a(26) = ((-2*v26(2))/(hs^2 + (hs*hb*h31)))+a(16); //correction factor
a(27) = ((-2*v27(2))/(hs^2 + (hs*hb*h31)))+a(17); //correction factor
a(28) = ((-2*v28(2))/(hs^2 + (hs*hb*h31)))+a(17); //correction factor
a(29) = ((-2*v29(2))/(hs^2 + (hs*hb*h31)))+a(17); //correction factor
a(30) = ((-2*v30(2))/(hs^2 + (hs*hb*h31)))+a(17); //correction factor

%%Locations of the center points of each sensor patch
x(1) = 1651/30;

for i=2:30
    x(i) = x(i-1)+(1651/30);
end
%%Calculate the displacement of the wing
z(1) = 0; // boundary condition
for i=2:30
    z(i) = (a(i)*(x(i)-x(i-1))) + z(i-1);
end
%%Plot the displacement of the wing
plot(x,z/815)

```

## REFERENCES

- [1] Mohamed, A., Massey, K., Watkins, S., & Clothier, R. (2014). The attitude control of fixed-wing MAVS in turbulent environments. *Progress in Aerospace Sciences*. doi:10.1016/j.paerosci.2013.12.003
- [2] Liguore, S., & Followell, D. (1995). Vibration fatigue of surface mount technology (SMT) solder joints. *Reliability and Maintainability Symposium, 1995. Proceedings., Annual*. doi:10.1109/RAMS.1995.513218
- [3] Williams, P. D., & Joshi, M. M. (2013). Intensification of winter transatlantic aviation turbulence in response to climate change. *Nature Clim. Change*, 3(7), 644–648. Retrieved from <http://dx.doi.org/10.1038/nclimate1866>
- [4] Gao, L., Lu, Q., Fei, F., Liu, L., Liu, Y., & Leng, J. (2013). Active vibration control based on piezoelectric smart composite. *Smart Materials and Structures*, 22(12), 125032. doi:10.1088/0964-1726/22/12/125032
- [5] Lams, C. F. (2011). An Investigation of Atmospheric Turbulence Probes with Ground Test Comparisons of Probe Head Designs and Evaluation of Suitability to Instrumented Aircraft.
- [6] Ellen, R., Roberts, P. ., & Greer, D. . (2005). An investigation into the next generation avionics architecture for the QUT UAV project. *Proceedings Smart Systems 2005 Postgraduate Research Conference, Brisbane., 2005*. Retrieved from <http://eprints.qut.edu.au/3111/1/3111.pdf>
- [7] Lissaman, P. (2009). Effects of Turbulence on Bank Upsets of Small Flight Vehicles. In *AIAA Aerospace Sciences Meeting Including The New Horizons Forum and Aerospace Exposition* (pp. 1–10).
- [8] Sven Marco Hoppe. (2000). *Gust Alleviation using direct Gust Measurement* (p. 95). Los Angeles.
- [9] Mohamed, A., Watkins, S., Clothier, R., & Abdulrahim, M. (2014). Influence of Turbulence on MAV Roll Perturbations, 6(3), 175–190.
- [10] Chen, T., Clothier, R., Mohamed, A., & Badawy, R. (2014). An Experimental Study of Human Performance in Controlling Micro Aerial Vehicles in Turbulent Environment.

- [11] Wang, S., Li, Y., & He, W. (2011). Flight attitude estimation for MAV based on M-estimation. *Consumer Electronics, Communications and Networks (CECNet), 2011 International Conference on*. doi:10.1109/CECNET.2011.5768718
- [12] Mohamed, a., Clothier, R., Watkins, S., Sabatini, R., & Abdulrahim, M. (2014). Fixed-wing MAV attitude stability in atmospheric turbulence, part 1: Suitability of conventional sensors. *Progress in Aerospace Sciences, 70*, 69–82. doi:10.1016/j.paerosci.2014.06.001
- [13] Zahui, M., & Thomas, R. (2014). Design of Beam Surface Displacement Sensors. *ASME International Mechanical Engineering Conference and Exposition 2014*, 1–7.
- [14] Rao, S. (2004). *Mechanical vibrations* (4th ed., p. 141,503,504,543). Reading, Massachusetts: Addison-Wesley.
- [15] Dorf, R., & Bishop, R. (2001). State Variable Models. In *Modern control systems* (9th ed., p. 166). Upper Saddle River, New Jersey: Prentice Hall.
- [16] Documentation. (2008, January 1). Retrieved March 4, 2015, from <http://www.mathworks.com/help/ident/state-space-models.html>
- [17] Sek, M. (2001). Frequency Response Function. *Victoria University*, 1–79. Retrieved from <http://www.staff.vu.edu.au/msek/FRF.pdf>
- [18] Ewins, D. (1984). Overview. In *Modal testing: Theory and practice* (p. 11). Letchworth, Hertfordshire: Research Studies Press
- [19] Elastic Supports. (2014). In *Mechanical Applications*, ANSYS Documentation. SAP IP.
- [20] A Normal and Tangential Elastic Foundation in Workbench Mechanical. (2014, January 1). Retrieved March 4, 2015, from <http://www.simutechgroup.com/FEA/a-normal-and-tangential-elastic-foundation-in-workbench-mechanical.html>
- [21] Odegard, G. M., Gates, T. S., Wise, K. E., Park, C., & Siochi, E. J. (2003). Constitutive modeling of nanotube – reinforced polymer composites, *63*, 1671–1687. doi:10.1016/S0266-3538(03)00063-0
- [22] Tatavolu, V. R., & Panchumarthy, S. R. (2013). Embedded Computer Based Active Vibration Control System for Vibration Reduction of Flexible Structures. *Journal of Computer Science, 9*(7), 838–846. doi:10.3844/jcssp.2013.838.846
- [23] Pinto, N. M. P., Frazão, O., Baptista, J. M., & Santos, J. L. (2006). Quasi-distributed displacement sensor for structural monitoring using a commercial OTDR. *Optics and Lasers in Engineering, 44*, 771–778. doi:10.1016/j.optlaseng.2005.07.009